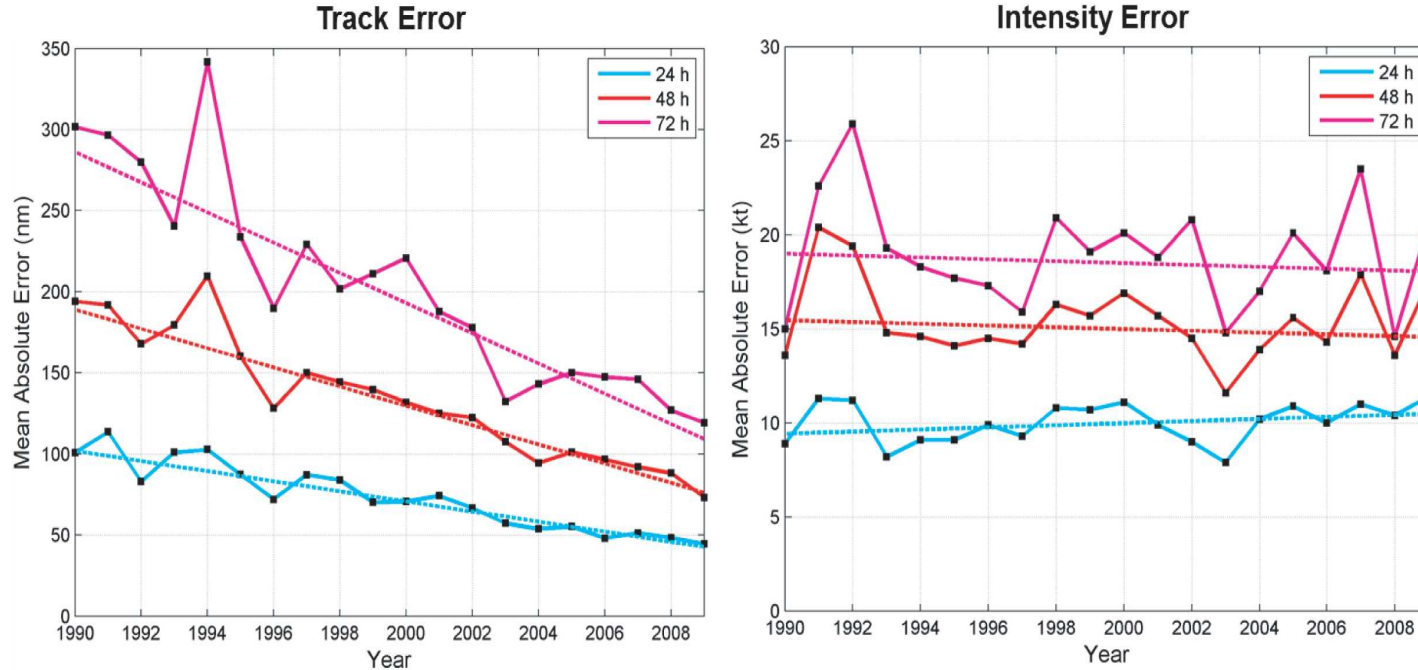


# WMO Training Course on Tropical Cyclones, La Réunion (October 2013)

1. Structure et variabilité internes
2. Influences externes
3. Variabilité climatique
4. Changements climatiques

## 1. Structure et variabilité internes

- Circulations primaire et secondaire
- Machine thermique
- Cycle de remplacement des murs de l'œil
- Bandes externes
- Circulation dans l'œil

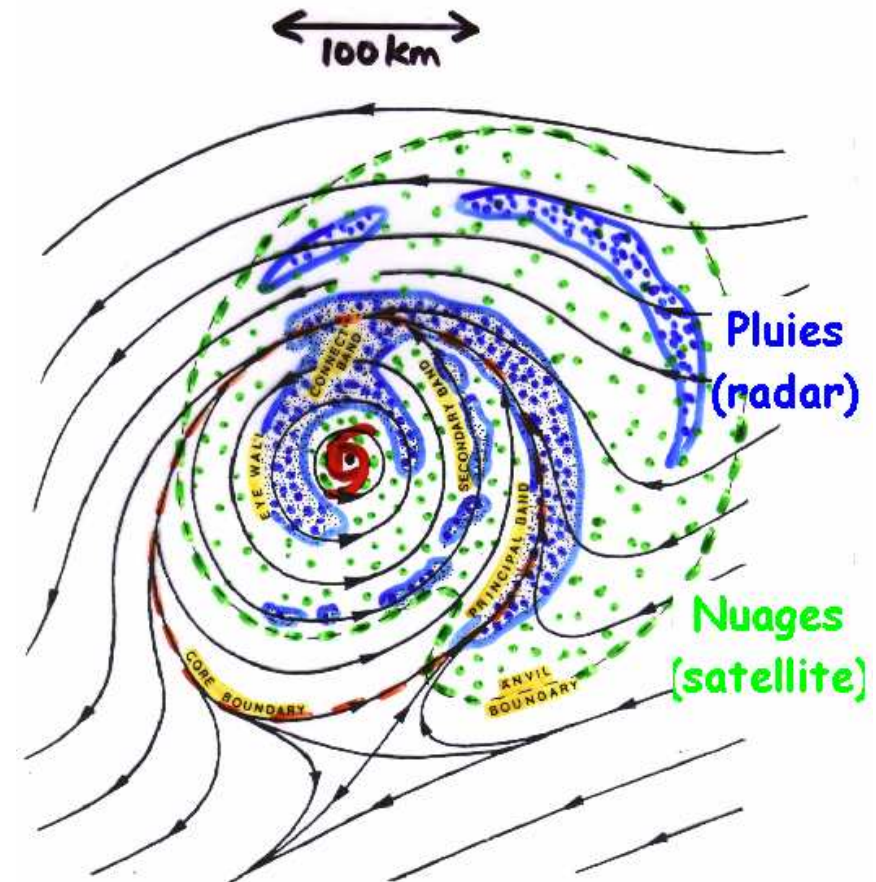
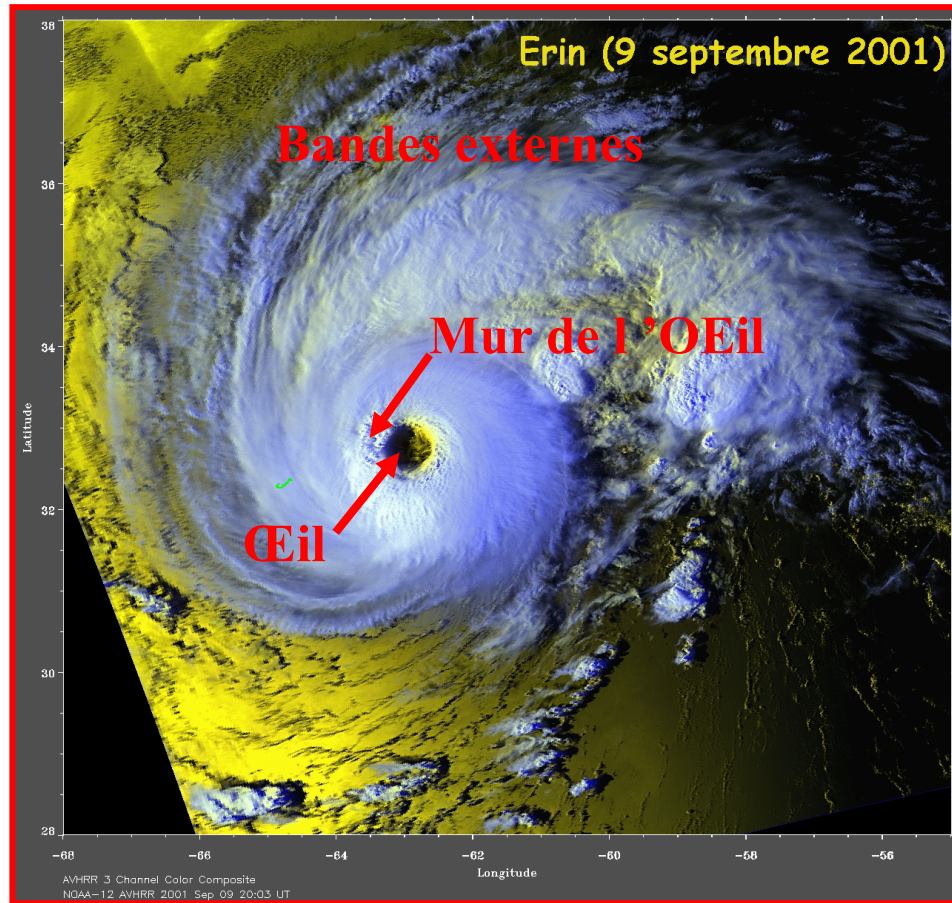


Average mean absolute errors for official TC track and intensity predictions at various lead times in the North Atlantic basin from 1990-2009.

## Quels facteurs contrôlent l'intensité d'un cyclone?

- Facteurs internes : équilibre thermodynamique, dynamique du Mur de l'Œil et des bandes externes, ...
- Facteurs externes : température de l'océan, cisaillement de vent, zones sèches, structures d'altitude, ...

# A L 'INTERIEUR DES CYCLONES TROPICAUX



Circulation primaire : tangentielle (qq 10 m/s)

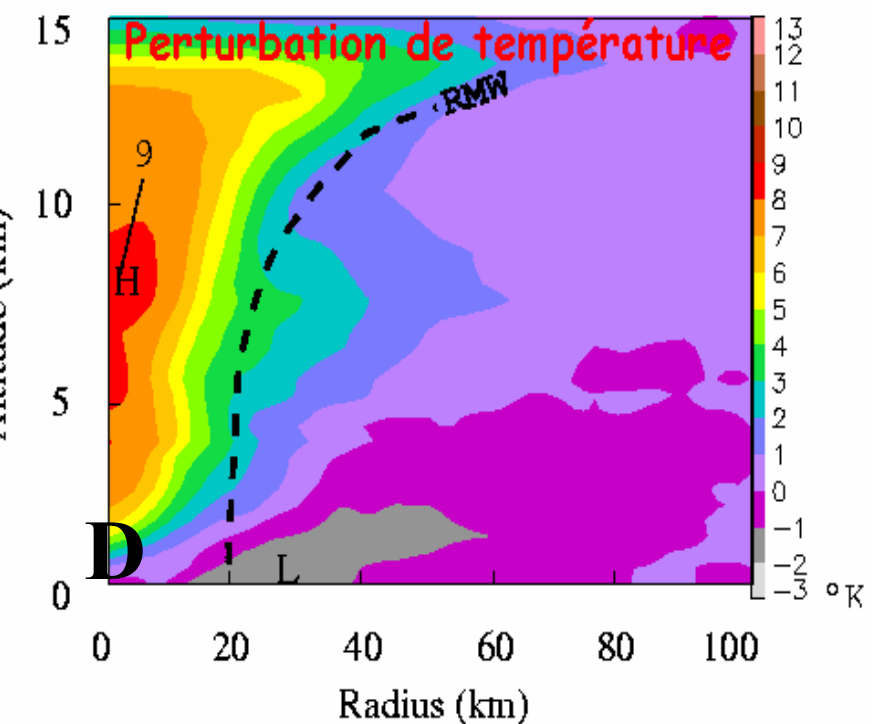
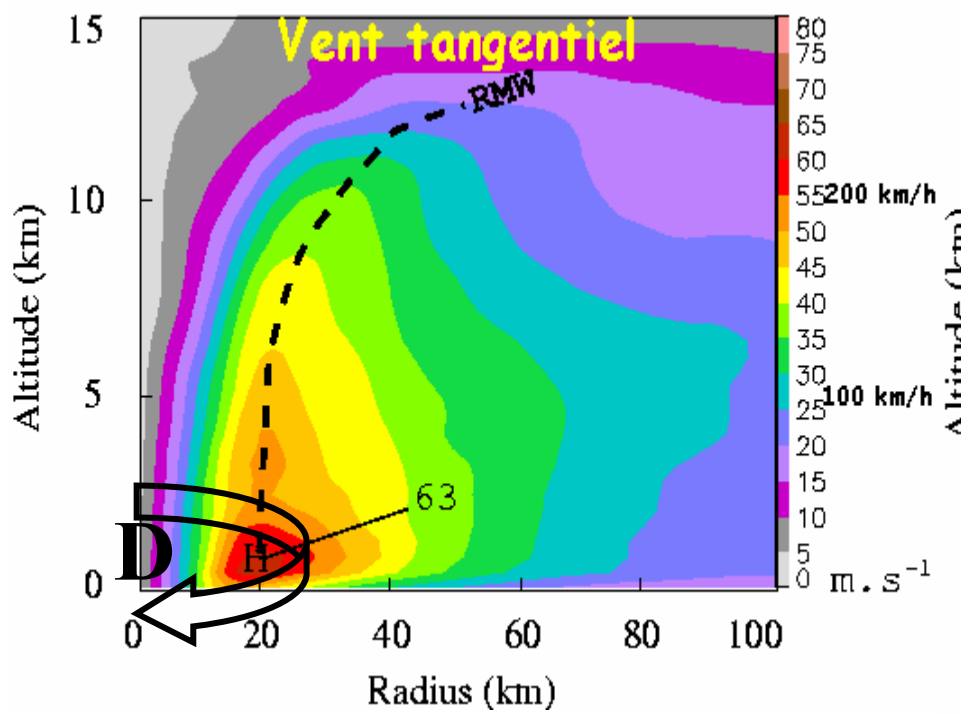
Circulation secondaire: radiale et verticale (qq m/s)

# LA CIRCULATION PRIMAIRE

L'accélération centrifuge du vent () équilibre la force centripète vers la dépression centrale (D) ;

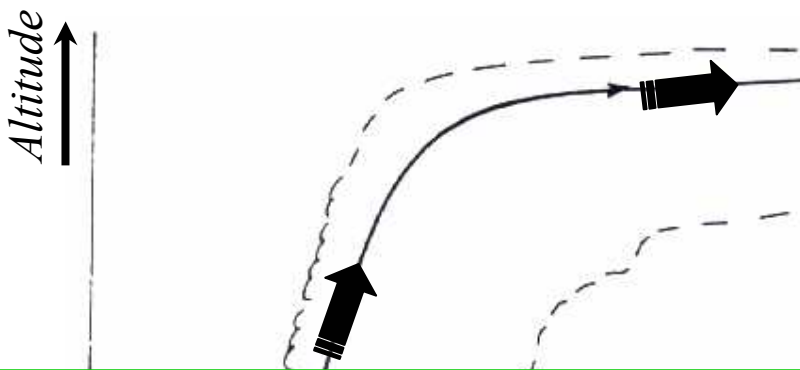
Cette dépression centrale (D) est due à la présence d'air chaud en altitude ;

→ EQUILIBRE DU VENT THERMIQUE



# LE CYCLONE VU COMME UNE MACHINE THERMIQUE :

## Le « Cycle de Carnot » équivalent [ Emanuel, 1986 : *J. Atmos. Sci.*, 43, 585-604 ]



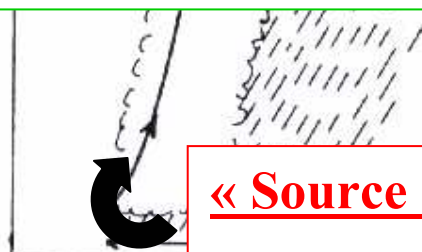
### Dans le Mur de l 'Œil :

$$\theta_{E1} > \theta_{E0} \text{ et } M_1 < M_0$$

Humidité de l 'air → Chaleur + Précip.

$D < 100 \text{ km} : 10 \text{ cm/jour} \Leftrightarrow 3000 \text{ W/m}^2$

[ 1 cyclone  $\approx 2500$  centrales nucléaires ]



### « Source Chaude » à $T=T_{OCEAN}$

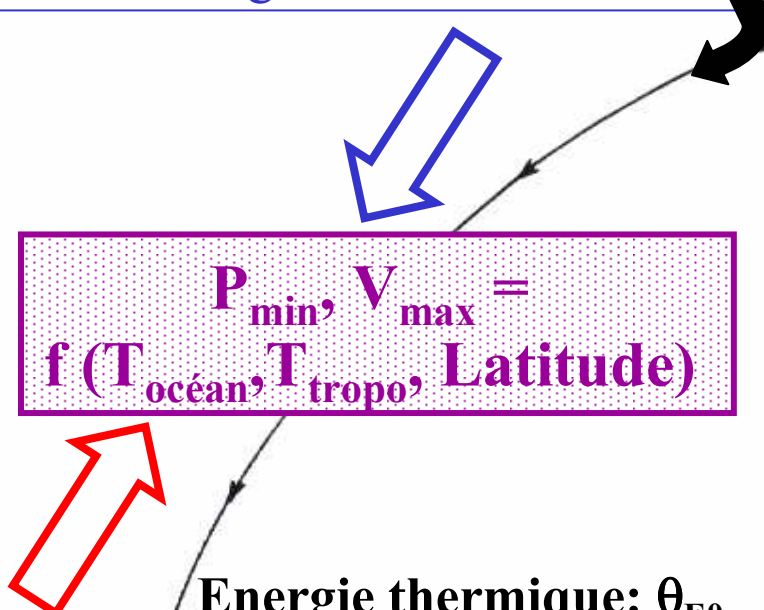
Flux d 'humidité  $\Rightarrow \theta_E \uparrow$

Frottement sur la surface  $\Rightarrow M \downarrow$

### « Source Froide » à $T=T_{TROPO}$

Rayonnement infrarouge  $\Rightarrow \theta_E \downarrow$

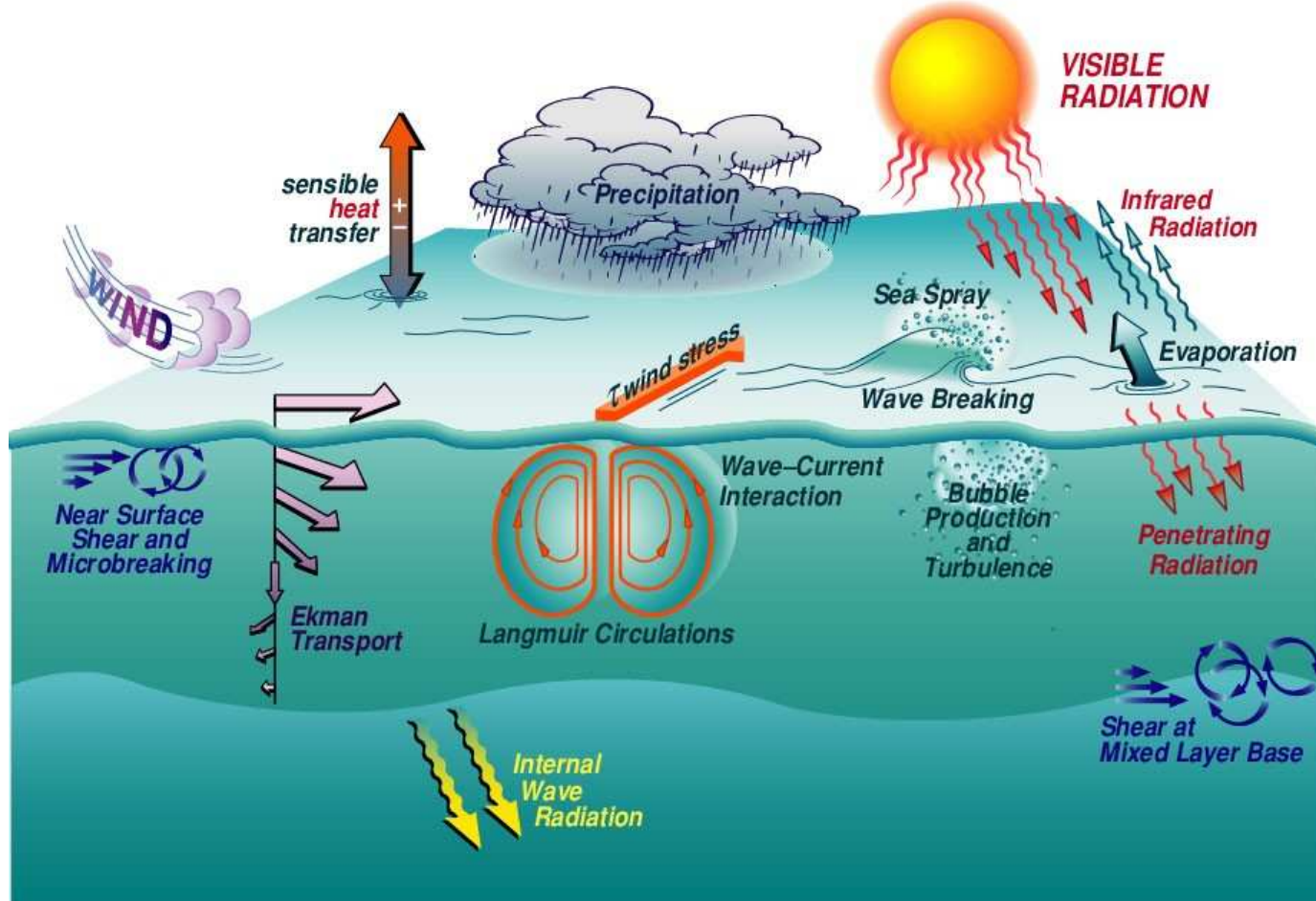
Circulation de grande échelle  $\Rightarrow M \uparrow$



Energie thermique:  $\theta_{E0}$   
Moment angulaire:  $M_0$

Distance au centre

# LE CYCLONE VU COMME UNE MACHINE THERMIQUE : Les interactions océan-atmosphère (1)



**CBLAST (Coupled Boundary Layers Air-Sea Transfer, 2003-04) :**  
améliorer notre compréhension des processus contrôlant les flux océan-atmosphère en conditions cycloniques avec vents forts, houles, embruns et circulations de couche limite

# LE CYCLONE VU COMME UNE MACHINE THERMIQUE :

## Les interactions océan-atmosphère (2)

Les flux de chaleur et d'humidité à la surface de l'océan représentent une source d'énergie pour la circulation atmosphérique.  
Réciproquement, le frottement du vent transfère de l'énergie vers l'océan en générant des vagues et des courants plus ou moins profonds.

La formulation « bulk » exprime ces flux en fonction des paramètres moyens de la circulation et de coefficients de transfert :

Flux de chaleur sensible :

$$Q_S = \rho C_S |\underline{V}_{air}| C_P (\theta_{surf} - \theta_{air})$$

Flux de chaleur latente :

$$Q_L = \rho C_L |\underline{V}_{air}| L (q_{surf} - q_{air})$$

[ Flux d'enthalpie :  $Q_E = Q_S + Q_L$  ]

Flux de quantité de mouvement (i) :  $Q_{Vi} = \rho C_D |\underline{V}_{air}| (V_{i,air})$

(  $\rho$  = densité de l'air,  $|\underline{V}_{air}|$  = module du vent horizontal,  $\theta$  = température,  $q$  = rapport de mélange,  $C_p$  = chaleur spécifique à P cste ,  $L$  = chaleur latente de vaporisation )

$C_S$  = nb de Stanton,  $C_L$  = nb de Dalton,  $C_D$  = coeff. de frottement

# LE CYCLONE VU COMME UNE MACHINE THERMIQUE : Les interactions océan-atmosphère (3)

CBLAST Hurricane Component (2003 & 2004) : mesures in situ et télédétection par avion + observations de surface et de sub-surface avec des bouées et instruments largués

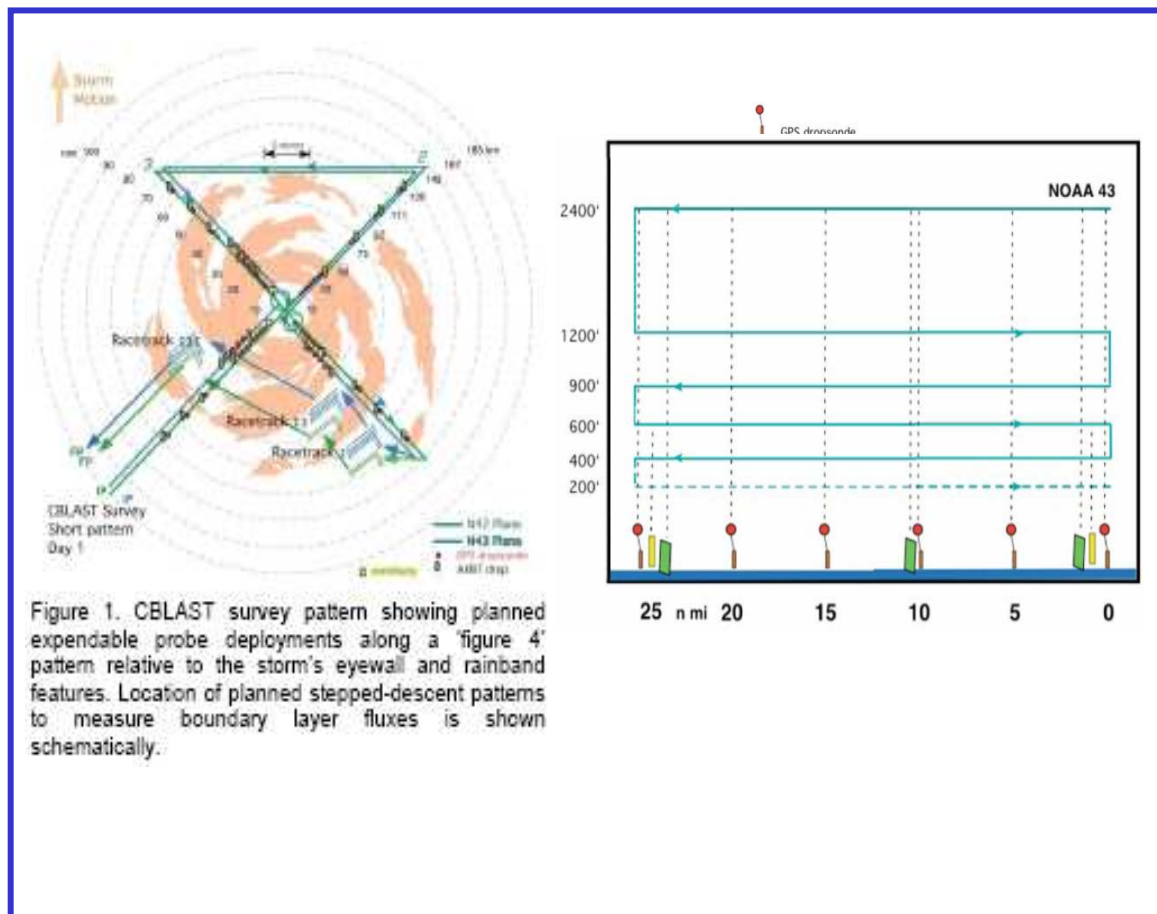


Figure 1. CBLAST survey pattern showing planned expendable probe deployments along a 'figure 4' pattern relative to the storm's eyewall and rainband features. Location of planned stepped-descent patterns to measure boundary layer fluxes is shown schematically.

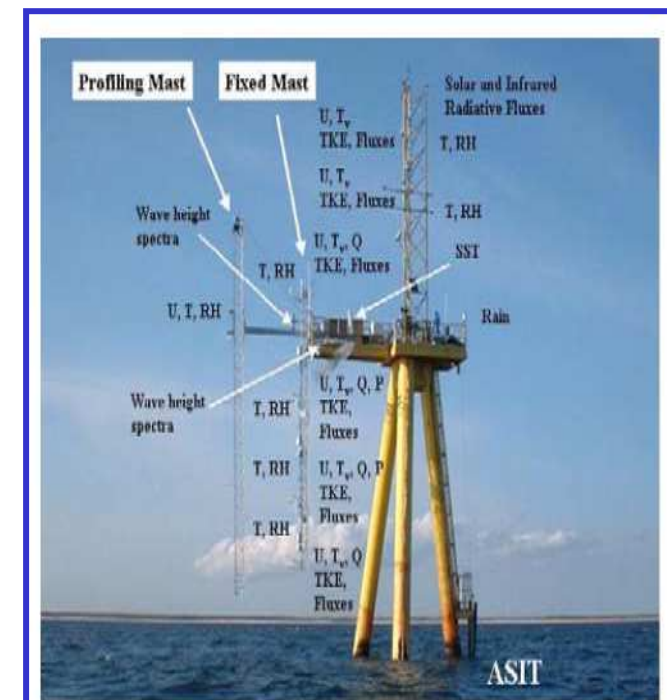
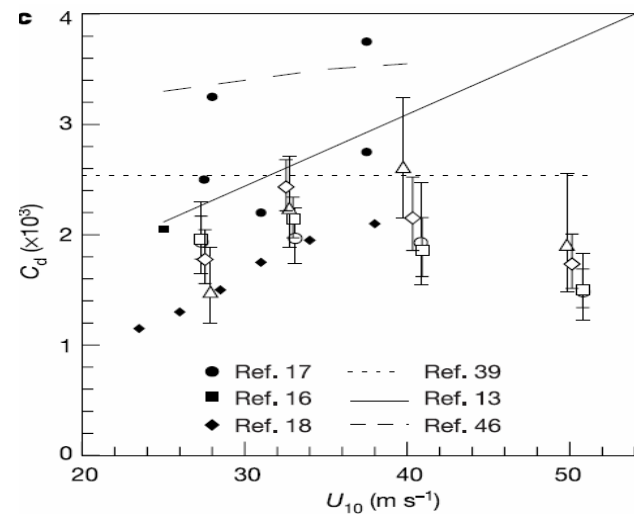


Figure 2. Experiment setup for the ASIT during CBLAST. The photo indicates where variables were measured on the met tower, fixed array, and profiling mast. The solar and infrared radiometers were measured 22-m above mean sea level.

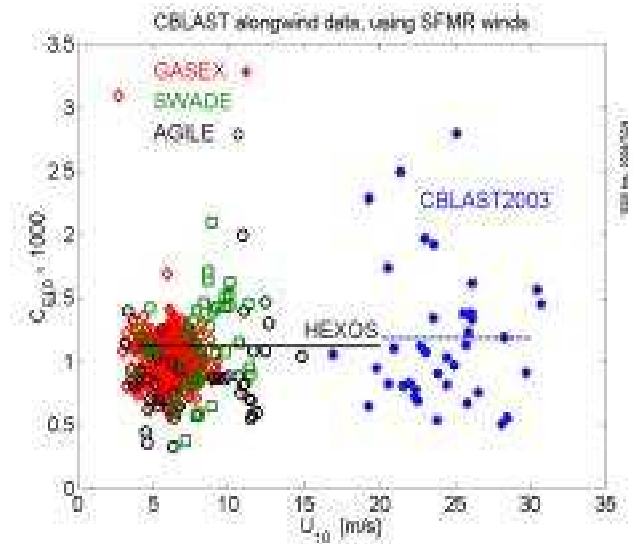
# LE CYCLONE VU COMME UNE MACHINE THERMIQUE : Les interactions océan-atmosphère (4)

[ Powell *et al.* 2003 : *Nature*, 422, 279-283 ]

Le coefficent de frottement turbulent  $C_d$  atteint un maximum pour un vent de 40 m/s et *semble diminuer lentement au-delà* ?



Le coefficent d'échange d'enthalpie  $C_e$  est constant pour des vents  $\leq 30 \text{ m/s}$ .  
Il pourrait augmenter au-delà de 50 m/s, en relation avec les embruns, les interactions entre houles, les circulations organisées dans la couche limite ?



# LE CYCLONE VU COMME UNE MACHINE THERMIQUE : Les interactions océan-atmosphère (5)

Black *et al.* 2007:  
*Bull. Amer. Meteor. Soc.*, **88**, 357-374

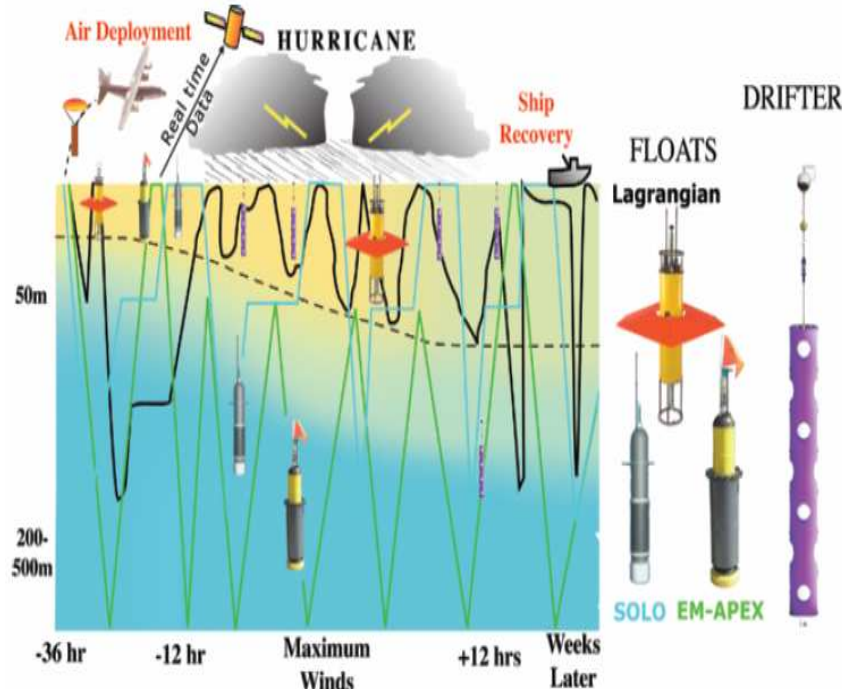


Fig. 13. Drawings of the three varieties of floats and a surface drifter as deployed into Hurricane Frances. Schematic depicts operations in Hurricane Frances (2004).

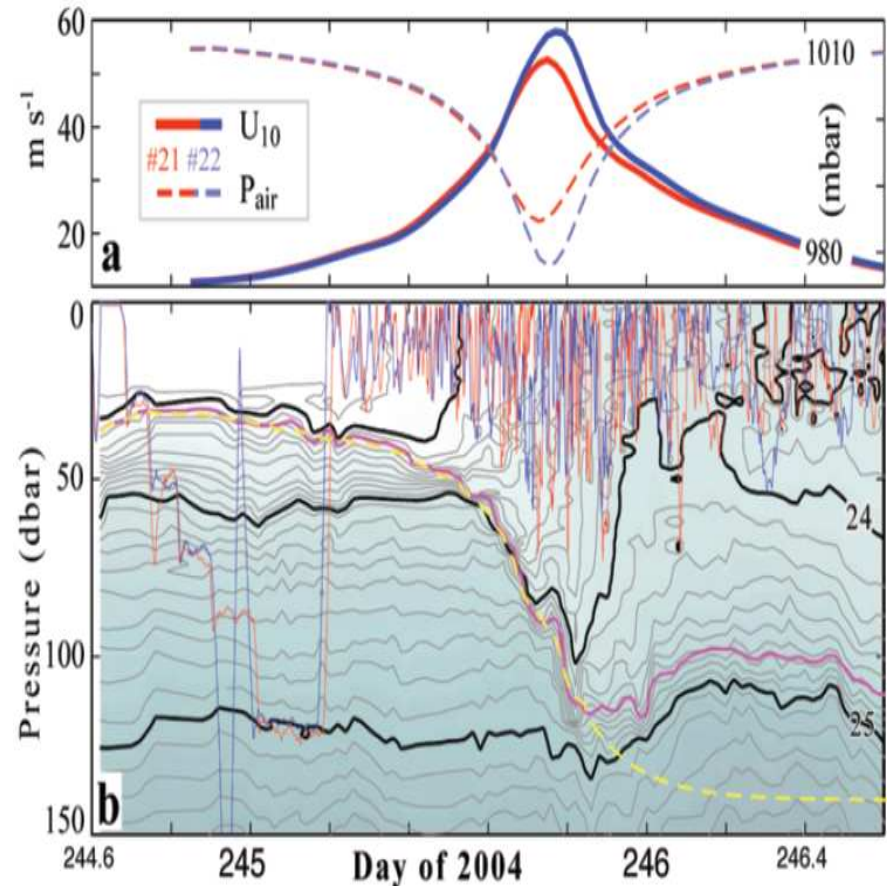
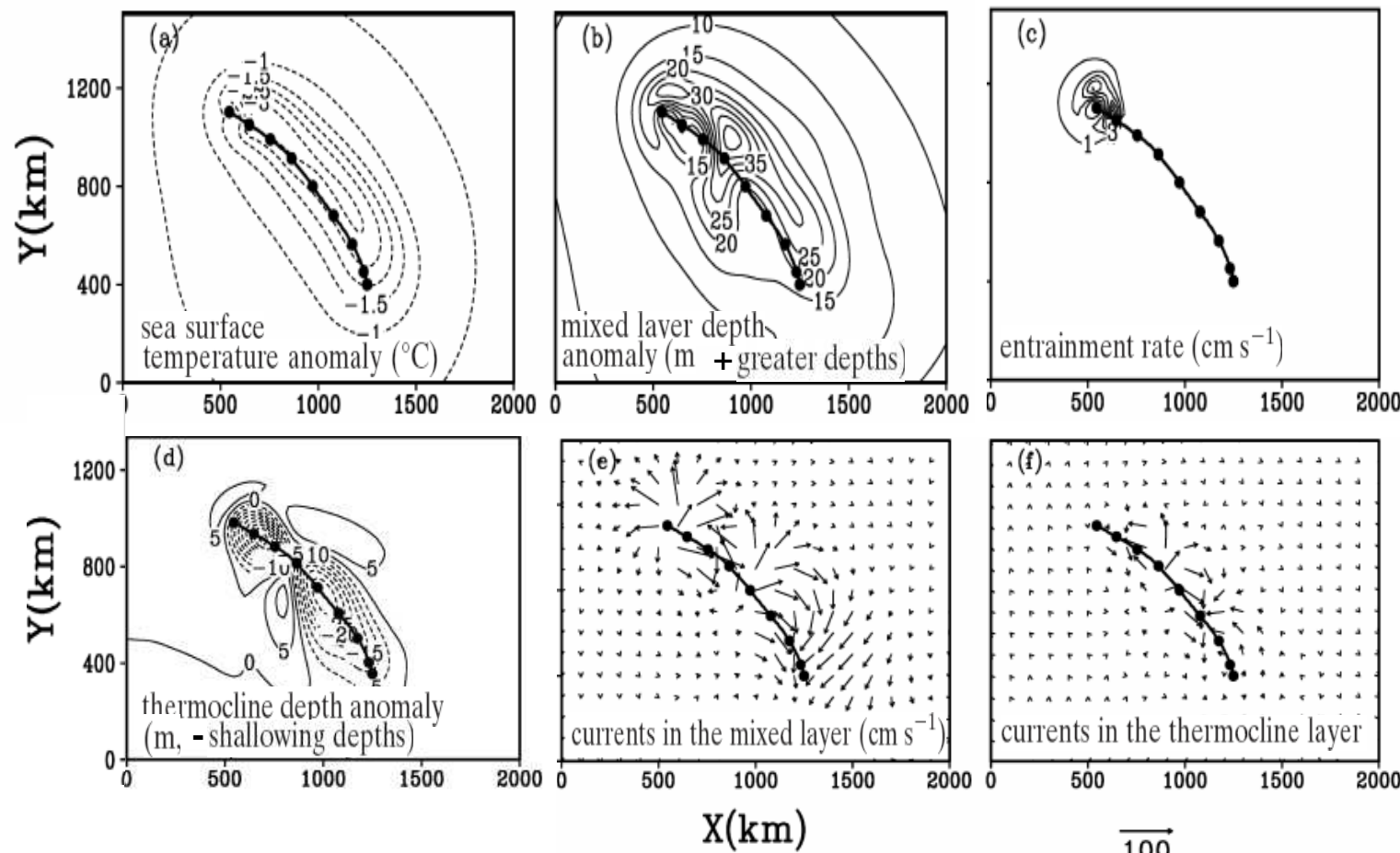


Fig. 16. Evolution of the density structure of the upper ocean near the radius of maximum winds of Hurricane Frances. (a) Wind speed and atmospheric pressure from HRD H\*WIND analysis at the two Lagrangian floats. (b) Potential density contours ( $kg m^{-3}$ ; in black), trajectories of Lagrangian floats (red and blue), measured depth of the mixed layer (magenta), and estimated depth of the mixed layer from a vertical heat budget (yellow, dashed).

# LE CYCLONE VU COMME UNE MACHINE THERMIQUE : Les interactions océan-atmosphère (6)

Wu *et al.* 2005 : *Mon. Wea. Rev.*, 133, 3299-3314

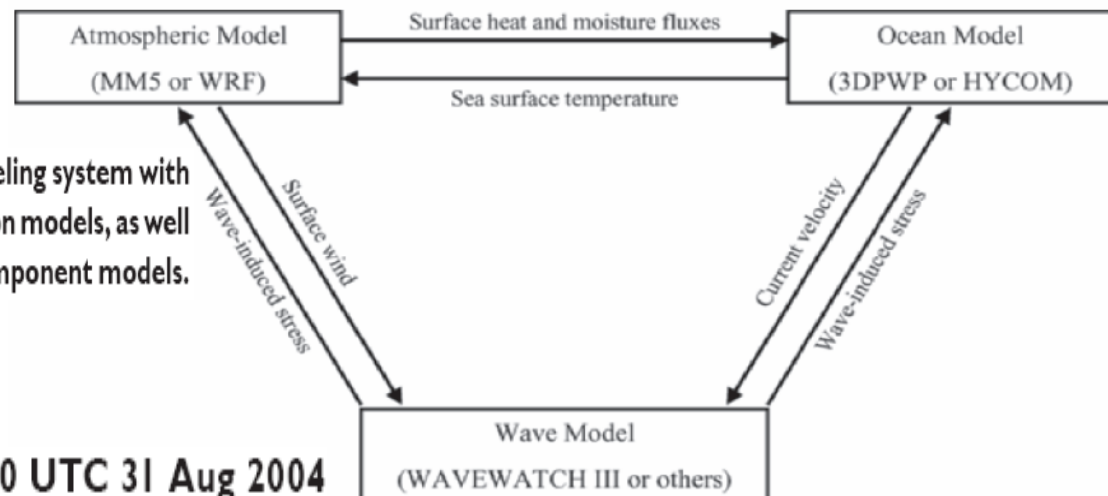


100

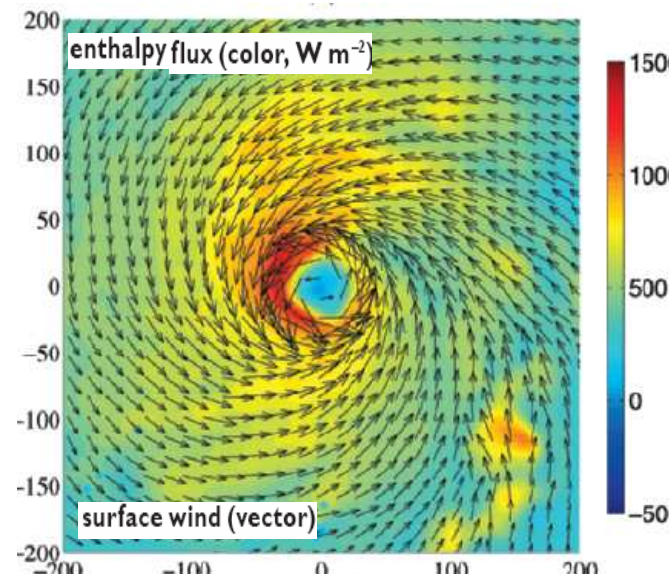
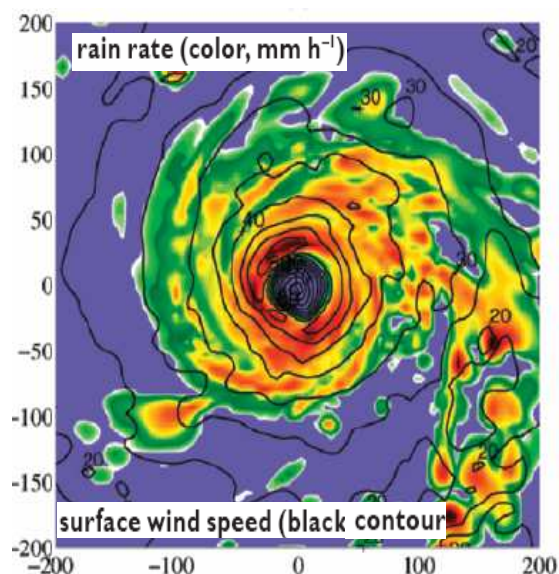
# LE CYCLONE VU COMME UNE MACHINE THERMIQUE : Les interactions océan-atmosphère (7)

Chen et al. 2007 : Bull. Amer. Meteor. Soc., 88, 311-317

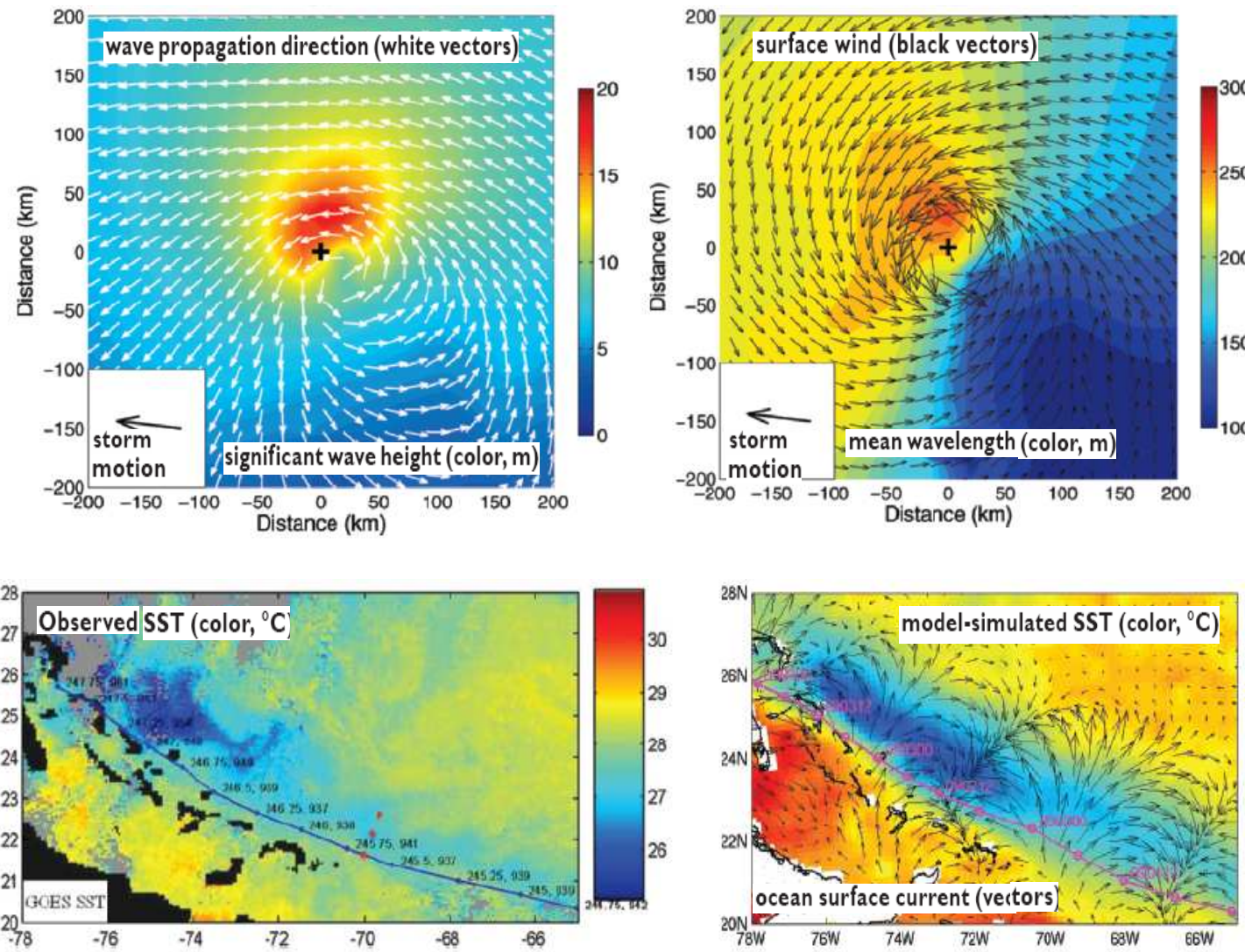
FIG. 1. Schematics of a coupled atmosphere-wave-ocean modeling system with the component atmosphere, surface wave, and ocean circulation models, as well as the coupling parameter exchanges between each of the component models.



Hurricane Frances at 1200 UTC 31 Aug 2004

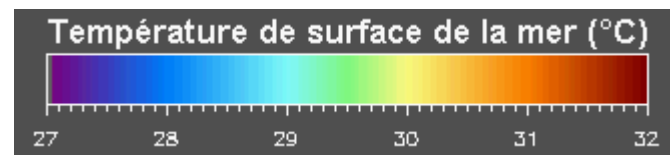
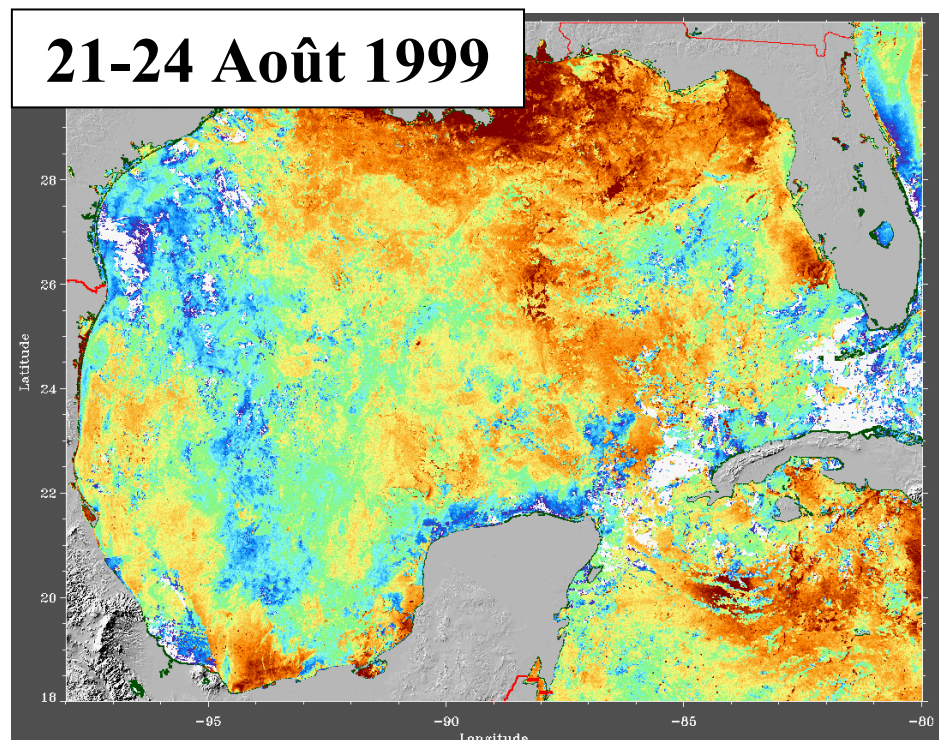
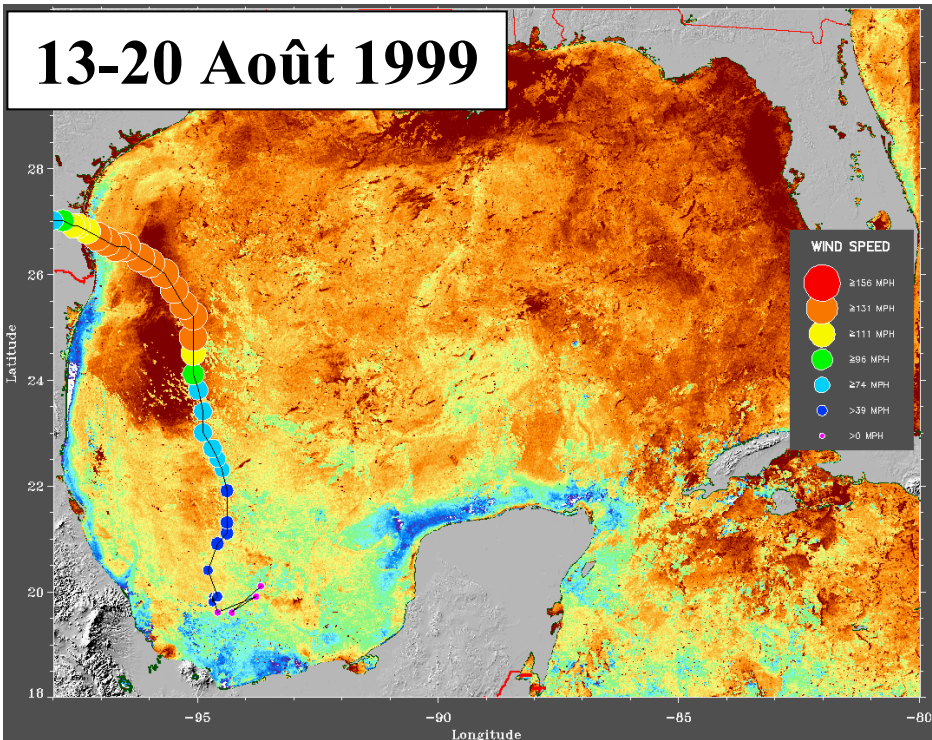


# LE CYCLONE VU COMME UNE MACHINE THERMIQUE : Les interactions océan-atmosphère (8)



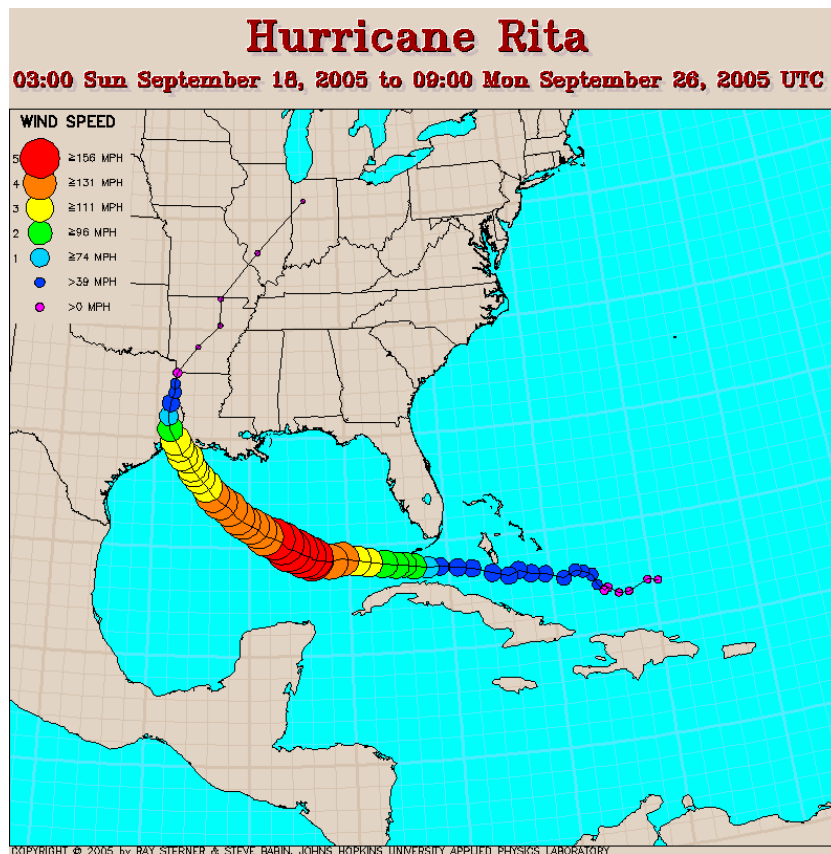
# LE CYCLONE VU COMME UNE MACHINE THERMIQUE : Pompage de la chaleur océanique (1)

## Hurricane Bret

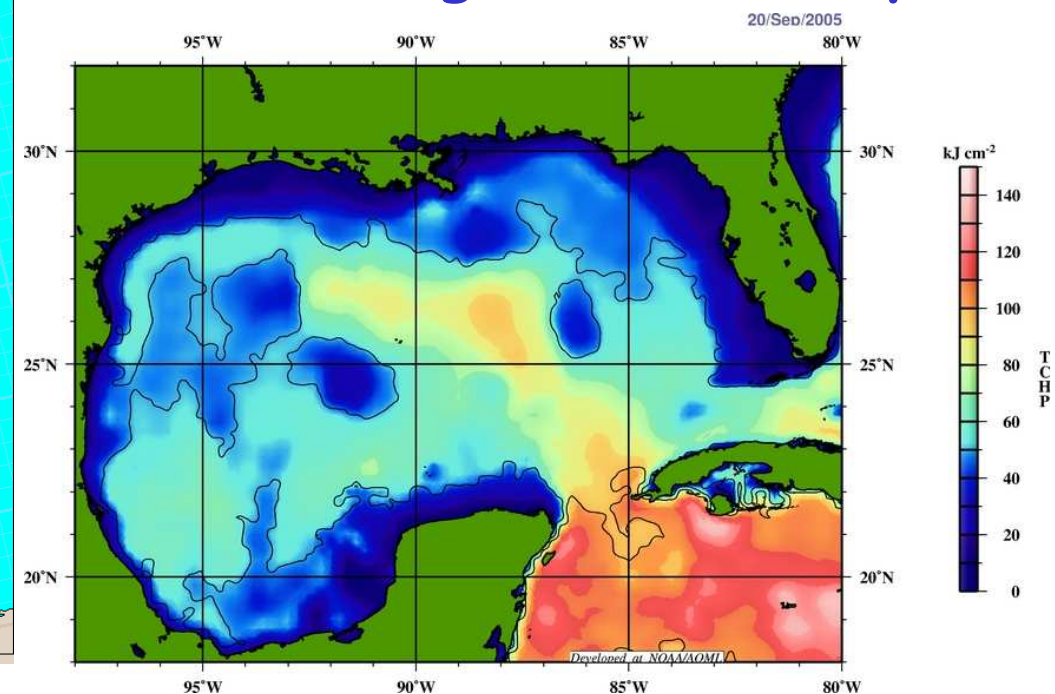


# LE CYCLONE VU COMME UNE MACHINE THERMIQUE : Pompage de la chaleur océanique (2)

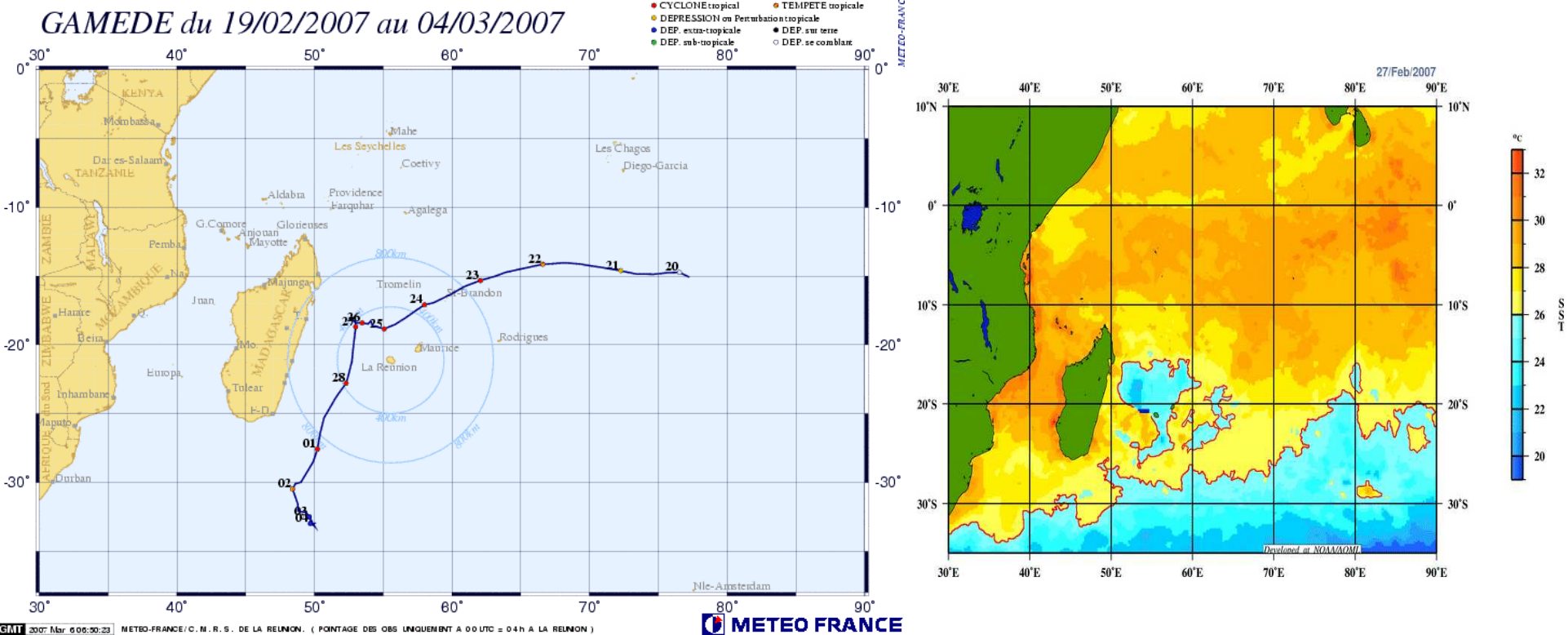
Diminution d'intensité de Rita  
avant l'arrivée sur la côte texane



Diminution de l'énergie  
thermique disponible  
dans le golfe du Mexique

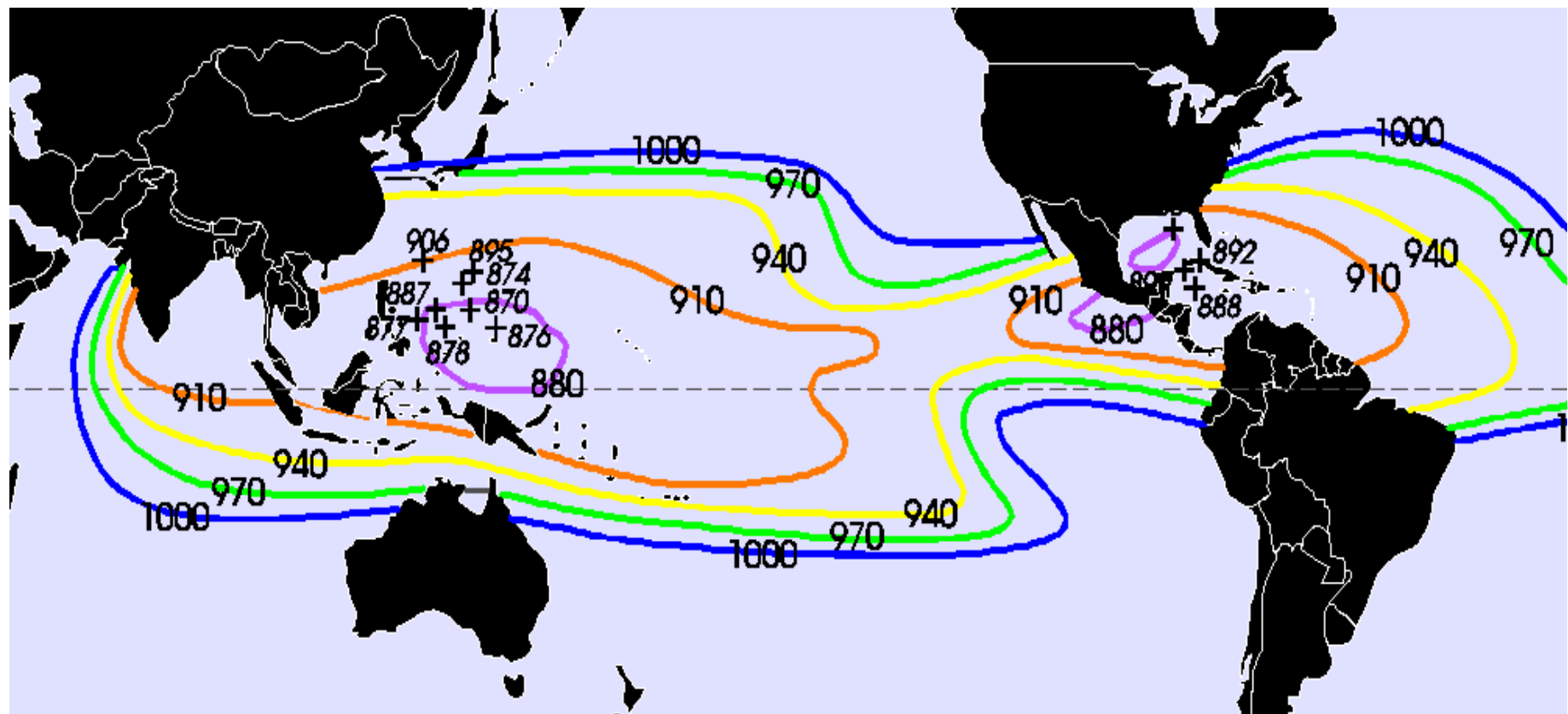


# LE CYCLONE VU COMME UNE MACHINE THERMIQUE : Pompage de la chaleur océanique (3)

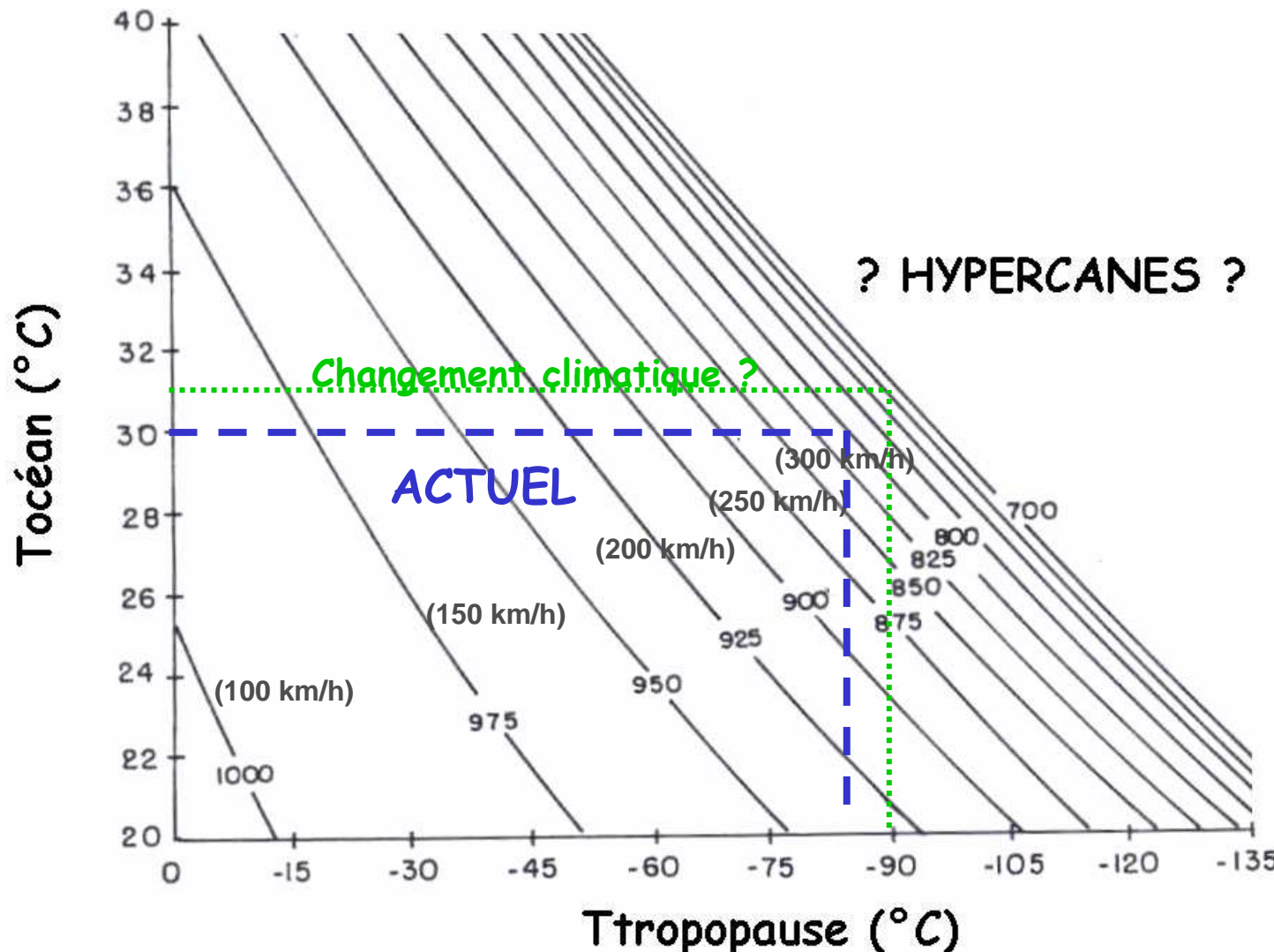


# LE CYCLONE VU COMME UNE MACHINE THERMIQUE : Intensité Maximum Potentielle « climatologique »

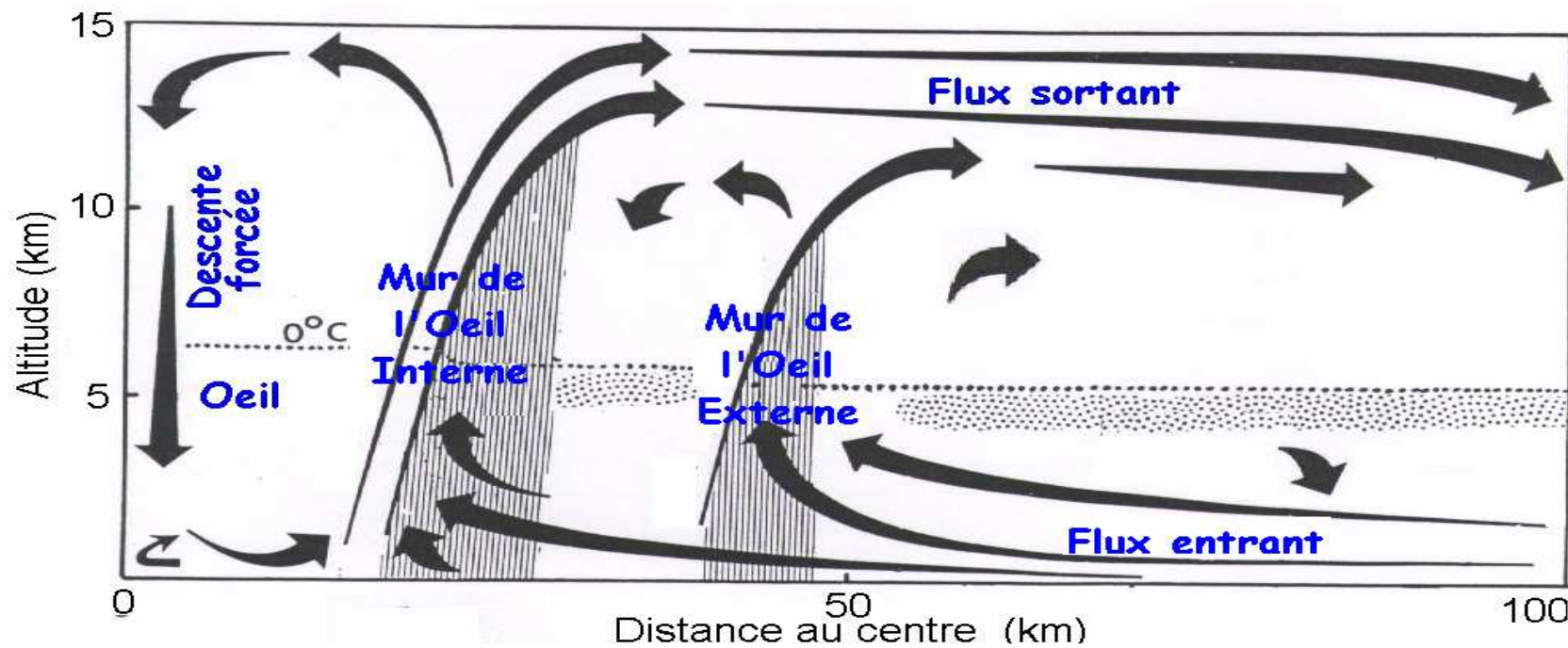
$$P_{\min}, V_{\max} = \\ f(T_{\text{ocean}}, T_{\text{tropo}}, \text{Latitude})$$



# LE CYCLONE VU COMME UNE MACHINE THERMIQUE : Intensité Maximum Potentielle (Pression mini, Vent maxi ) (latitude = 20°)

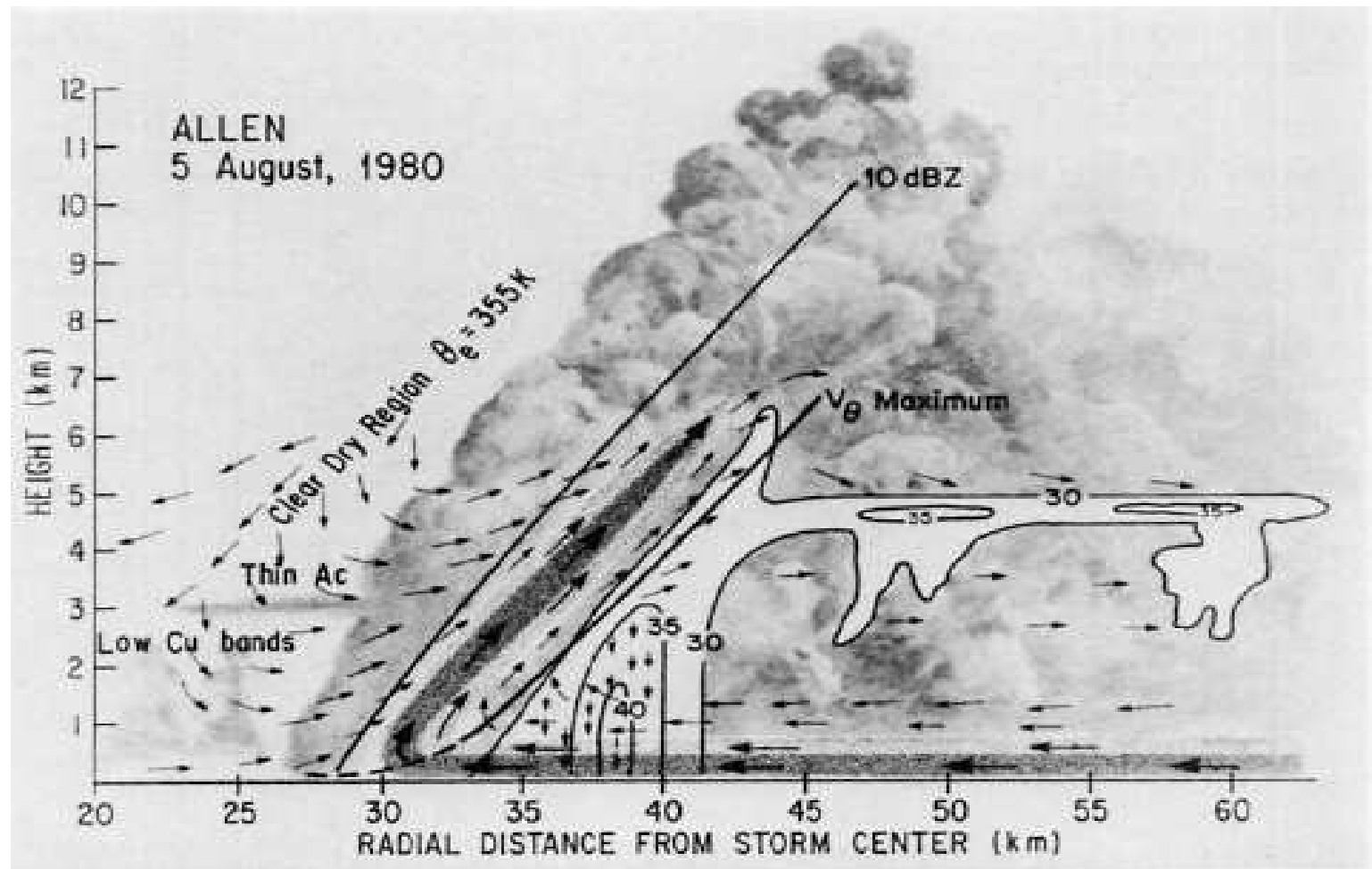


# LA CIRCULATION SECONDAIRE



# LA CIRCULATION SECONDAIRE observations (1)

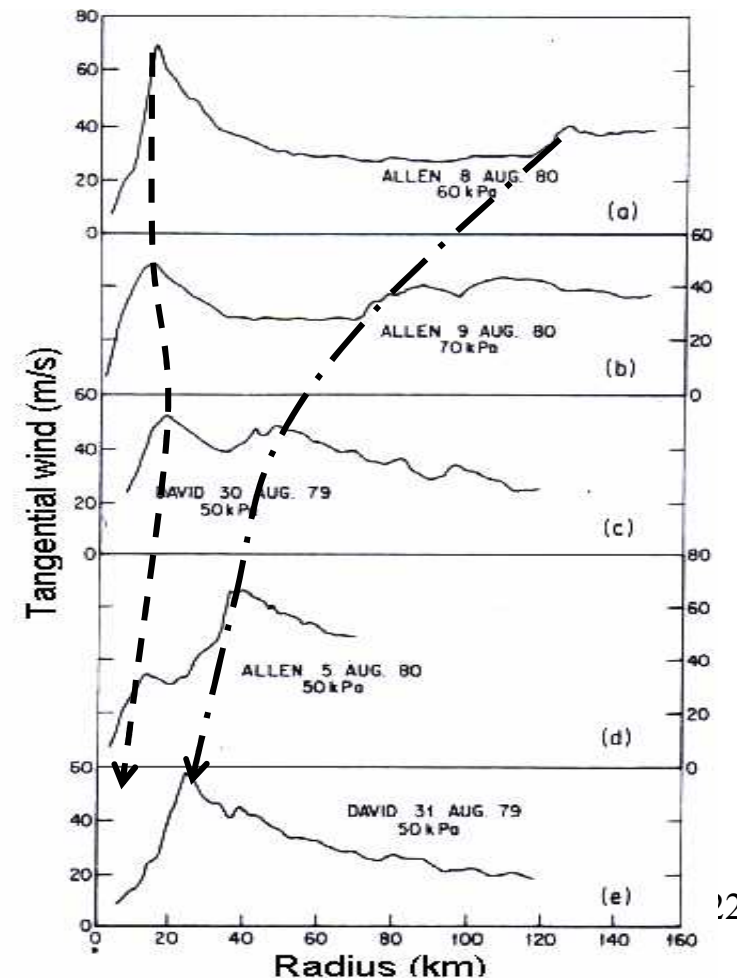
Jorgensen, 1984 [ *J. Atmos. Sci.*, 41, 1287-1311 ] :  
a conceptual model for the inner core of Hurricane Allen (1980)



# LA CIRCULATION SECONDAIRE observations (2)

Willoughby *et al.*, 1982 [ *J. Atmos. Sci.*, 39, 395-411 ] :  
a mechanism for the formation of concentric eyewalls

An illustration of the concentric eye cycle  
made up from individual profiles in  
Hurricanes David (1979) and Allen (1980)

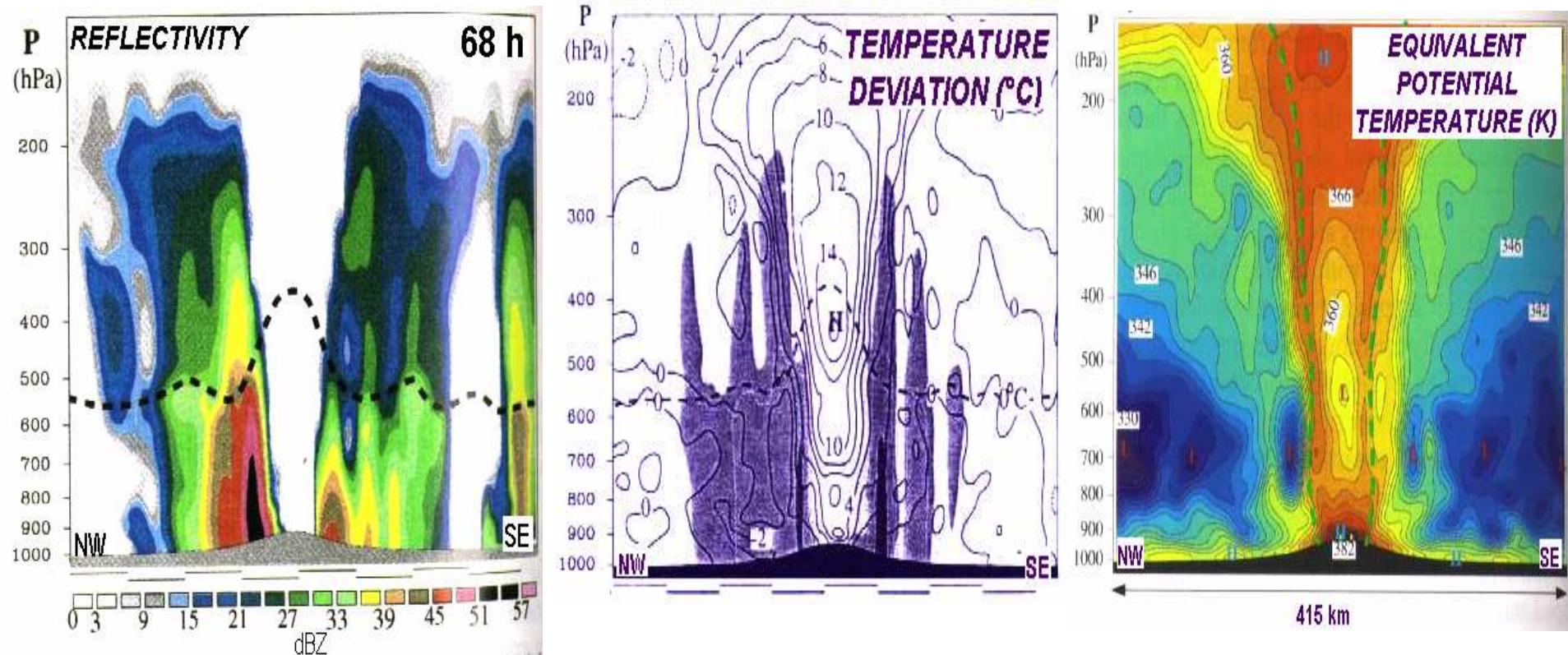


# LA CIRCULATION SECONDAIRE

## modélisation (1)

Liu *et al.*, 1997 [ *Mon. Wea. Rev.*, 125, 3073-3093 ]

Many simulated kinematics, thermodynamics and microphysics structures in the simulated core region compare favorably to previous observations of hurricanes.



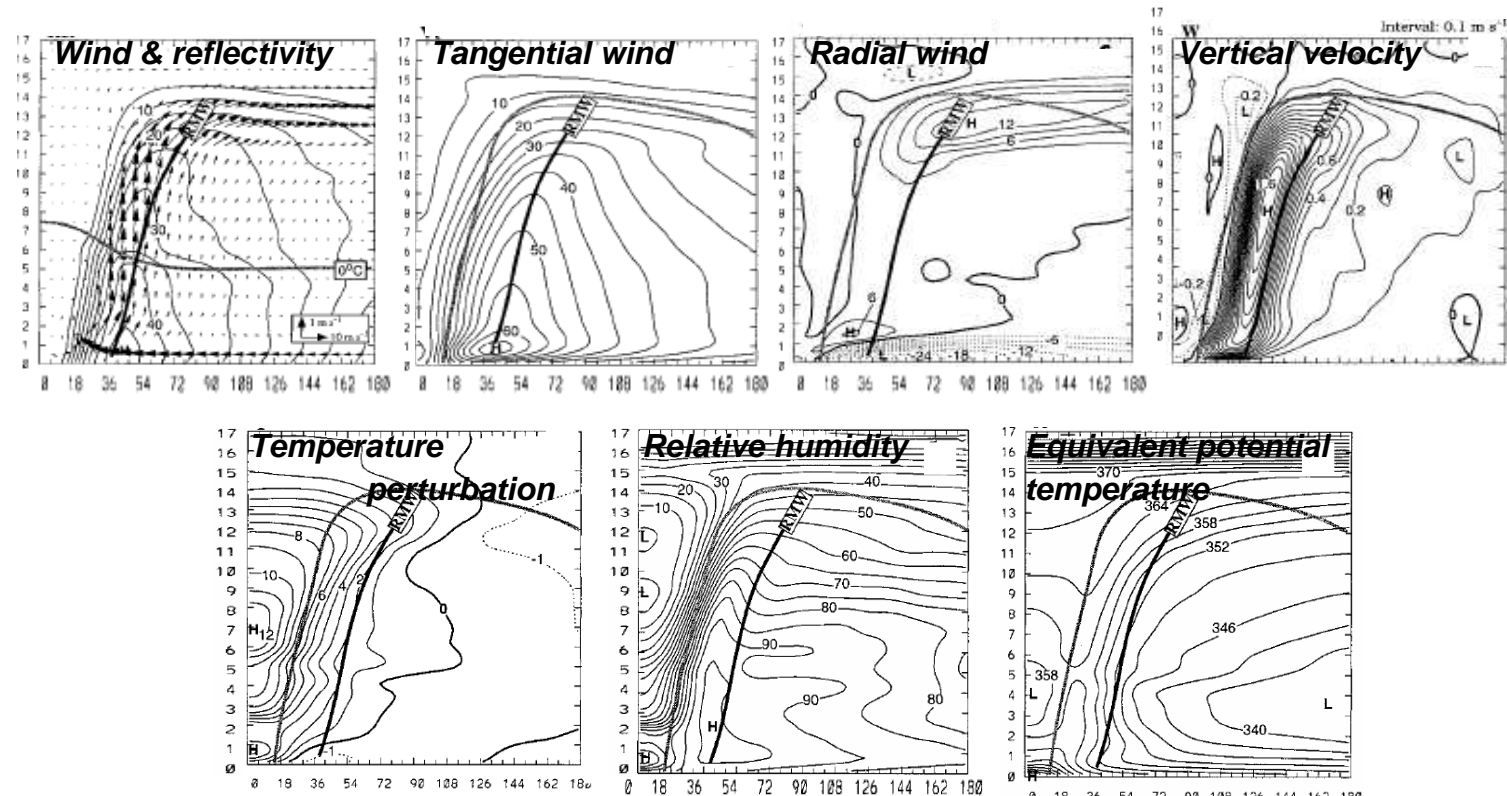
# LA CIRCULATION SECONDAIRE

## modélisation (2)

Liu *et al.*, 1999 [ *Mon. Wea. Rev.*, 127, 2597-2616 ]

Axisymmetric structure of the storm (6-km horizontal grid) :

- moist inflow (outflow) in the boundary layer (upper troposphere) and slantwise ascent in the eyewall where the tangential wind is maximum ;
- penetrative dry downdraft at the inner edge of the eyewall ;
- weak subsiding motion in the eye with warming/drying above an inversion, below, warm/moist air coming from the low-level inflow and downdraft.



# LA CIRCULATION SECONDAIRE

## modélisation (3)

Zhang *et al.*, 2000 [ *Mon. Wea. Rev.*, 128, 3772-3788 ]

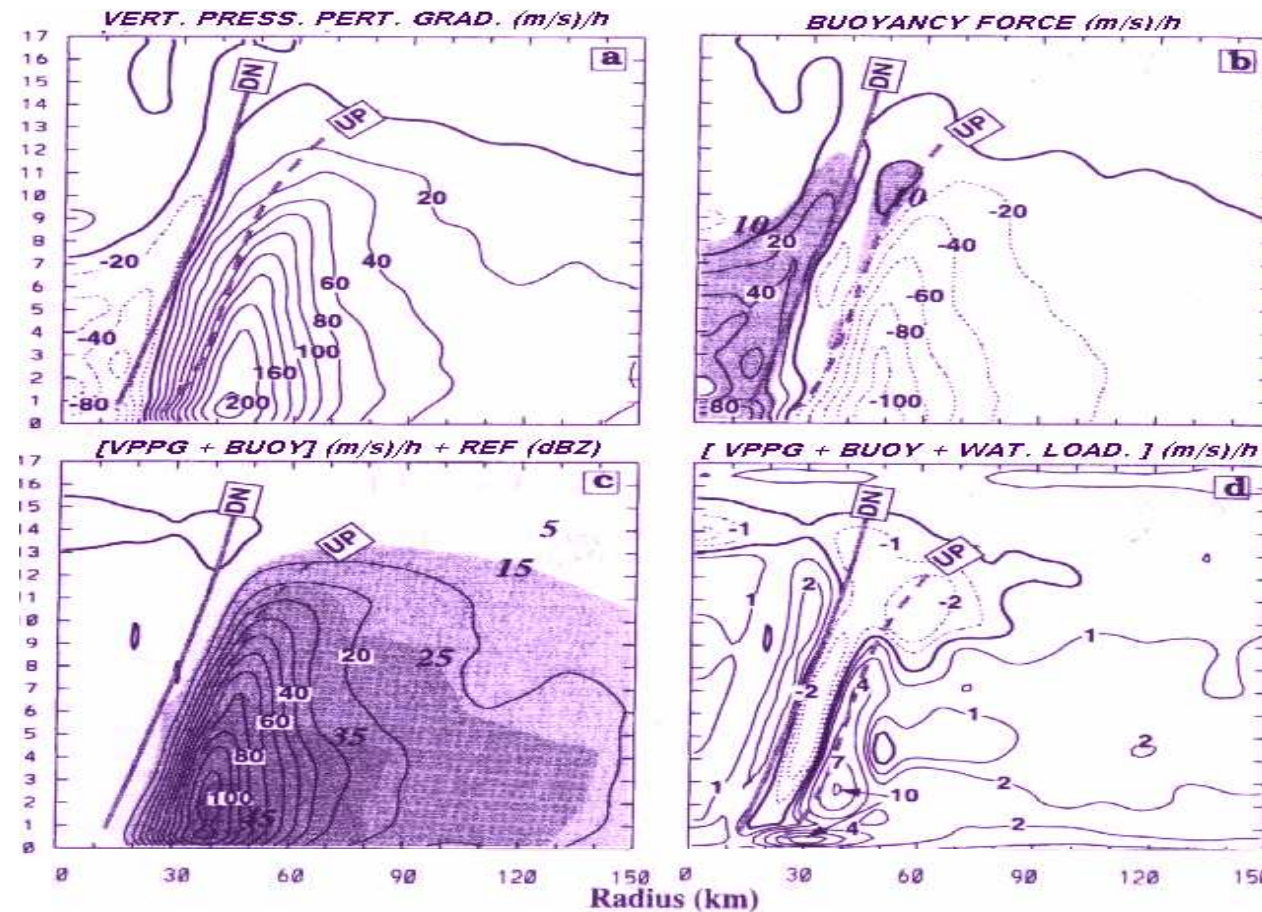
analysis of the vertical momentum budget in the inner-core region :  
vertical acceleration in the eyewall is a small difference between  
vertical pressure gradient force, buoyancy and water loading.

$$\underbrace{\frac{Dw}{Dt}}_{\text{total tendency}} = \underbrace{\frac{\partial w}{\partial t}}_{\text{local tendency}} + \underbrace{(V \cdot \nabla) w}_{\text{total advection}} = \underbrace{-D(w)}_{\text{turbulent diffusion}} - C_p \theta_{v0} \underbrace{\frac{\partial \pi_1}{\partial z}}_{\text{vertical pressure perturbation gradient force}} + g \underbrace{\frac{\theta_{v1}}{\theta_0}}_{\text{thermal buoyancy}} - \underbrace{g q_p}_{\text{liquid+ice water loading}}$$

# LA CIRCULATION SECONDAIRE

## modélisation (3)

Zhang *et al.*, 2000 [ *Mon. Wea. Rev.*, 128, 3772-3788 ]  
analysis of the vertical momentum budget in the inner-core region :  
vertical acceleration in the eyewall is a small difference between  
vertical pressure gradient force, buoyancy and water loading.



# LA CIRCULATION SECONDAIRE

## modélisation (4)

*Zhang et al. 2001 [ Mon. Wea. Rev., 129, 92-107 ]*

validity of the « thermal wind balance » : « supergradient » flows and accelerations are well organized from the bottom of the eye center to the upper outflow layer in the eyewall.

$$\underbrace{\frac{Du}{Dt}}_{\substack{\text{total} \\ \text{tendency}}} = \underbrace{\frac{\partial u}{\partial t}}_{\substack{\text{local} \\ \text{tendency}}} + \underbrace{(V \cdot \nabla) u}_{\substack{\text{total} \\ \text{advection}}} = \underbrace{-D(u)}_{\substack{\text{turbulent} \\ \text{diffusion}}} - C_p \theta_{v0} \underbrace{\frac{\partial \pi_1}{\partial r}}_{\substack{\text{radial} \\ \text{pressure} \\ \text{perturbation} \\ \text{gradient} \\ \text{force}}} + \underbrace{\frac{v^2}{r}}_{\substack{\text{centrifugal} \\ \text{force}}} + \underbrace{fv}_{\substack{\text{Coriolis} \\ \text{force}}}$$

$u$  = radial wind component ;  $v$  = tangential wind component

super-gradient wind :

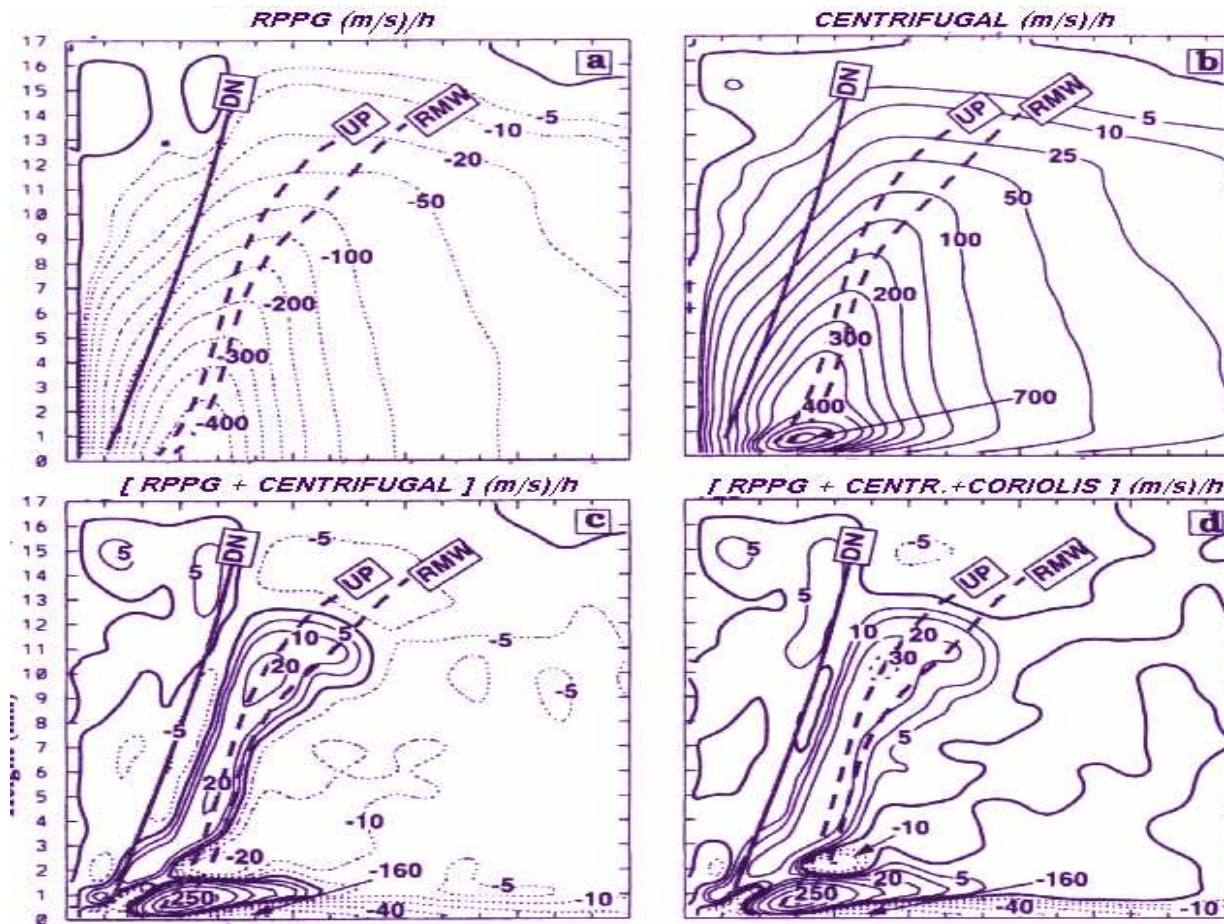
when "centrifugal + Coriolis" forces > "rad. press. pert. grad." force

# LA CIRCULATION SECONDAIRE

## modélisation (4)

Zhang *et al.*, 2001 [ *Mon. Wea. Rev.*, 129, 92-107 ]

validity of the « thermal wind balance » : « supergradient » flows and accelerations are well organized from the bottom of the eye center to the upper outflow layer in the eyewall.



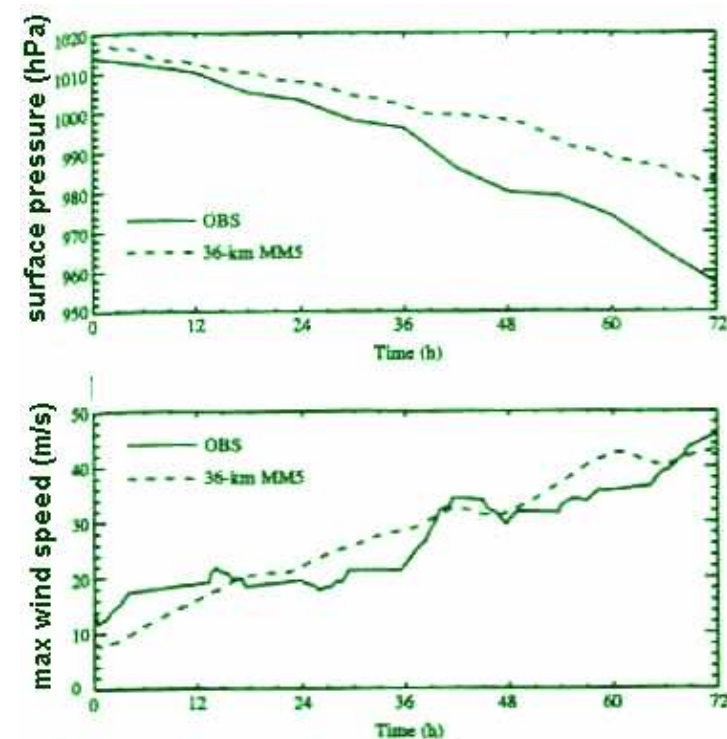
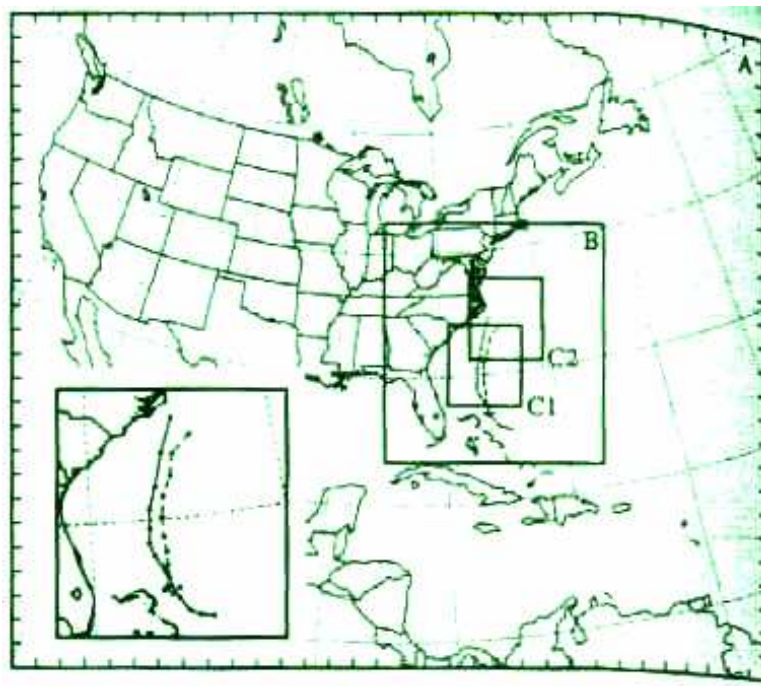
$V_T^2/r + f V_T > 1/\rho \partial p / \partial r$   
because of angular momentum conservation  
→ net outward radial force

# LA CIRCULATION SECONDAIRE

## modélisation (5)

Braun and Tao, 2000 [ *Mon. Wea. Rev.*, 128, 1573-1592 ]

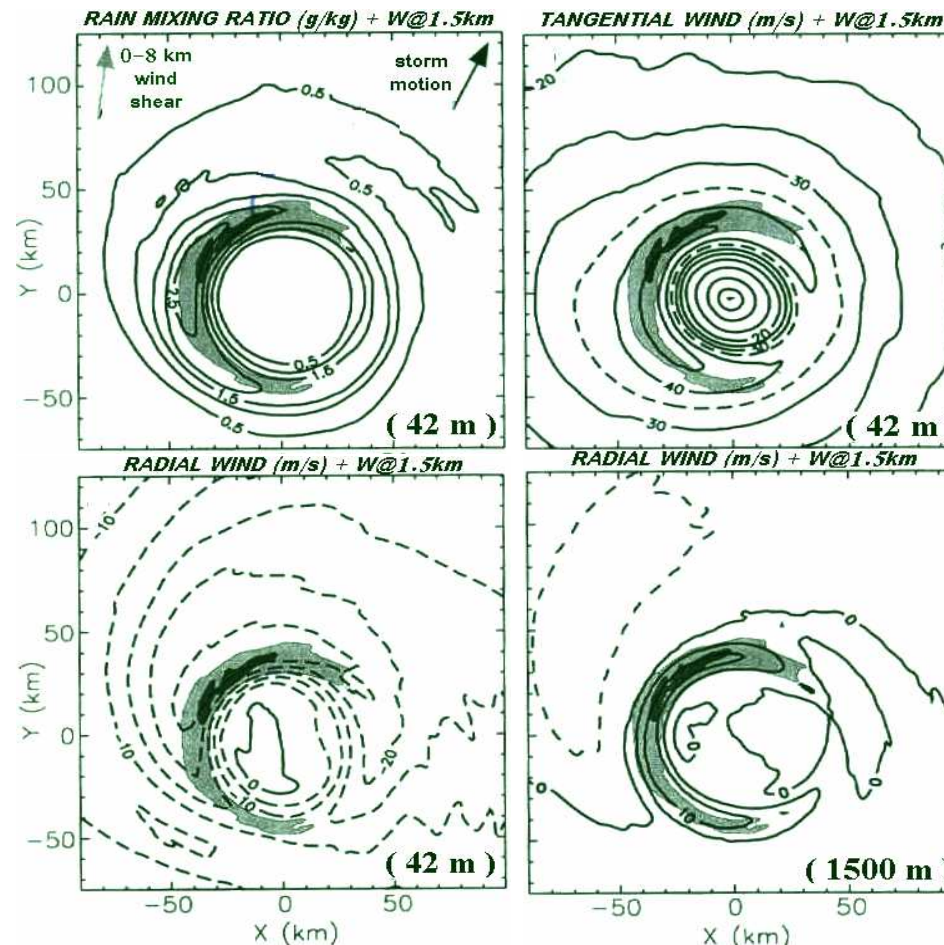
- 72-h simulation of Hurricane Bob (1991) [16 Aug 00 UTC → 19 Aug 00 UTC] using a 36-km grid **A**
- at 48 h, one-way nested 12-km grid **B** and a two-way nested 4-km grid **C** are activated (hourly boundaries from the 36-km grid)
- at 62 h ( $\langle V \rangle_{\max} = 58 \text{ ms}^{-1}$ ,  $P_{\min} = 970 \text{ hPa}$ ), a two-way nested 1.3-km grid **D** is initialized. Both 4-km and 1.3-km grids are moved with the storm



# LA CIRCULATION SECONDAIRE

## modélisation (6)

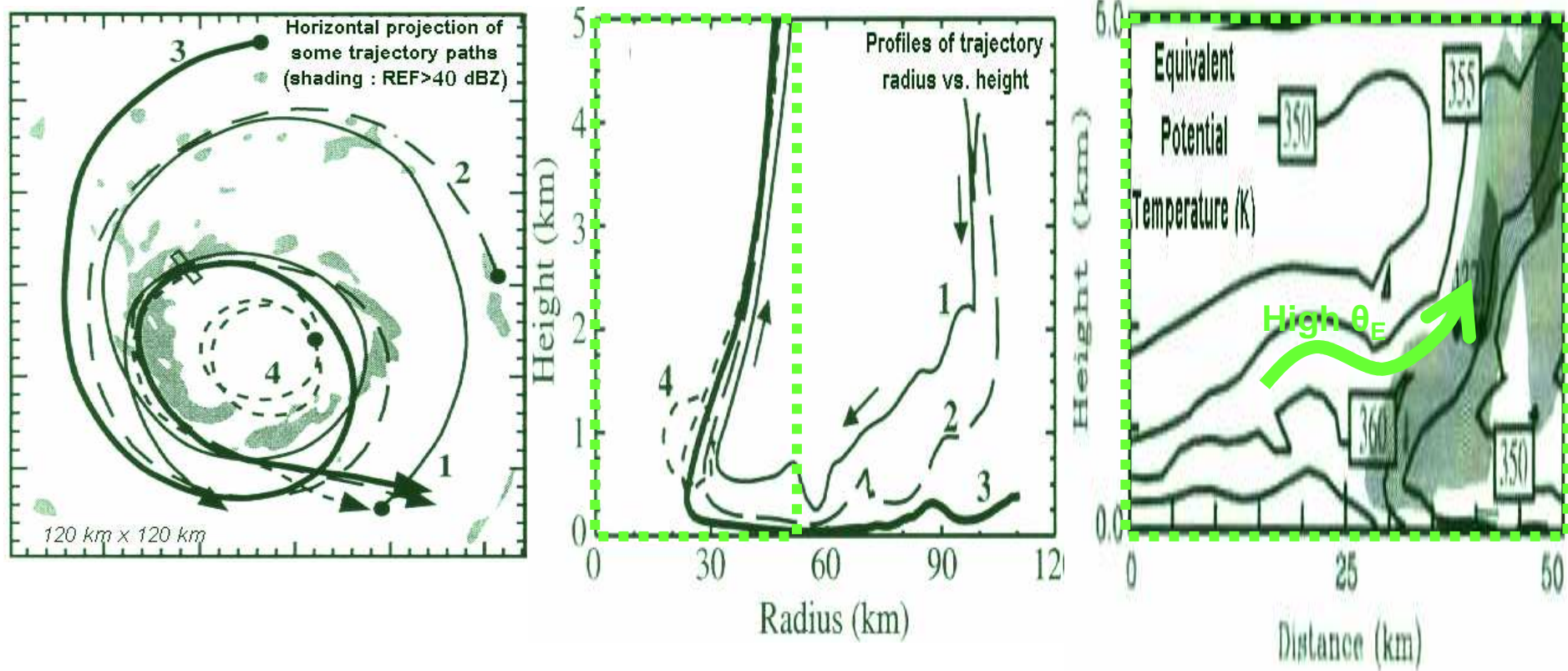
- Time-average structure of the horizontal flow is characterized by a wavenumber-1 asymmetry (relative to the nearly aligned storm motion and wind shear vector) in the low-level vertical motions, near surface tangential wind, inflow and outflow above the boundary layer



# LA CIRCULATION SECONDAIRE

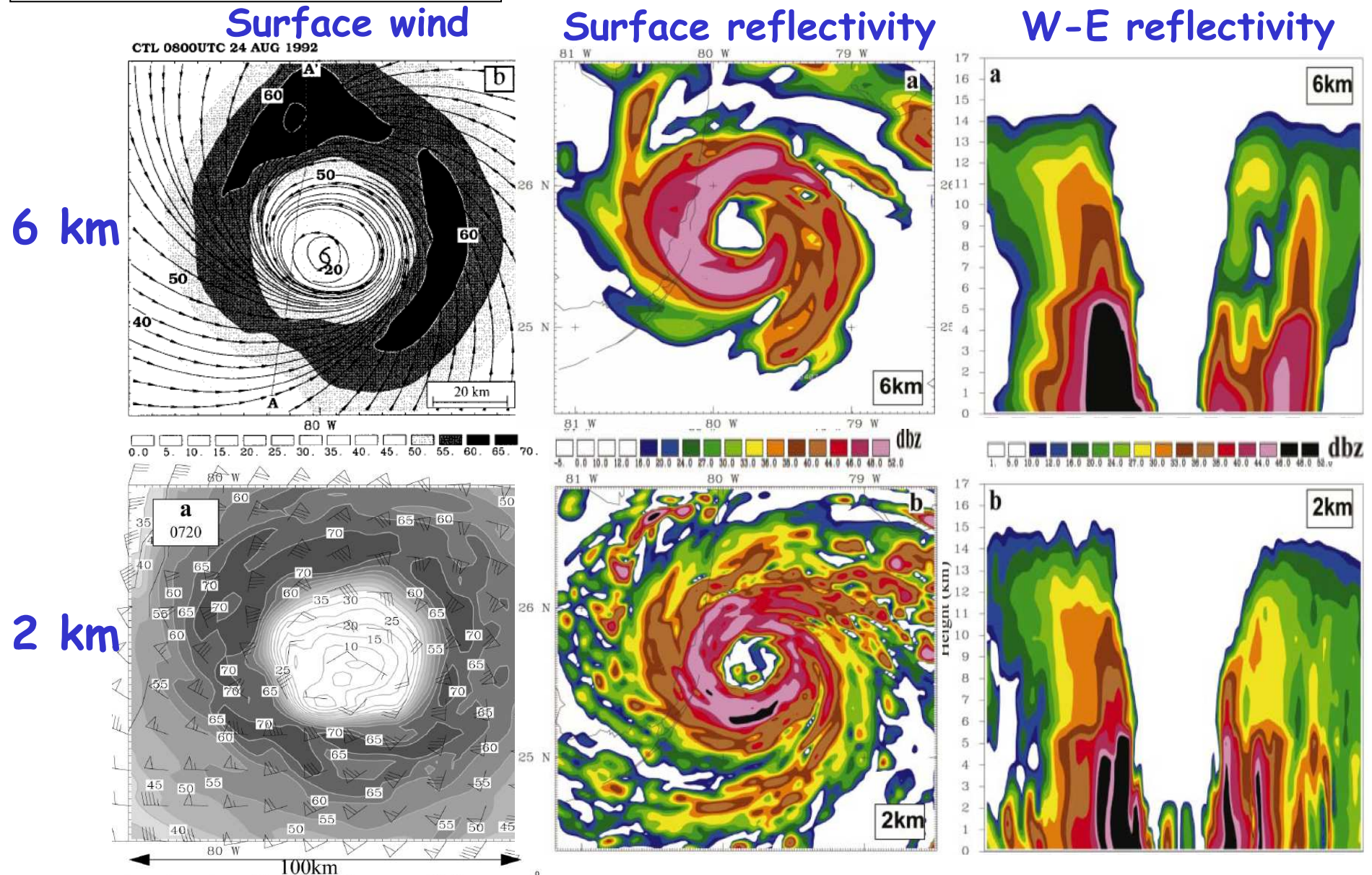
## modélisation (7)

- Some air parcels originating from outside the eyewall in the lowest part of the boundary layer penetrate furthest into the eye, then accelerate outward sharply while rising out of the boundary layer
- Occasionally high- $\theta_e$  air from the eye is drawn into the eyewall updraft, through episodic rather than continuous venting of the eye air into the eyewall

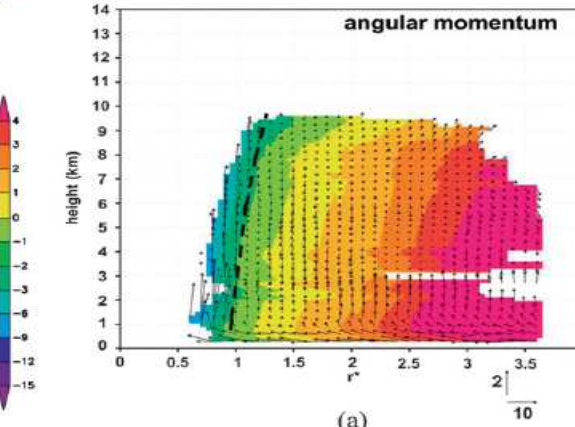
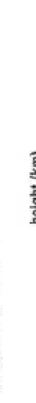
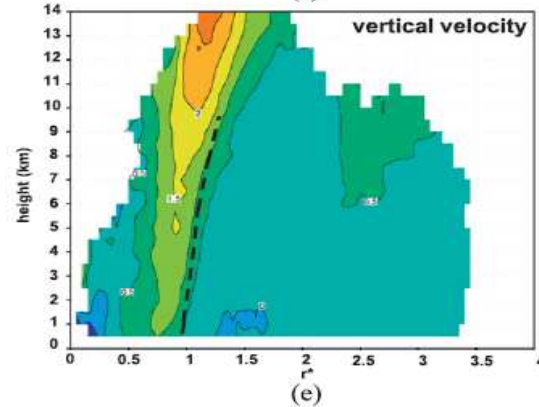
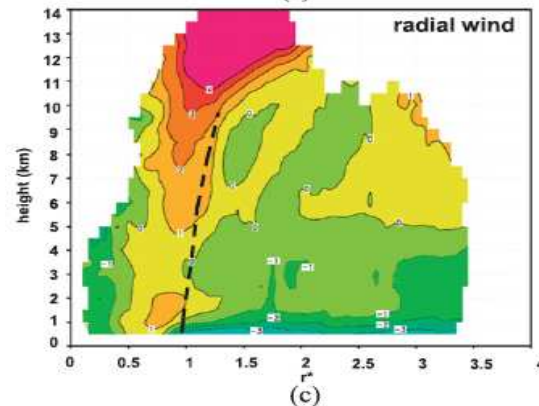
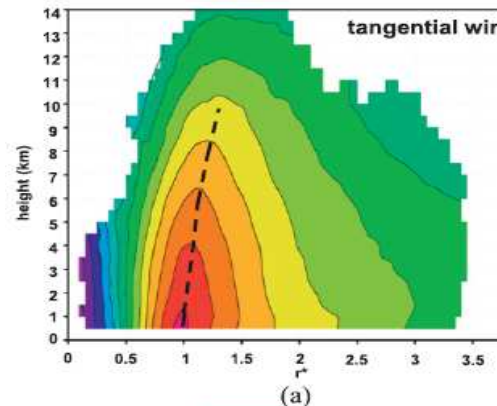


# LA CIRCULATION SECONDAIRE modélisation (8)

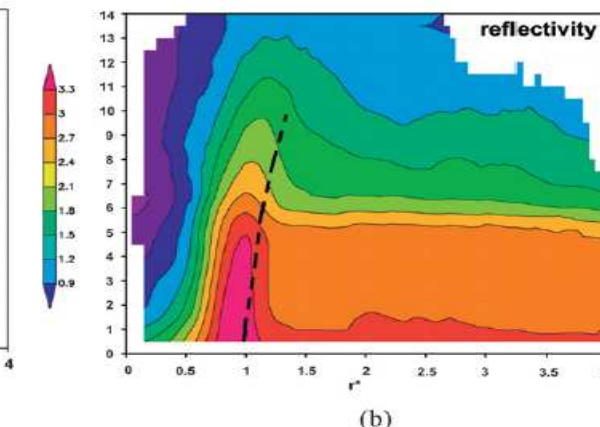
Yau et al., 2004 :  
*Mon. Wea. Rev.*, 132, 3299-3314



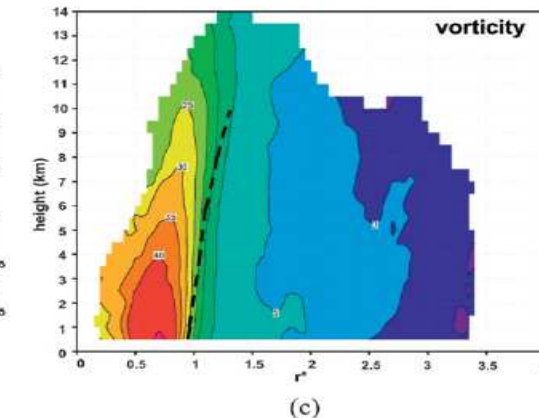
# LA CIRCULATION SECONDAIRE composite of airborne Doppler observations



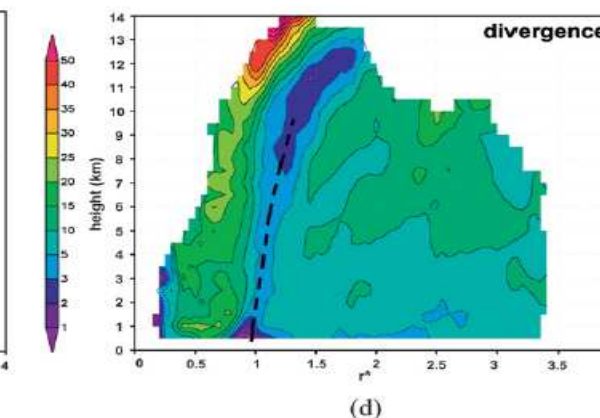
(a)



(b)



(c)

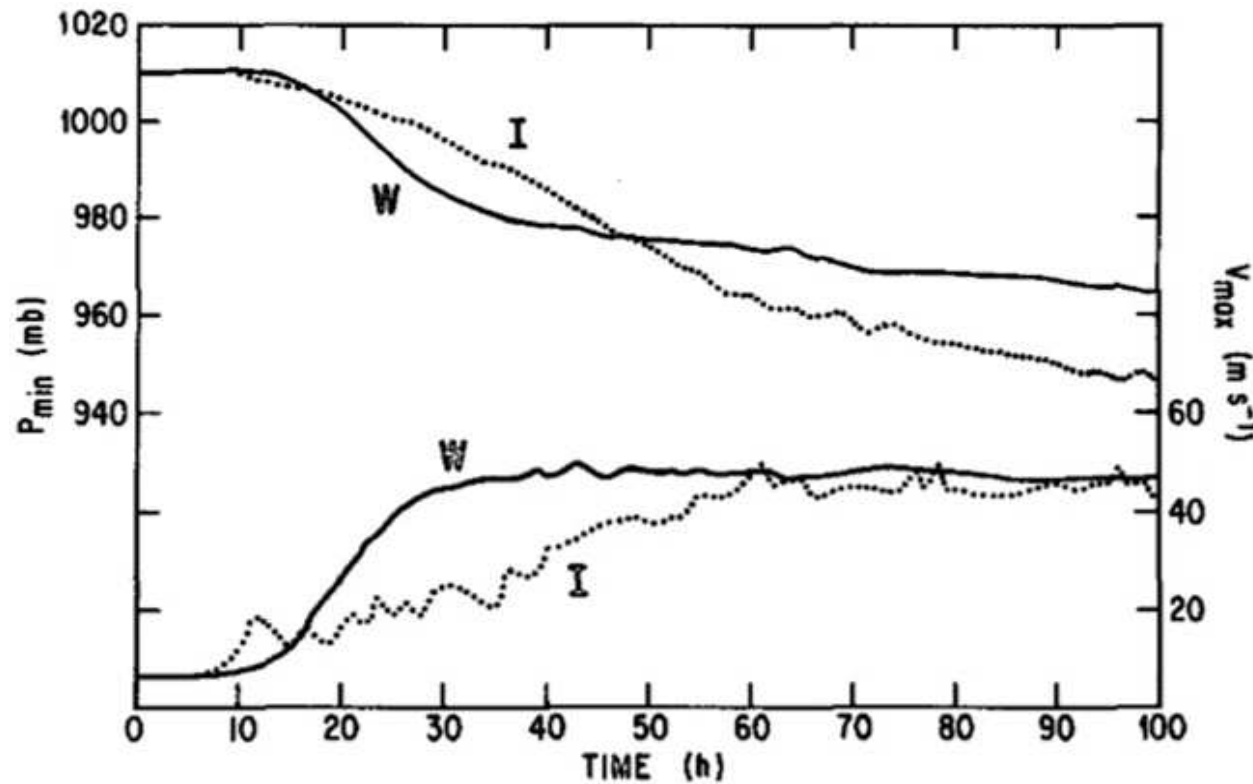


(d)

Rogers *et al.*, 2012 :  
*Mon. Wea. Rev.*, 140, 77-99

# LA CIRCULATION SECONDAIRE : microphysique (1)

Willoughby *et al.*, 1984 [ *J. Atmos. Sci.*, 41, 1169-1186 ]  
impact of cloud microphysics on tropical cyclone structure and intensity  
using a 2D axis-symmetric non-hydrostatic model  
with 2 km horizontal grid size



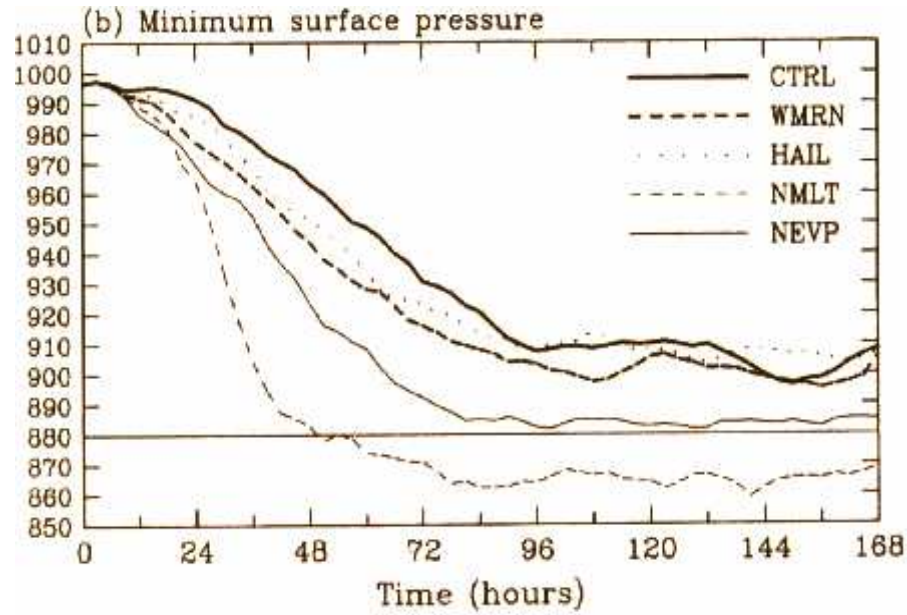
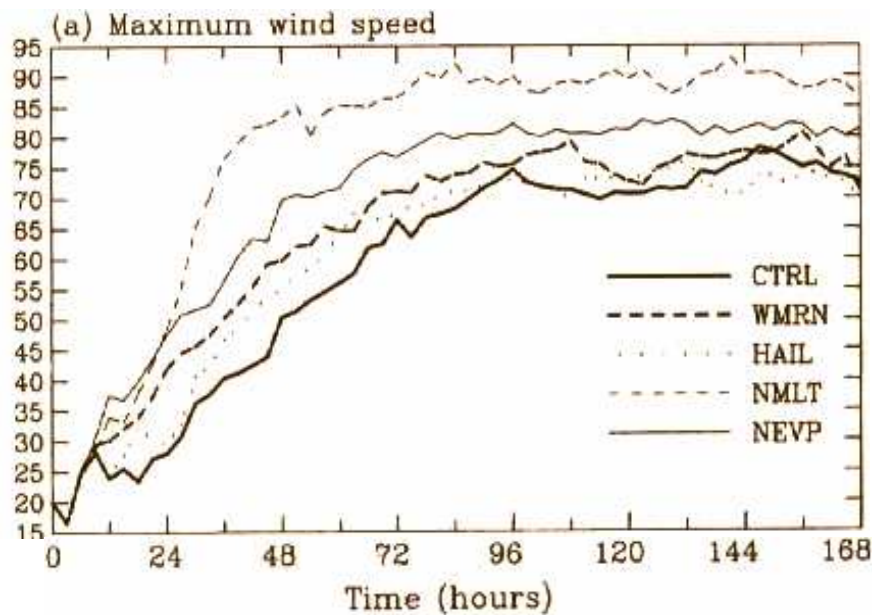
Time series of minimum surface level pressure (MSLP) and maximum tangential winds at 3.1 km in water (W) and ice (I) models.

# LA CIRCULATION SECONDAIRE : microphysique (2)

Wang, 2002a [ *Mon. Wea. Rev.*, 130, 3022-3036 ]

→ sensitivity of the simulated TC structure and intensity to the details of cloud microphysics parameterization :

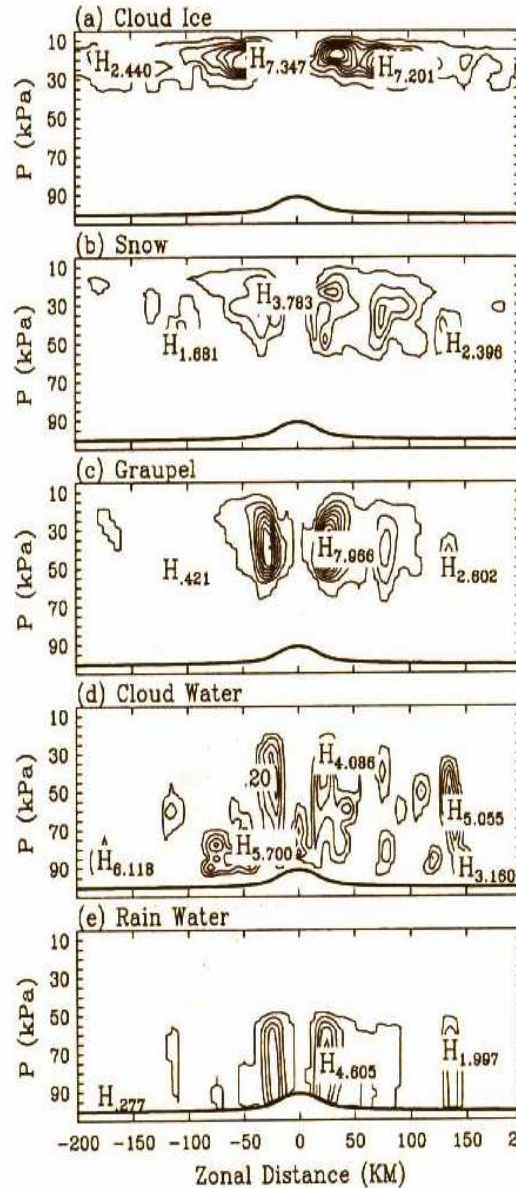
warm-rain only (WMRN), ice : crystal-snow-graupel (CTRL), ice : crystal-snow-hail (HAIL), no evaporation of rain (NEVP), no melting (NMLT)



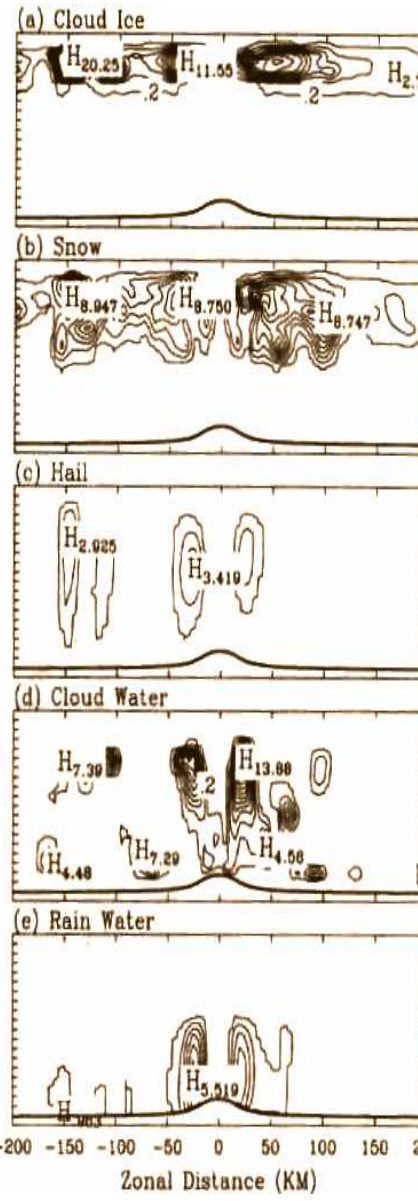
The simulated TC develops more rapidly and reaches a stronger intensity for « warm-rain only », « no evaporation » and « no melting » experiments

# LA CIRCULATION SECONDAIRE : microphysique (3)

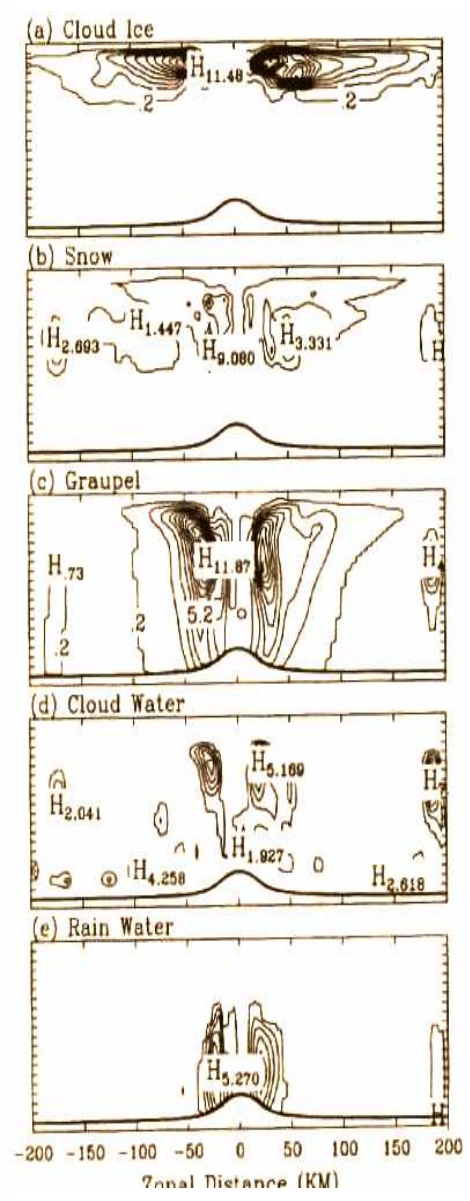
**CTRL**



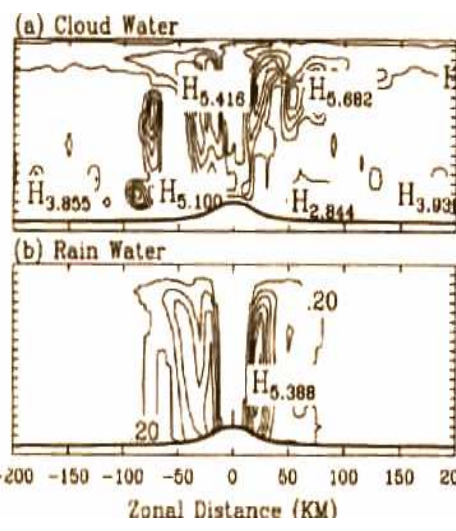
**HAIL**



**NMLT**



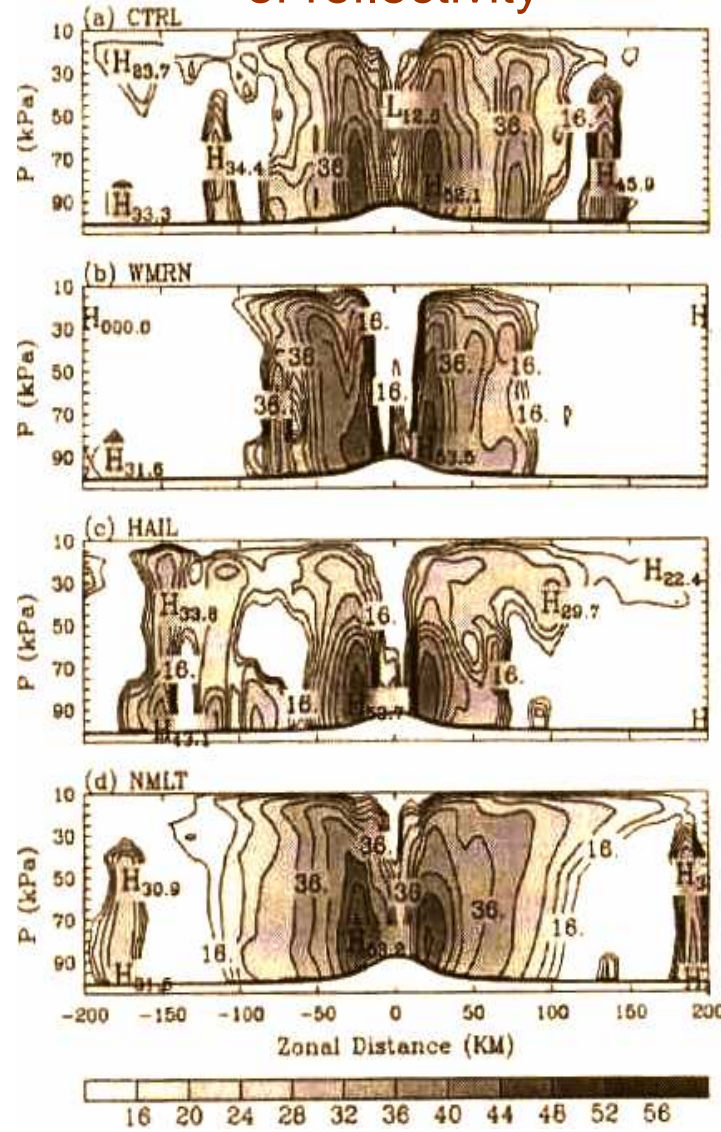
**WMRN**



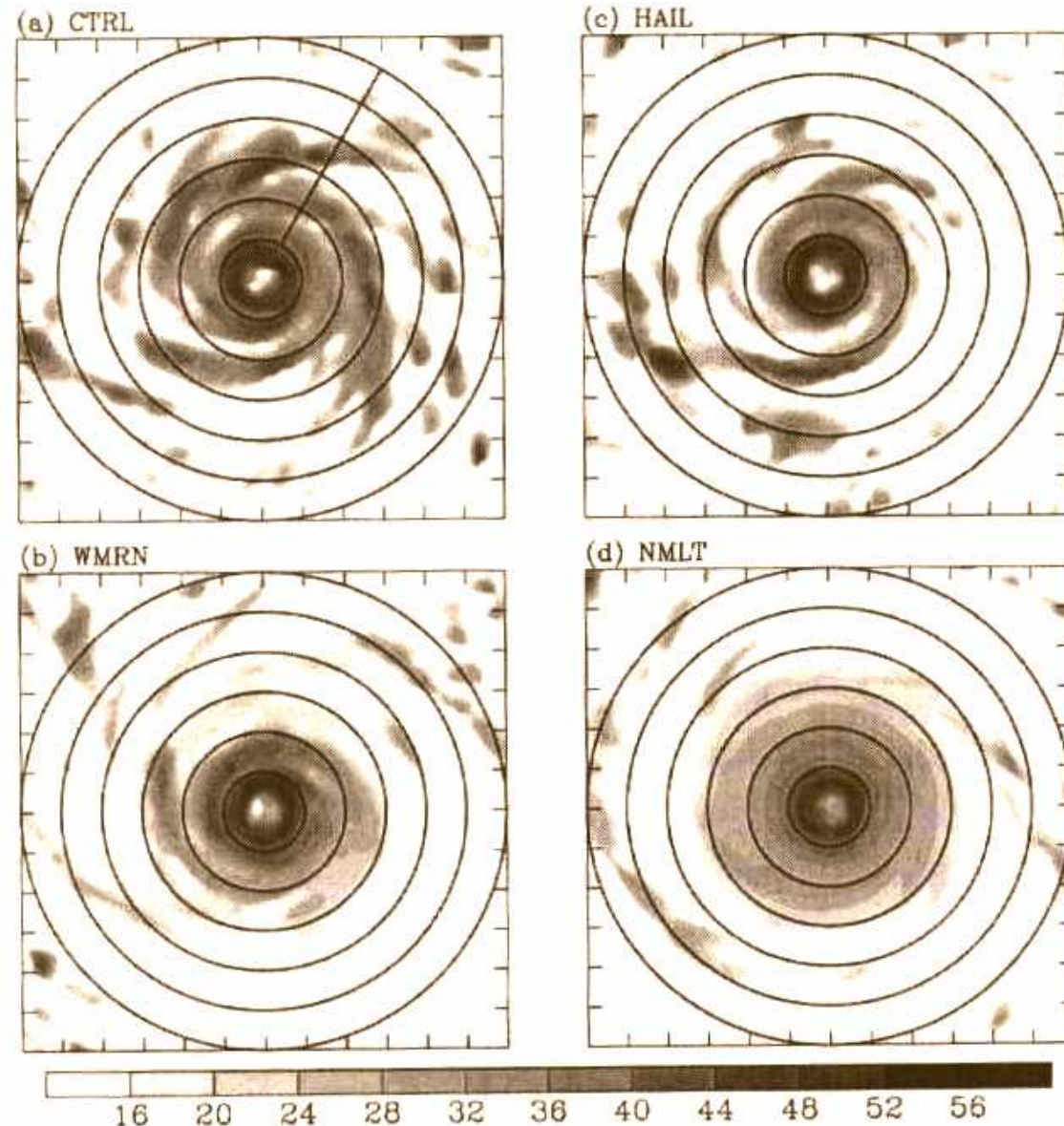
Zonal Distance (KM)

# LA CIRCULATION SECONDAIRE : microphysique (4)

Zonal vertical cross-section  
of reflectivity



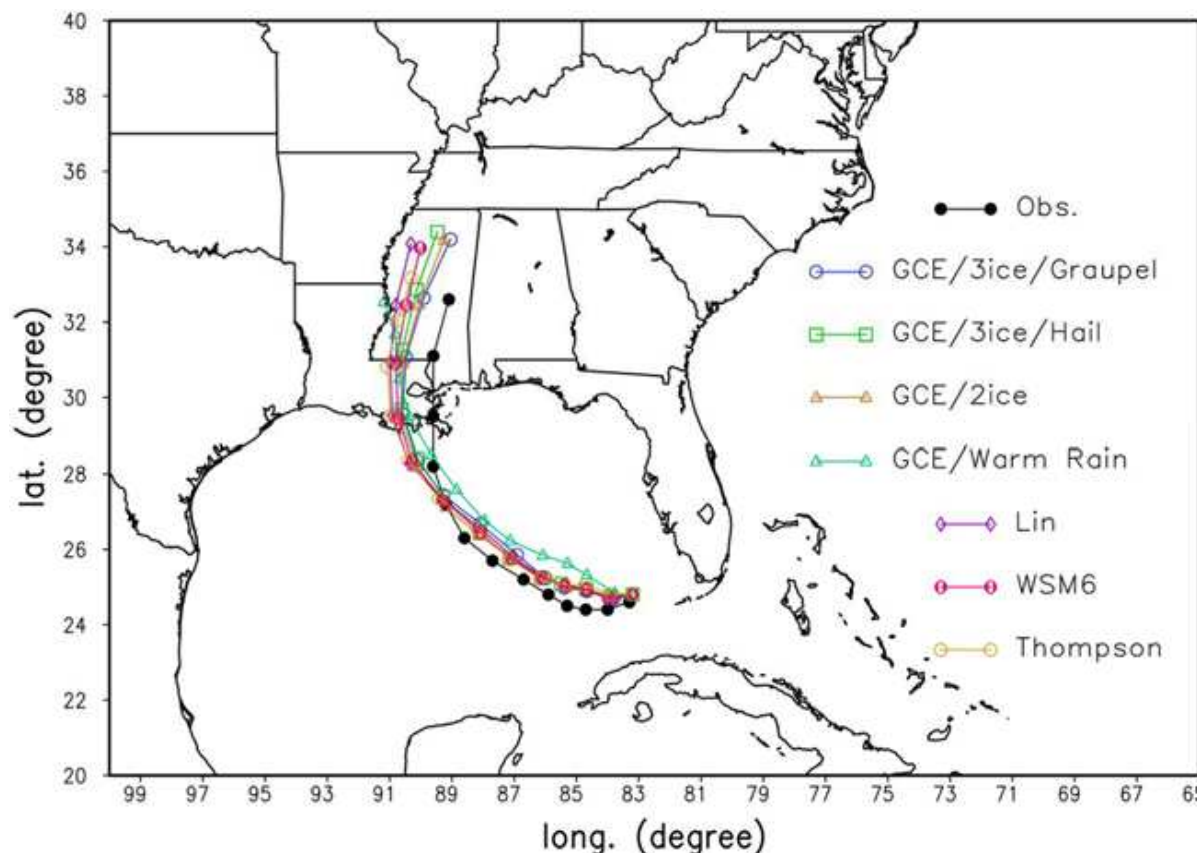
Surface reflectivity in 360 km x 360 km



# LA CIRCULATION SECONDAIRE : microphysique (5)

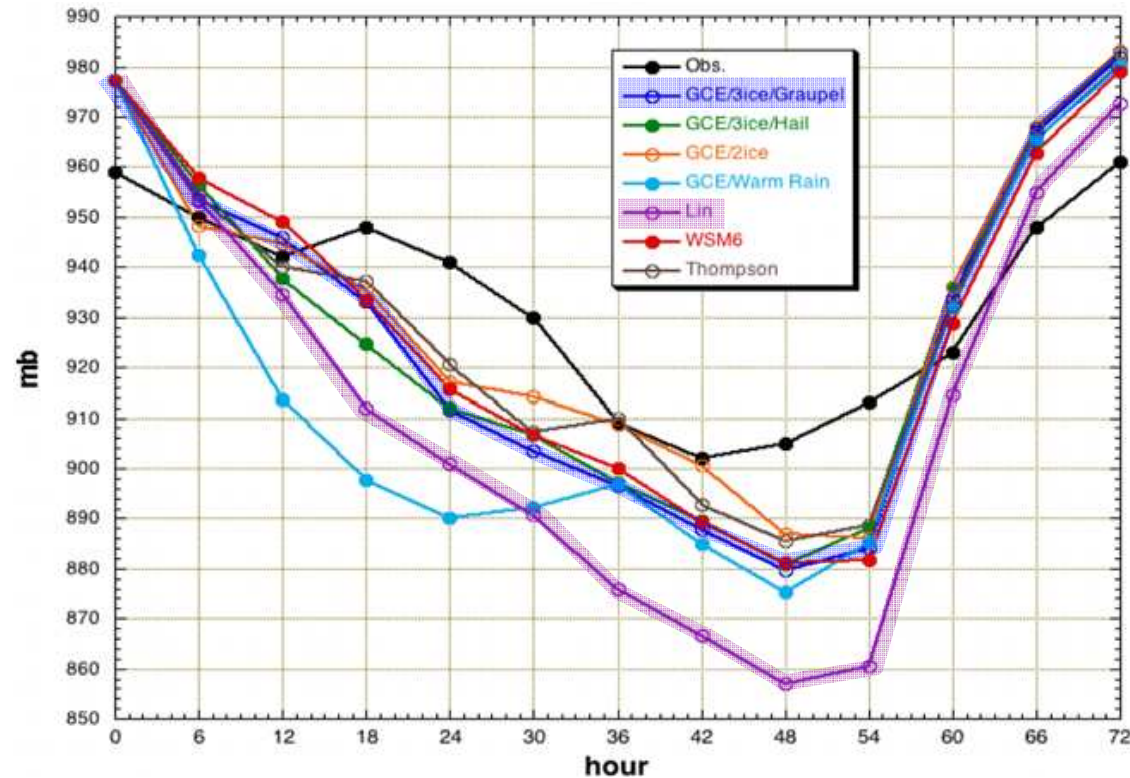
Tao *et al.*, 2011 :  
*Asia-Pacific J. Atmos. Sci.*, 47, 1-16

Simulation of Hurricane Katrina (2005) with the triple-nested (15, 5 and 1.667 km) WRF model with six different microphysical schemes (including the ice phase)



The sensitivity tests show no significant difference in track among the different microphysical schemes

# LA CIRCULATION SECONDAIRE : microphysique (6)

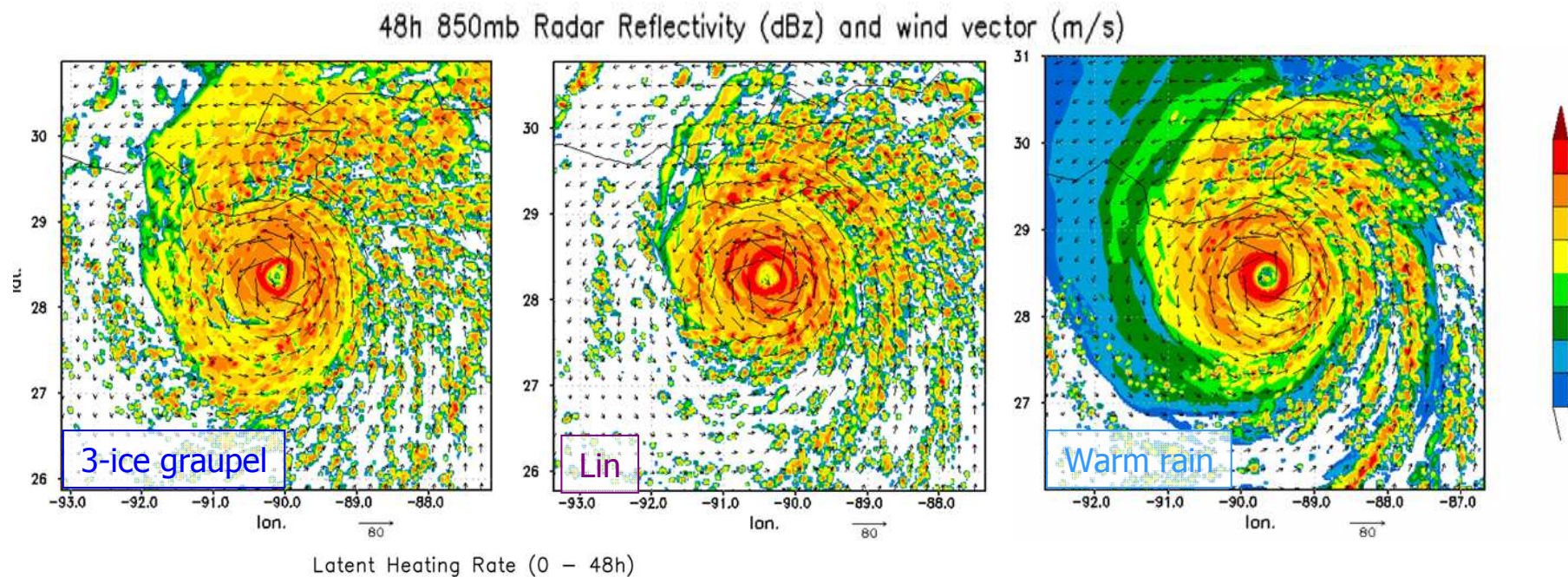


Minimum sea level pressure (hPa) obtained from WRF forecasts of Hurricane Katrina using six different microphysical schemes

	3ICE-Hail	3ICE-Graupel	2ICE	WSM6	Lin	Thompson
Liquid hydrometeor	46.6%	36.4%	24.8%	50.4%	65.3%	34.2%
Solid Hydrometeor	53.4%	63.6%	75.2%	49.6%	34.7%	65.8%

Domain- and 72-h time-average accumulated liquid (warm rain) and solid (ice) water species for the Hurricane Katrina case.

# LA CIRCULATION SECONDAIRE : microphysique (7)



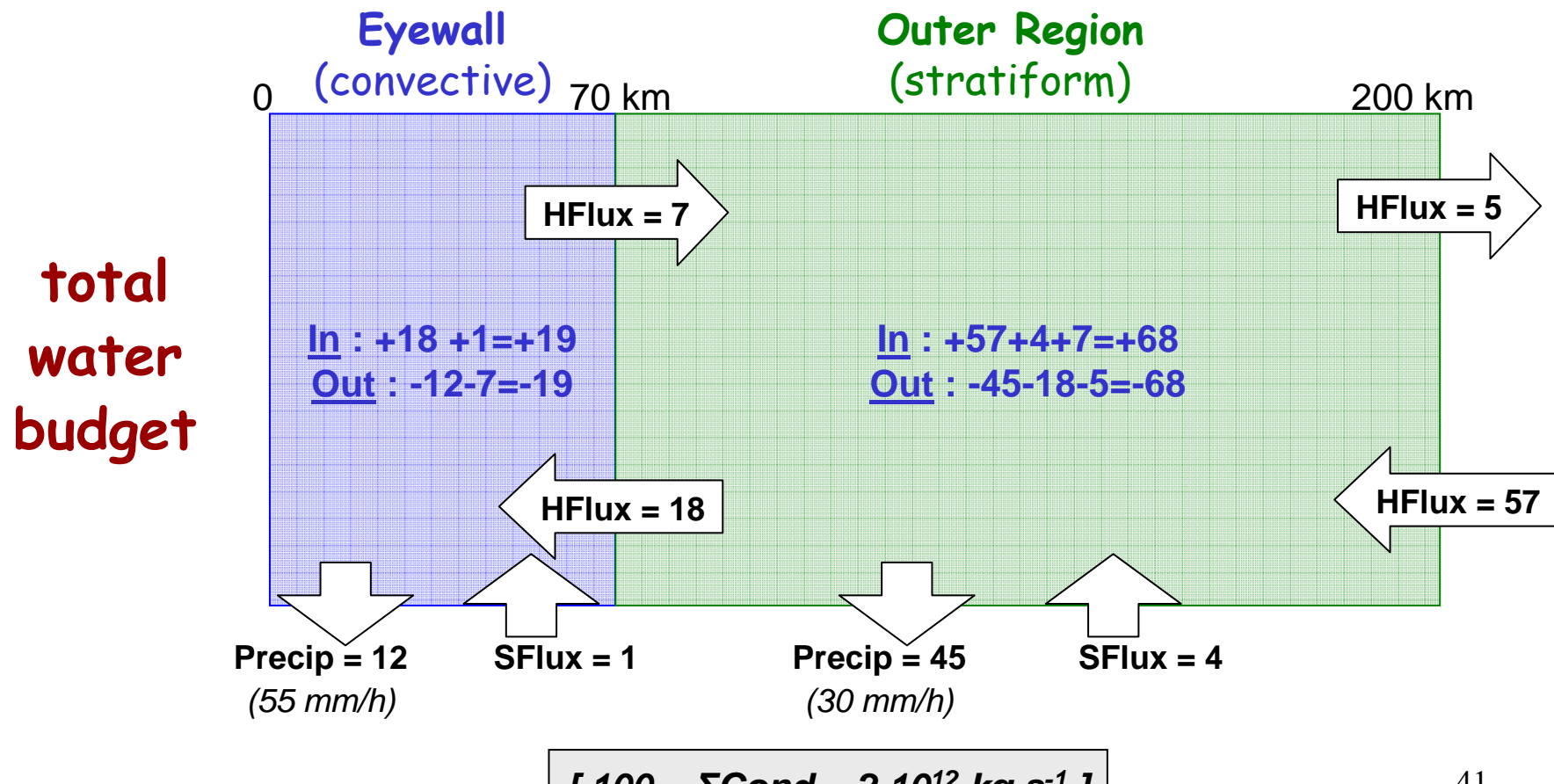
Latent heating is largest in the lower and middle troposphere for the warm rain only physics, whereas it is larger aloft in both « ice » schemes.  
 → modeling studies suggest that the larger the latent heating is in the lower and middle troposphere, the stronger the storm intensity and the larger the eyewall can be.

# LA CIRCULATION SECONDAIRE : microphysique (8)

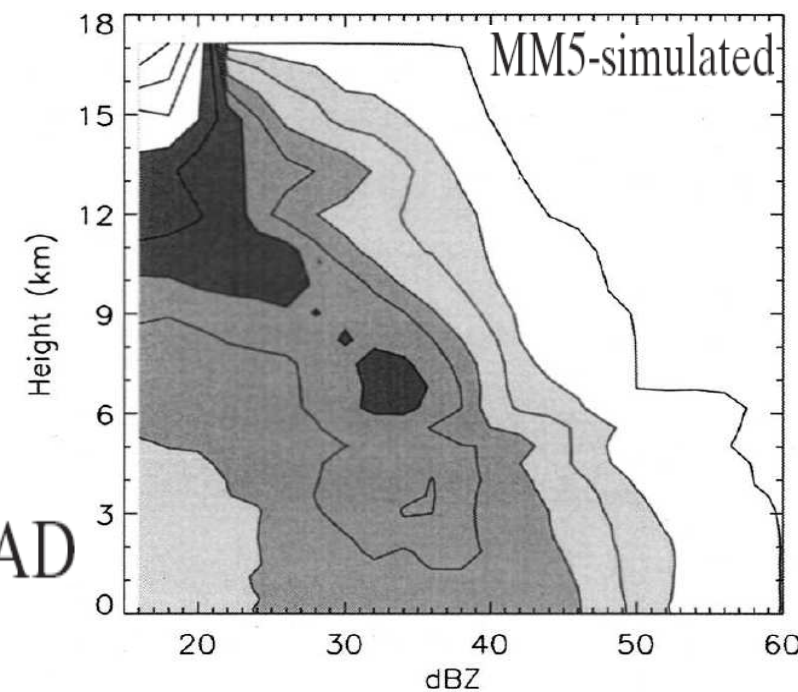
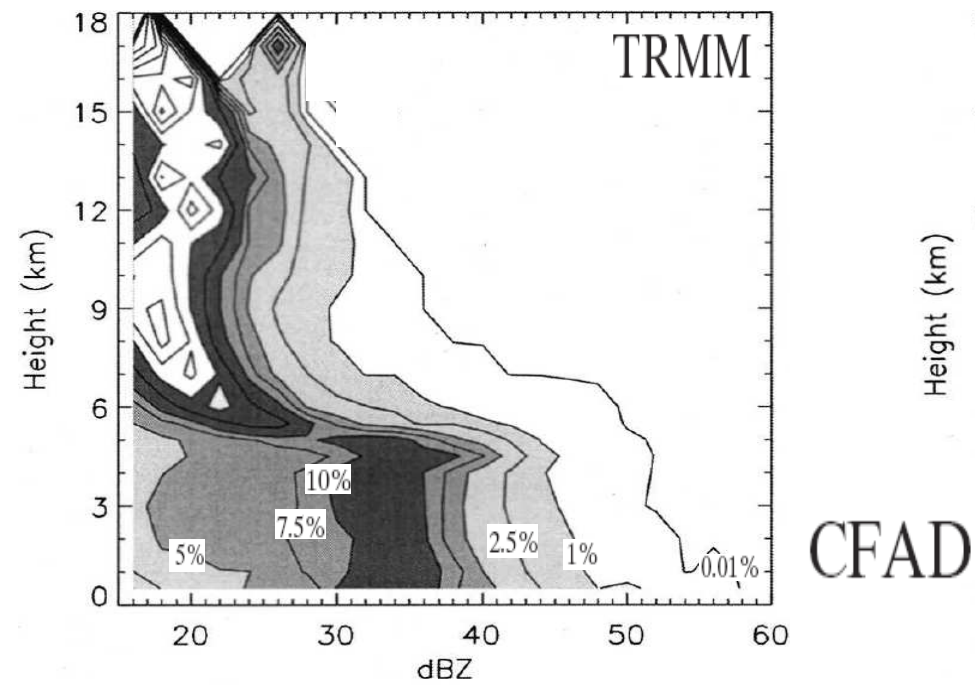
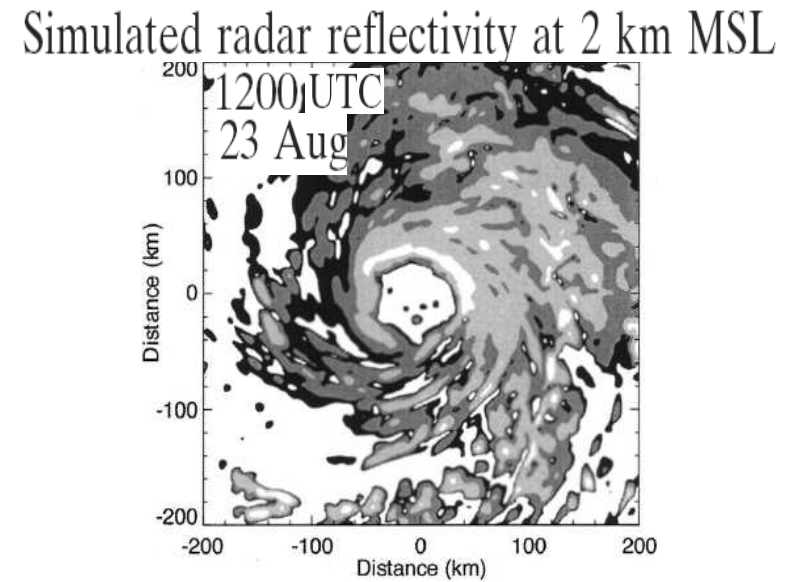
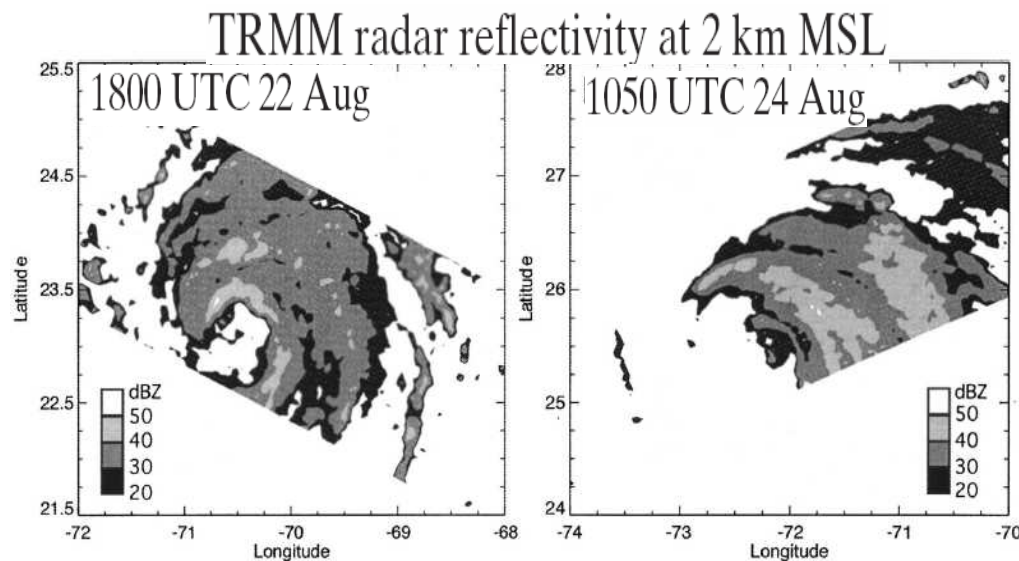
Braun, 2006 [ *J. Atmos. Sci.*, 63, 43-64 ]

Numerical simulation of Hurricane Bonnie (23 Aug 1998)

→ Water vapor, cloud condensate & precipitation budget

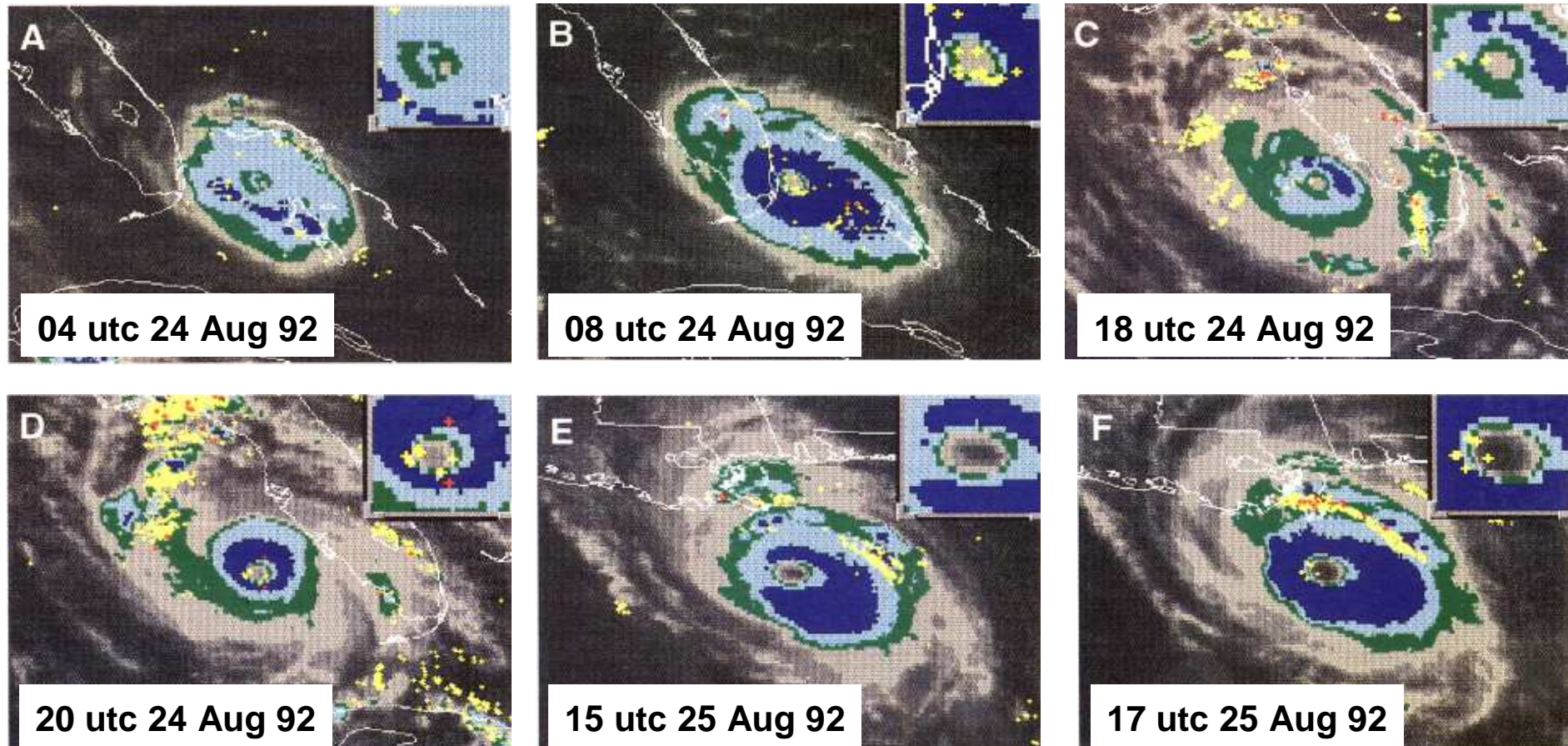


# LA CIRCULATION SECONDAIRE : microphysique (9)



# LA CIRCULATION SECONDAIRE : activité électrique (1)

Molinari *et al.*, 1994 [ *J. Geophys. Res.*, 99, 16665-16676 ]



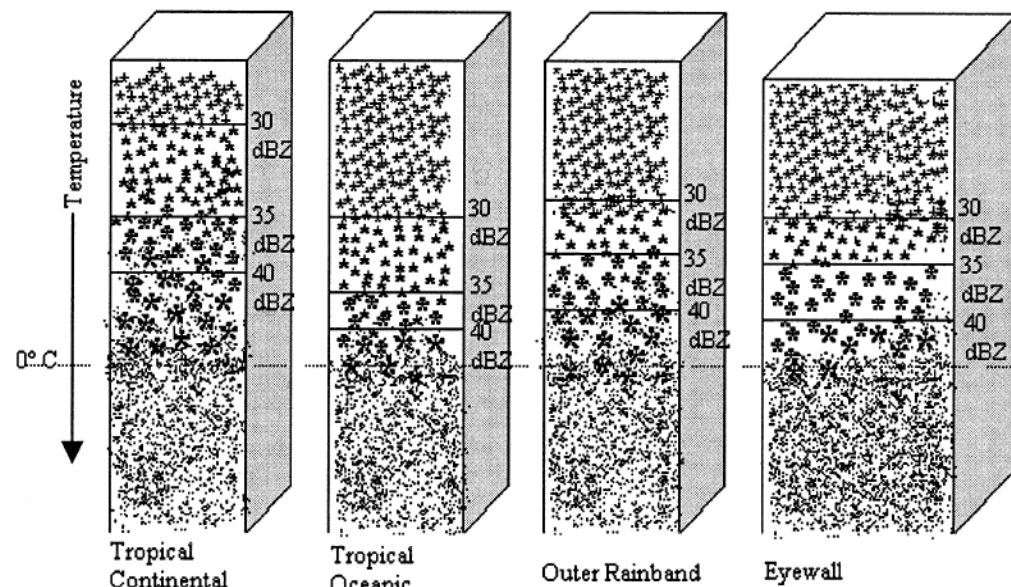
Variation of lightning in Hurricane Andrew, superimposed on infrared satellite images. The insets show a 2X view of the eye and eyewall.

# LA CIRCULATION SECONDAIRE : activité électrique (2)

Molinari *et al.*, 1999 [ *Mon. Wea. Rev.*, 127, 520-534 ]

Ground flash density (from NLDN) for 9 Atlantic hurricanes :

- weak maximum in the eyewall region (↑ before/during intensification)  
→ *≈ weakly electrified oceanic monsoonal convection*
- minimum 80-100 km outside the eyewall (positive flashes)  
→ *mostly stratiform precipitation*
- strong maximum in outer rainbands (200-300 km radius)  
→ *more convective*

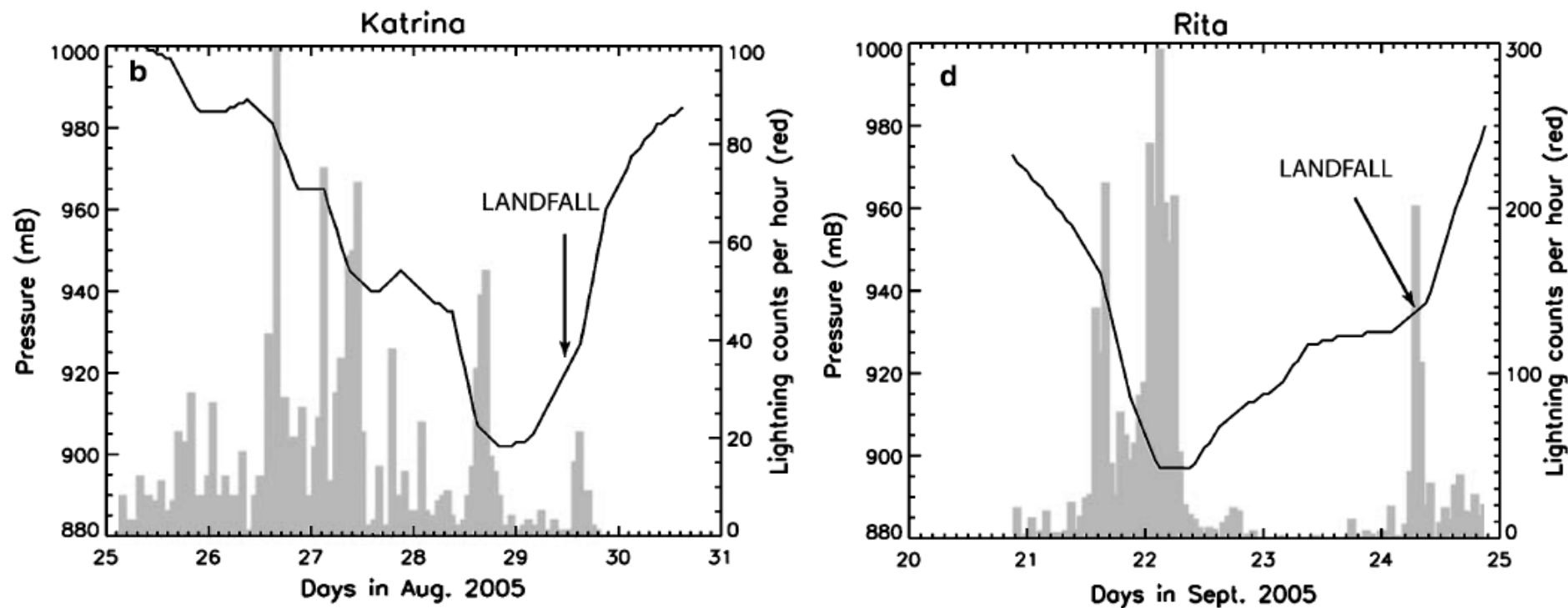


- Dots indicate liquid hydrometeors ;
- Stars indicate frozen hydrometeors with increasing symbol size representing larger graupel or hail.

Cecil & Zipser, 2002 :  
*Mon. Wea. Rev.*, 130, 785-801

## LA CIRCULATION SECONDAIRE : activité électrique (3)

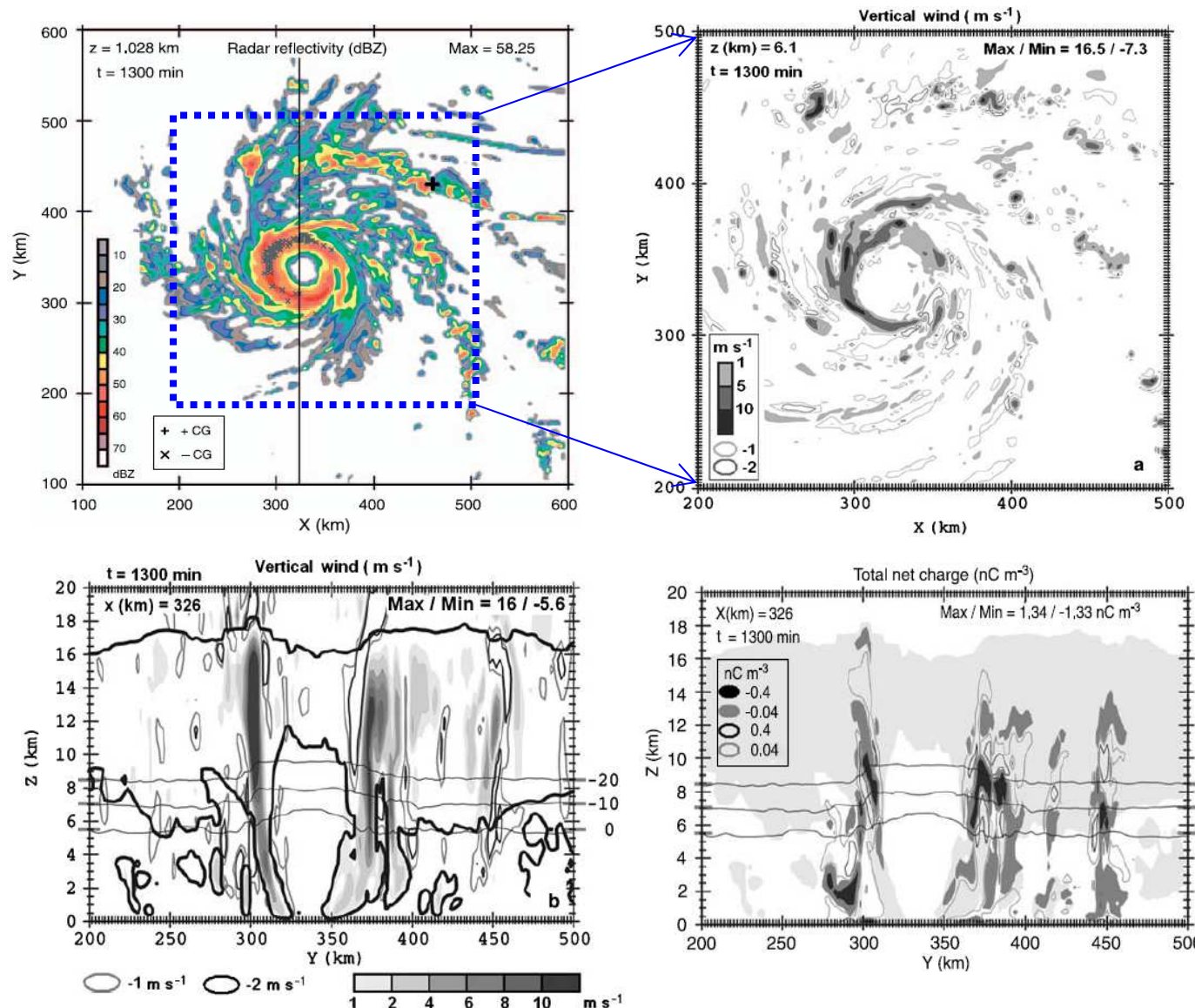
Fierro *et al.*, 2007 [ *Meteor. Atmos. Phys.*, 98, 13-33 ]



Hourly eyewall total lightning flash rate detected for Hurricanes Katrina and Rita of 2005 by LASA (Los Alamos National Laboratory's Sferic Array)  
→ The increasing flash rates suggest that eyewall lightning outbreaks might be a useful forecast tool to predict imminent changes in hurricane intensity and therefore to diagnose storm intensification.

# LA CIRCULATION SECONDAIRE : activité électrique (4)

Fierro *et al.*, 2007 [ *Meteor. Atmos. Phys.*, 98, 13-33 ]

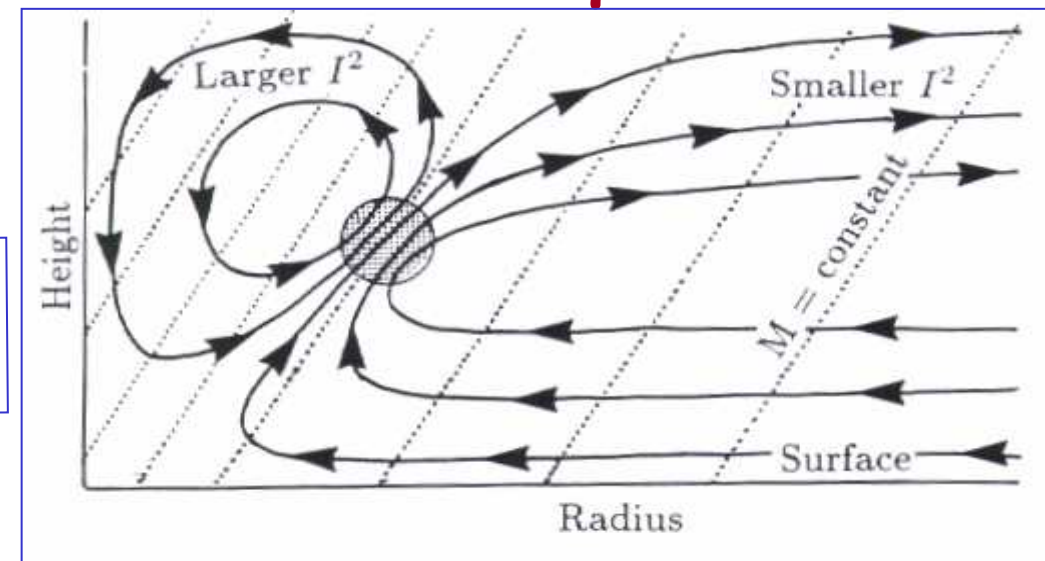


Since the eyewall and the strongest rainbands contained the largest updrafts and mixing ratios of graupel and cloud water, these regions were more conducive for collisional « Non-Inductive » charging processes to operate. Consequently, these regions also produced the largest flash rates in the TC.

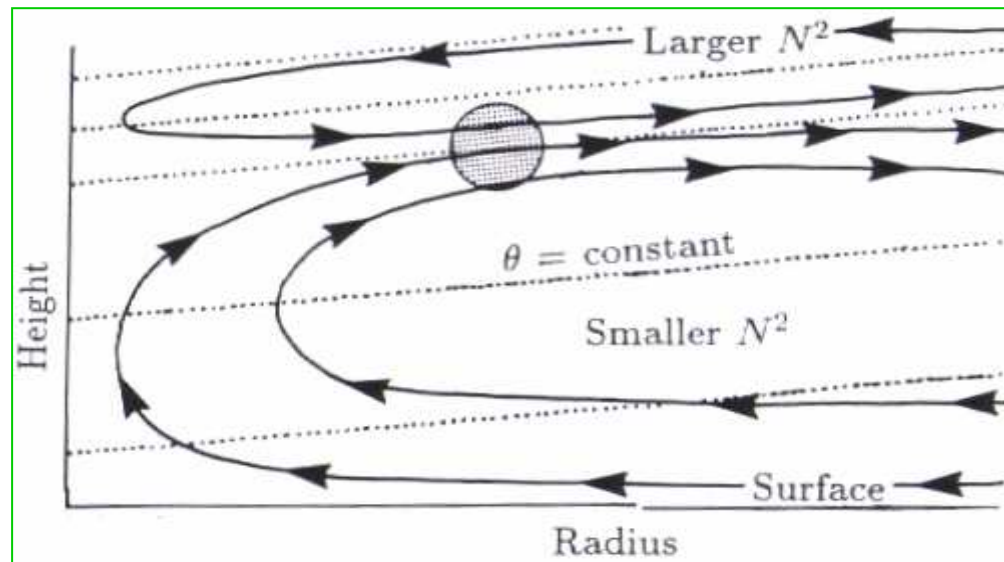
# LA CIRCULATION SECONDAIRE : Sources « convectives » dans un environnement en équilibre du vent thermique

Willoughby et al., 1982  
*J. Atmos. Sci.*, 39, 395-411

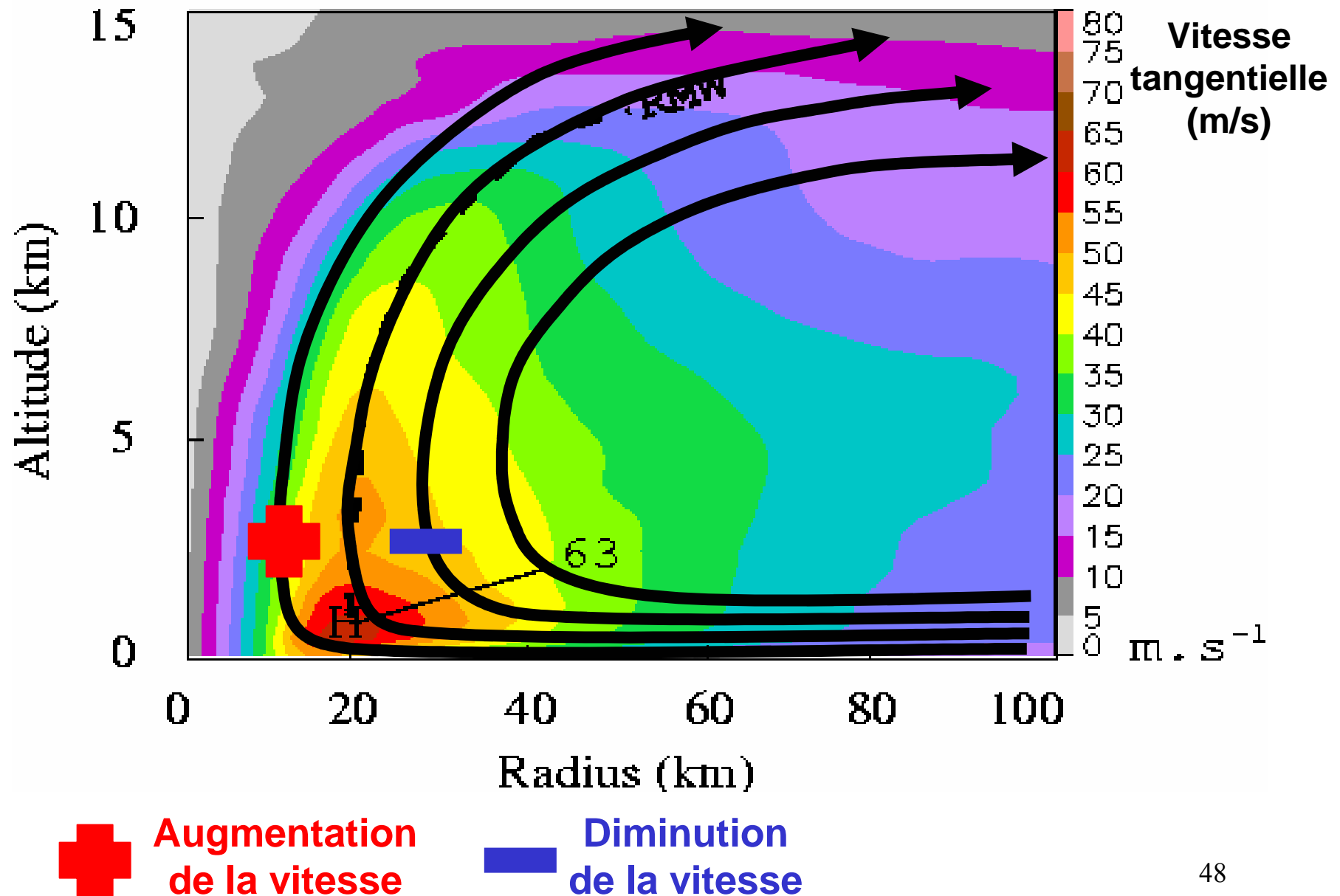
Source  
de chaleur



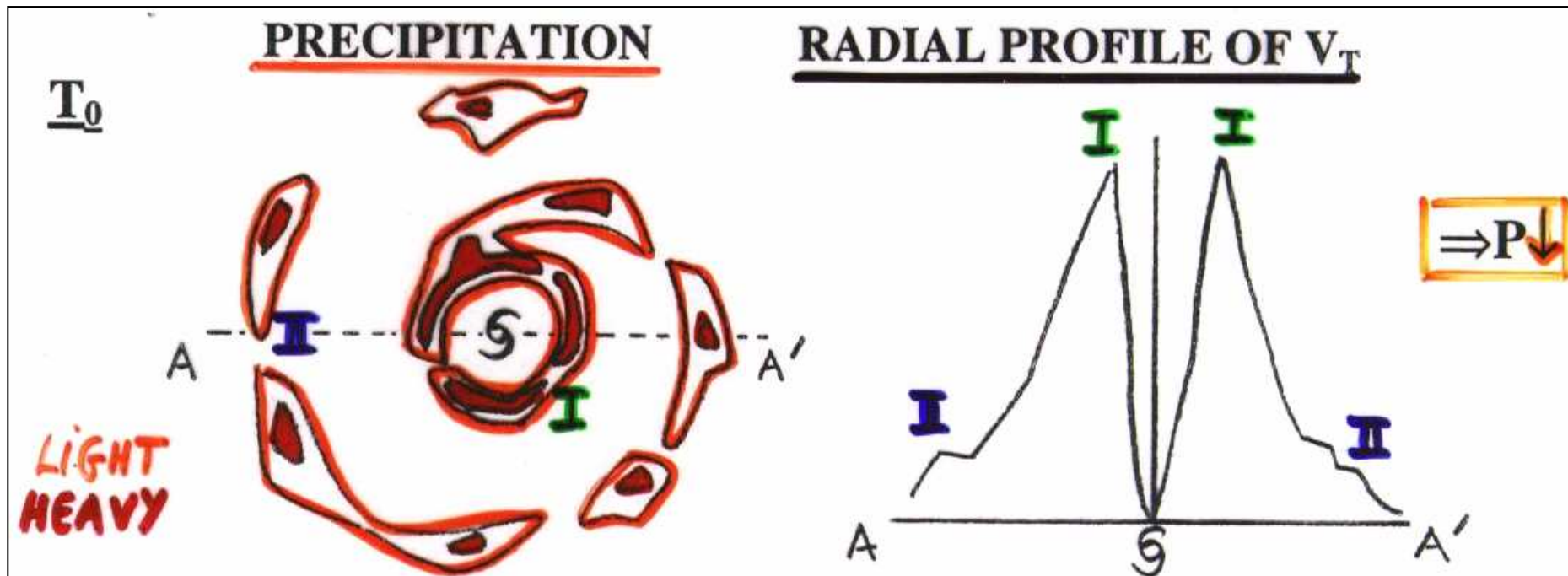
Source  
de moment



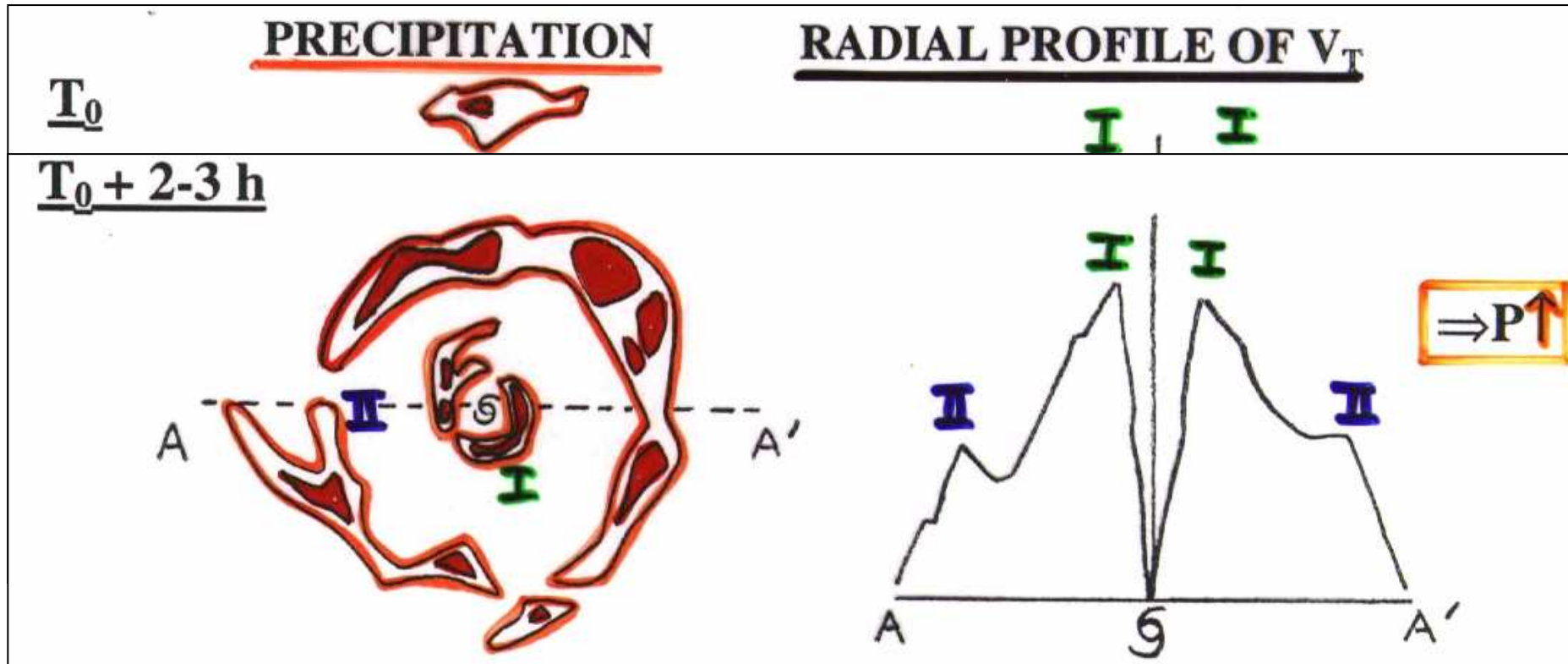
# LA CIRCULATION SECONDAIRE : Evolution



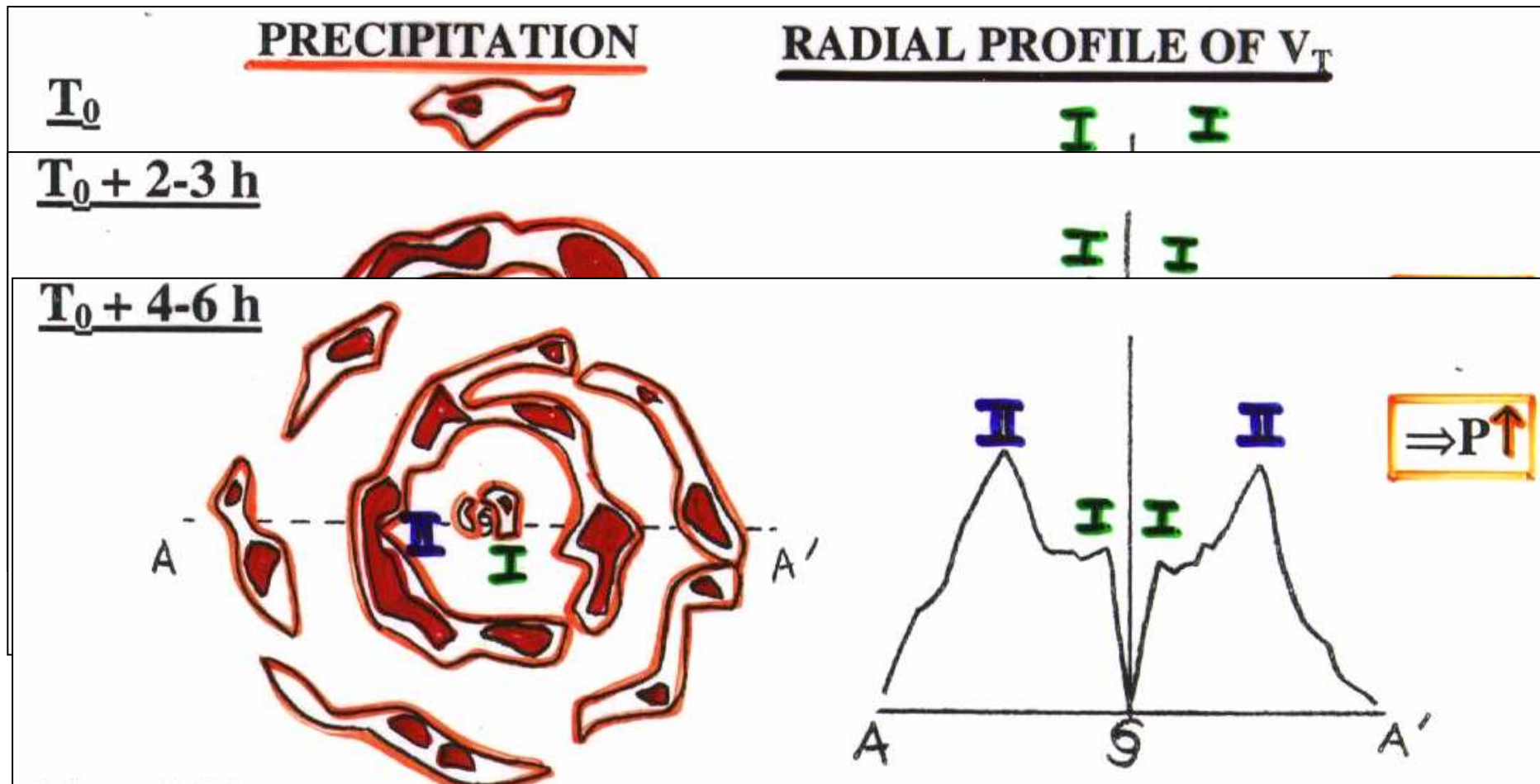
# LA CIRCULATION SECONDAIRE : Cycle de remplacement des Murs de l'Œil (1a)



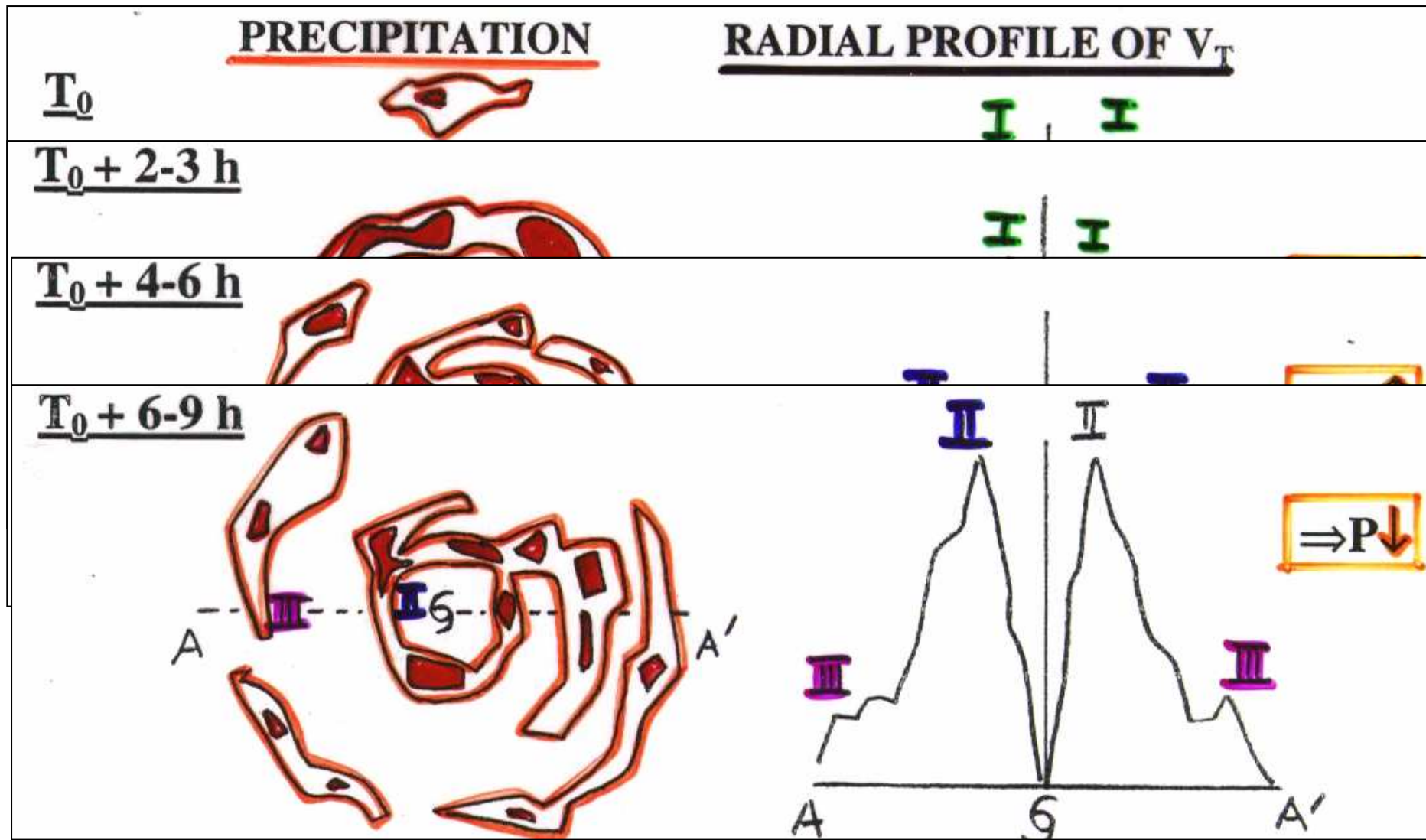
# LA CIRCULATION SECONDAIRE : Cycle de remplacement des Murs de l 'Œil (1b)



# LA CIRCULATION SECONDAIRE : Cycle de remplacement des Murs de l 'Œil (1c)



# LA CIRCULATION SECONDAIRE : Cycle de remplacement des Murs de l'Œil (1d)



# LA CIRCULATION SECONDAIRE : Cycle de remplacement des Murs de l'Œil (2)

Hurricane Intensity and Eyewall Replacement

Robert A. Houze, Jr., et al.  
Science 315, 1235 (2007);

RAINEX

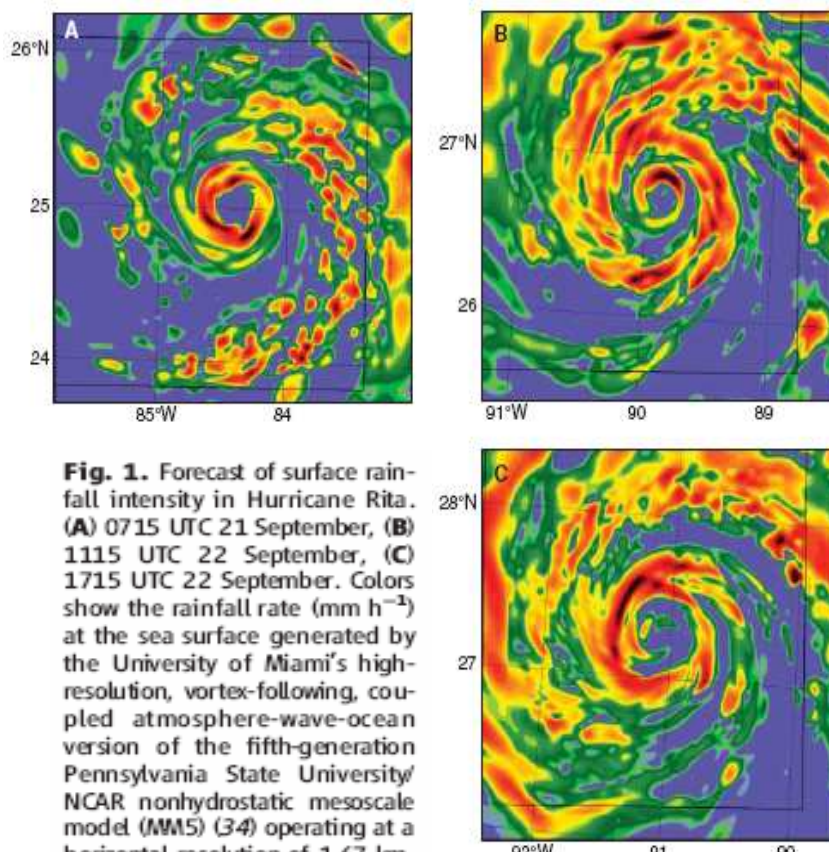


**Fig. 1.** Forecast of surface rainfall intensity in Hurricane Rita. (A) 0715 UTC 21 September, (B) 1115 UTC 22 September, (C) 1715 UTC 22 September. Colors show the rainfall rate ( $\text{mm h}^{-1}$ ) at the sea surface generated by the University of Miami's high-resolution, vortex-following, coupled atmosphere-wave-ocean version of the fifth-generation Pennsylvania State University/NCAR nonhydrostatic mesoscale model (WM5) (34) operating at a horizontal resolution of 1.67 km. Initial fields at 0000 UTC 20 September 2005 and lateral boundary conditions are from the NOGAPS global numerical forecast model (35).

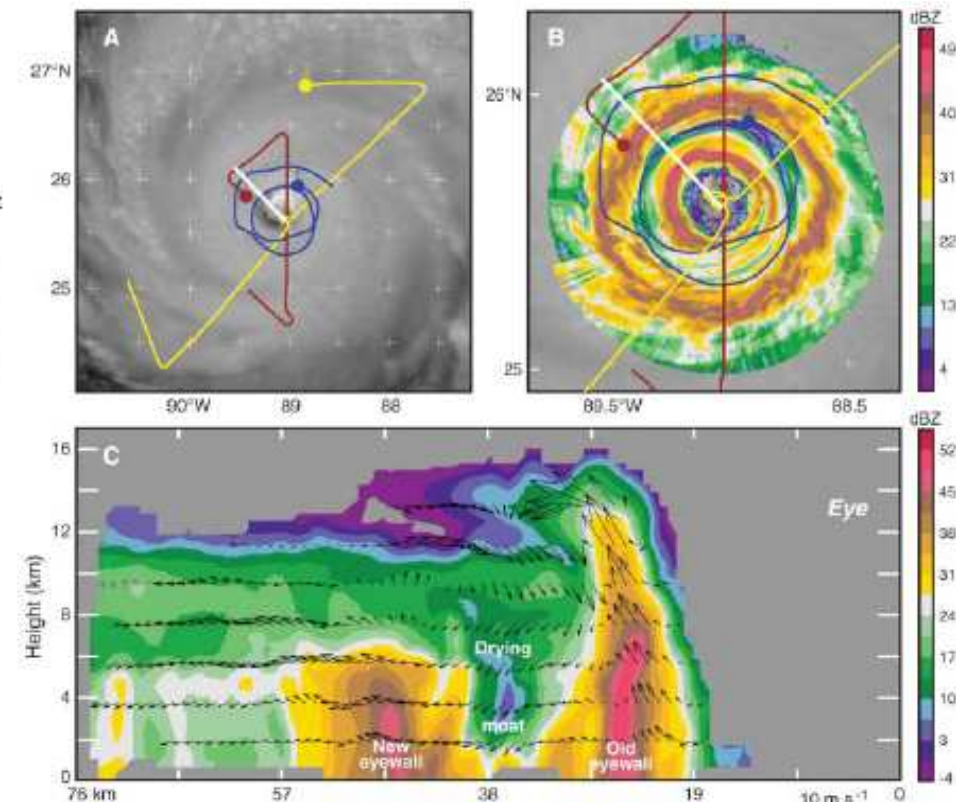
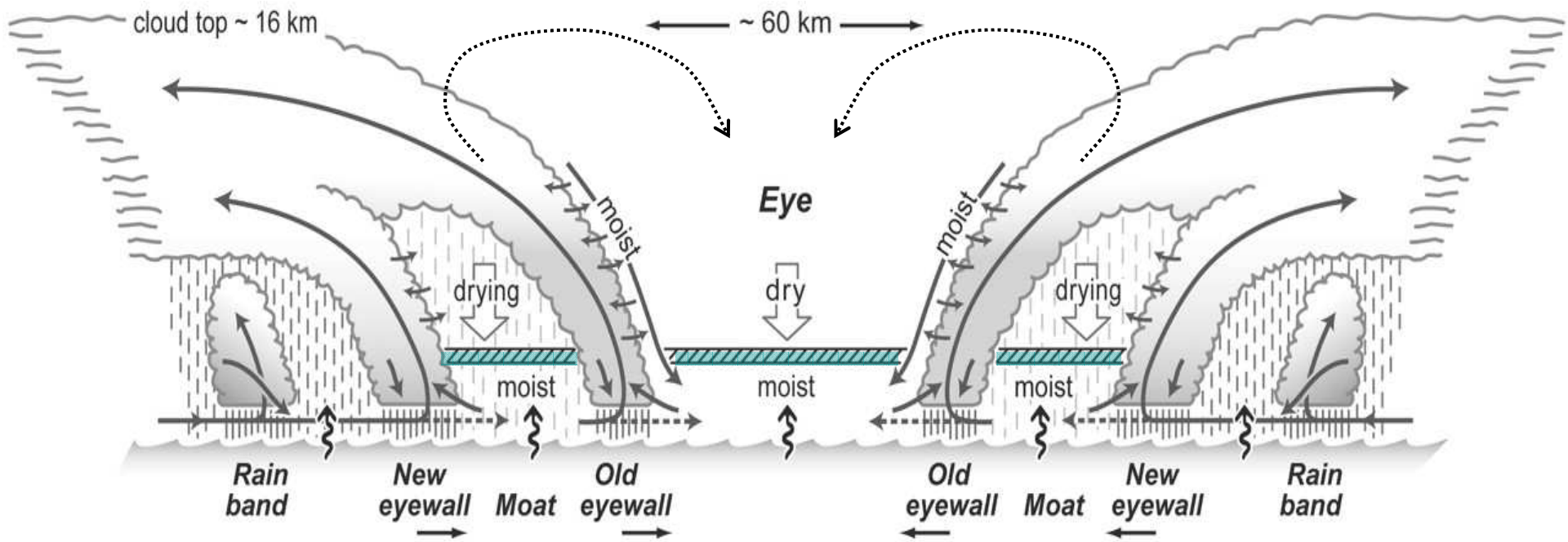


**Fig. 2.** Aircraft data collected in Hurricane Rita between 1800 and 1820 UTC 22 September 2005. (A) and (B) are plan views; (C) is a vertical cross section across the northwest side of the storm (along the white line in the plan views). Colored lines in (A) denote the flight tracks of the three RAINEX aircraft: yellow and red are the NOAA aircraft tracks; blue is the NRL aircraft, which was instrumented with ELDORA. The dots show aircraft locations as of 1830 UTC. The yellow track segment is for the 80 min preceding that time; the red and blue track segments are for the preceding 45 min. The yellow NOAA track was part of a wide pattern to determine the broad-scale structure of the cyclone vortex. The red NOAA track was part of an intermediate pattern, with shorter legs across the center of the storm to monitor the two eyewalls. The blue NRL track was the circumnavigation that obtained the key radar and sounding data referred to in this article. The



Two interacting eyewalls, separated by the moat, were contracting inward. The vertical lines below the clouds indicates precipitation.

The thin arrows show the direction of air motion relative to the storm. Dashed segments indicate partially interrupted flow.

The wavy arrows at the sea surface indicate upward water vapor flux.

The broad arrows indicate the downward motion induced by the heating in the eyewall and (possibly) momentum mixing across the inner edges of the eyewalls.

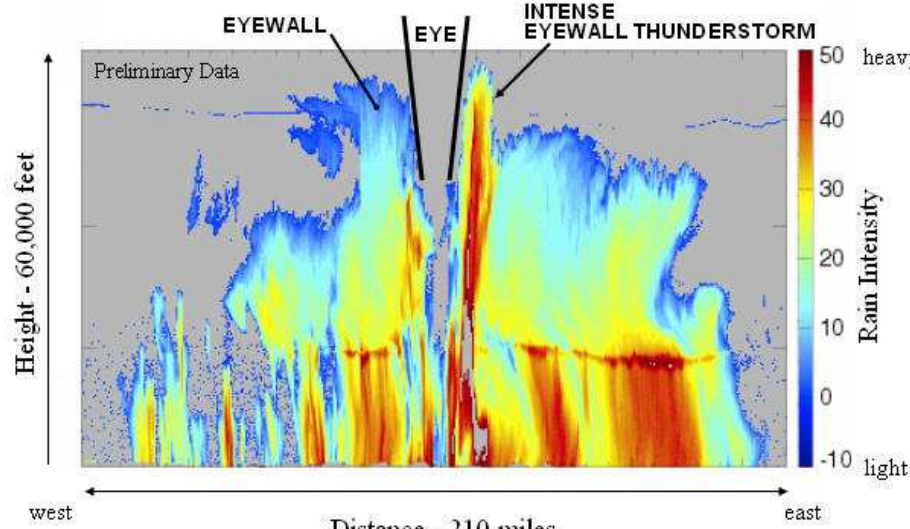
The hatched zone shows the top of the near-surface moist layer, which is capped by the stabilizing and drying effect of subsiding air above.

# LA CIRCULATION SECONDAIRE : Développements dans le Mur de l 'Œil

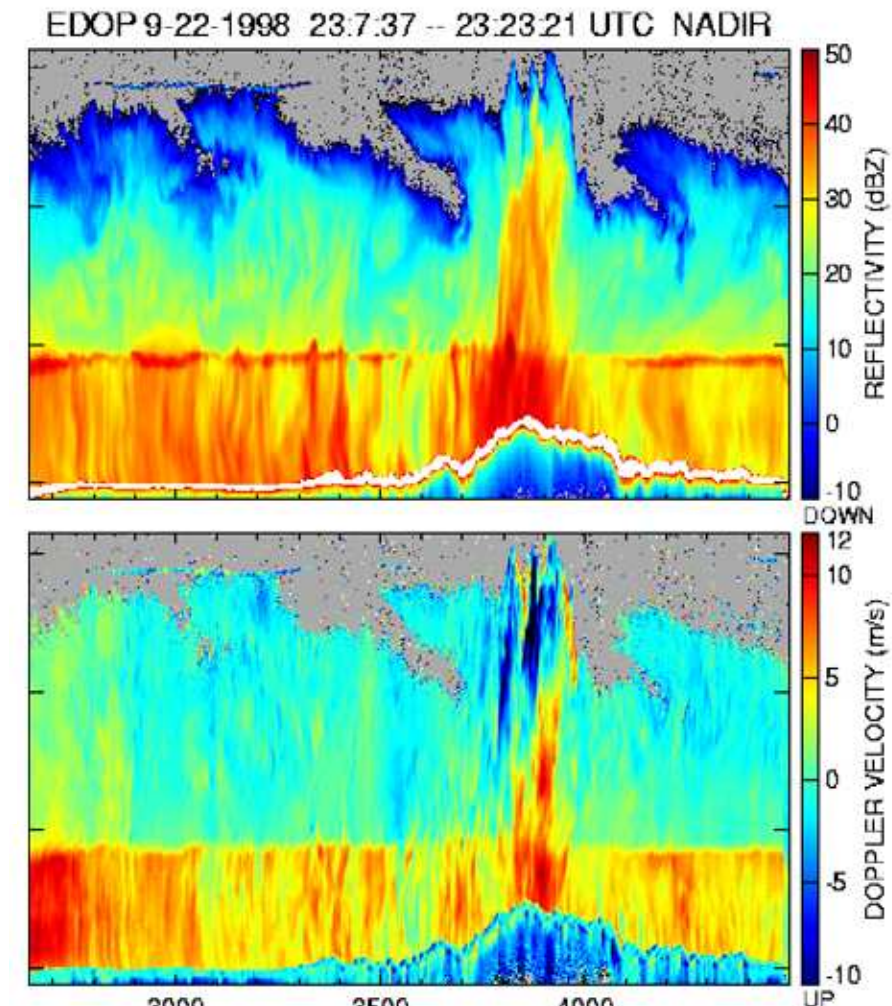


ER-2 Doppler Radar (EDOP) Views Detailed Super-Anatomy  
Of Intense Hurricane Emily During NASA's TCSP Experiment

Principal Investigator: Dr. Gerald Heymsfield, NASA GSFC



Vertical slice showing rain structure across the entire storm -  
1:30 - 2:00 AM CST July 17, 2005



Hurricane Georges over Hispaniola

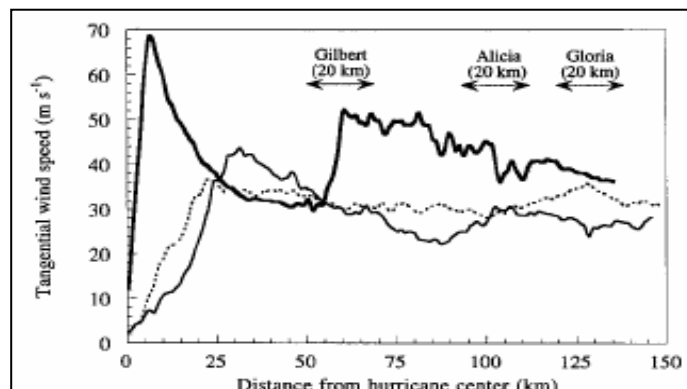
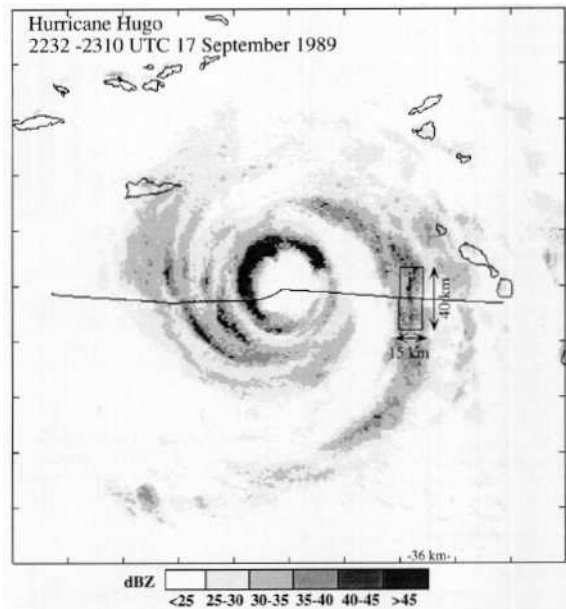


FIG. 2. Storm-relative tangential wind profiles of Hurricane Gilbert from 1012 to 1029 UTC 14 September 1988 (bold, solid line), Hurricane Alicia from 1352 to 1413 UTC 17 August 1983 (thin, solid line), and Hurricane Gloria from 1932 to 1951 UTC 26 September 1985 (thin, dashed line). The three shaded regions delineate the 20

Samsury & Zipser, 1995 [ *Mon. Wea. Rev.*, 123, 3502-3517 ] ≈30% des bandes externes présentent un maximum secondaire de vent tangentiel

## BANDES EXTERNES (1)

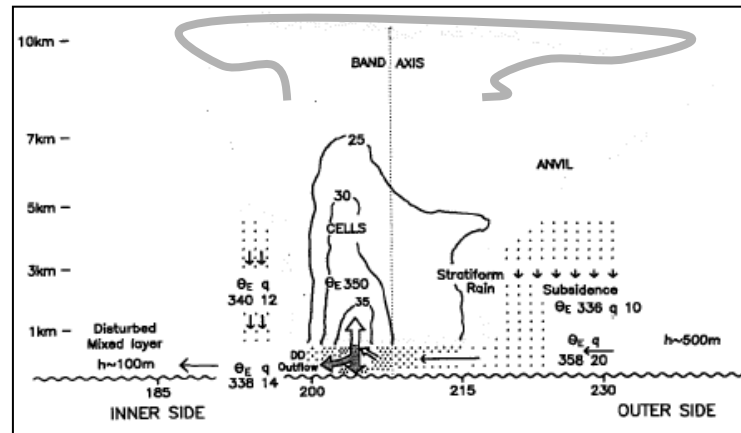
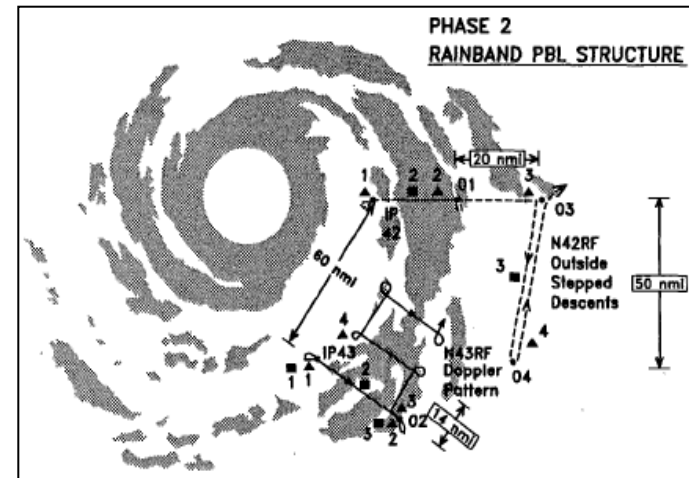


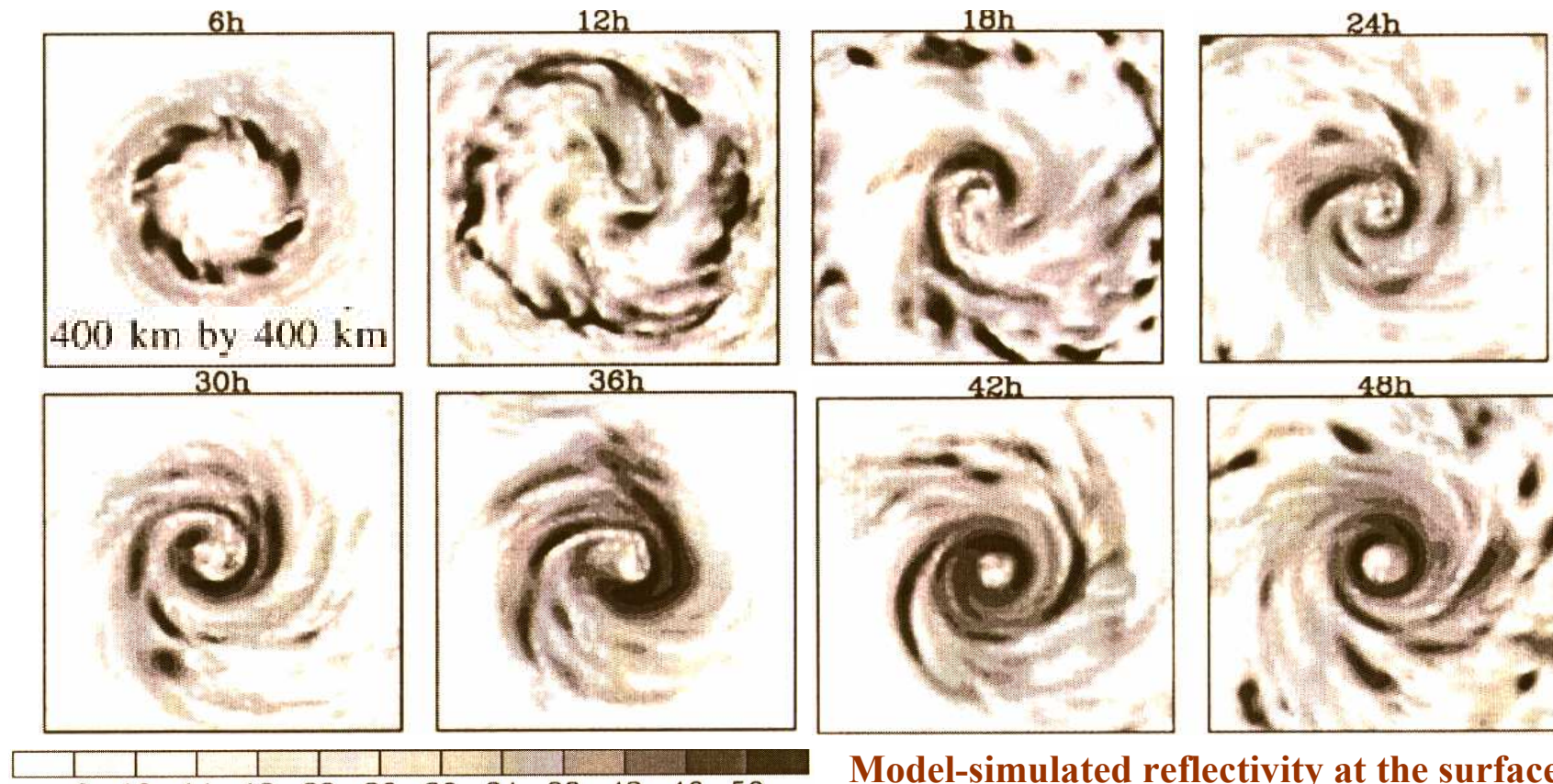
FIG. 14. Schematic cross section of the thermodynamic structure in the Hurricane Earl rainband. Outer solid contour indicates band cloud edges while other contours represent radar reflectivity. Horizontal arrows represent crossband component of the wind, bold vertical arrows indicate convective core updrafts and downdrafts, small downward arrows indicate mesoscale subsidence regions and larger downward arrows indicate penetrative downdrafts originating in the inner anvil region.

Powell, 1990 [ *Mon. Wea. Rev.*, 118, 891-938 ] les courants descendants diminuent  $\theta_E$  en basses couches

## BANDES EXTERNES (2)

Wang, 2001 [ *Mon. Wea. Rev.*, 129, 1370-1394 ]

triply-nested, two-way interactive, movable mesh model using hydrostatic primitive equations, with explicit « liquid+ice » microphysics and improved physical parameterizations, initialized with an axisymmetric vortex embedded in uniform easterly flow of 5 m/s on a « f-plane »



Model-simulated reflectivity at the surface  
up to 48h in the control experiment

# BANDES EXTERNES (3)

Romine & Wilhelmsen, 2006 [ *Mon. Wea. Rev.*, 134, 1121-1139 ]

TABLE 1. Summary of hypotheses that have been proposed to explain the formation of core and outer spiral rainbands within hurricanes. Small-scale bands are defined as observed bands that have  $\sim 10$  km horizontal scale.

Case	Proposed banding mechanism	Brief description	Comments
1	Inertia-buoyancy waves (Kurihara 1976)	Outward-propagating disturbance excited by eyewall convection	Three gravity wave modes, all with horizontal scales much larger than small-scale bands (25–200 km)
2	Inertia-buoyancy waves (Willoughby 1977)	Outward-propagating disturbance excited by eyewall convection	Favored horizontal scale $\sim 20$ km
3	Inertia-buoyancy waves (Willoughby 1978)	Inward- and outward-propagating Eliassen–Palm waves	Unrealistic phase speeds relative to observations, large variation in proposed horizontal scale with radius
4	Rayleigh instability (Fung 1977)	Ekman shear-induced circulations in the boundary layer, outward propagating	20–60-km horizontal scale, increasing with radius, slow to stationary phase speed
5	Symmetric instability (Braun 2002)	Primarily attributed to eyewall convection	May act as a trigger mechanism for gravity or potential vorticity waves of varying scale
6	Boundary layer rolls (GTH98)	Outward propagating, driven by boundary layer shear with deep convection	Deep horizontal roll vortices, structure and propagation similar to small-scale bands
7	Boundary layer rolls (Wurman and Winslow 1998)	Shear parallel boundary layer rolls	Shallow roll vortices, over one order of magnitude smaller scale than small-scale bands, not suggested to cause rainbands
8	Potential vorticity waves (Montgomery and Kallenbach 1997)	Vortex shedding (outward) and/or potential vorticity source entrainment (inward)	Slow outward velocity and horizontal scale increasing with radius from center of 20–50 km
9	Kelvin–Helmholtz instability [Testud et al. (1980) based on mode III waves proposed by Lalas and Einaudi (1976)]	Propagating gravity wave mode generated under extreme shear conditions	Scale and propagation characteristics similar to small-scale bands, applied to rainbands associated with postfrontal precipitation

# BANDES EXTERNES (4)

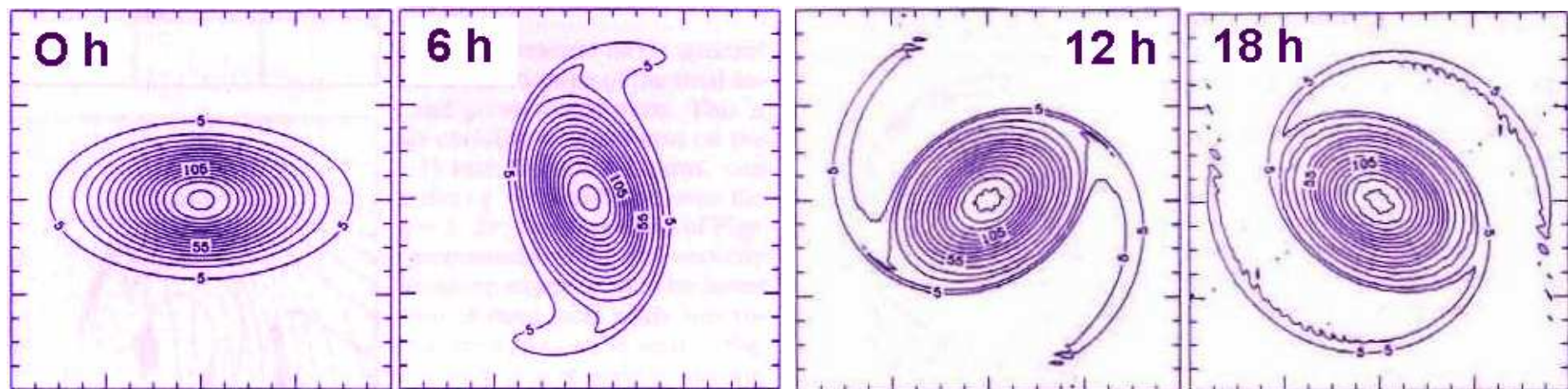
MacDonald, 1968 [Tellus, 20, 138-150]

- potential vorticity :  $PV = \frac{1}{\rho_{air} \text{ density}} \left[ (\nabla \times \underline{v} + fk) \cdot \frac{\nabla \theta}{\text{potential temperature gradient}} \right]$
- equation for PV :  $\frac{D(PV)}{Dt} = \frac{\zeta_a}{\rho} \cdot \frac{\nabla \dot{\theta}}{\text{latent heating}} + \frac{1}{\rho} \left( \nabla \times \frac{F}{\text{friction}} \right) \cdot \nabla \theta$
- Rossby PV waves : in a basic state with a horizontal gradient of PV, a perturbation of the PV contours (*which are material contours in an adiabatic flow*) propagates relative to the basic flow.  
In a tropical cyclone, the axi-symmetric PV field, with highest values in the center, is a basic state on which such waves can propagate.

# BANDES EXTERNES (5)

Guinn & Schubert, 1993 [ *J. Atmos. Sci.*, 50, 3380-3403 ]

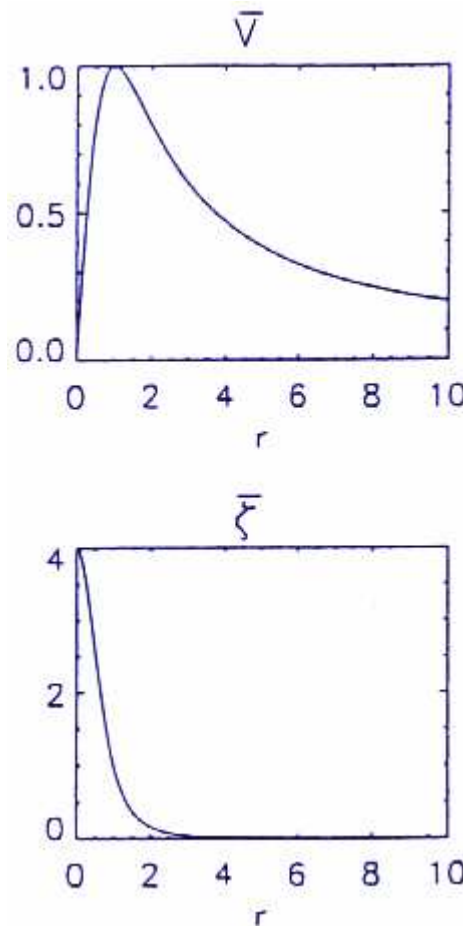
linearized non-divergent barotropic model : the non-linear breaking of Rossby waves in a TC-like PV field leads to irreversible distortion of the PV contours and a horizontal spreading of PV, until an axi-symmetric distribution is reached, with highest values in the center.



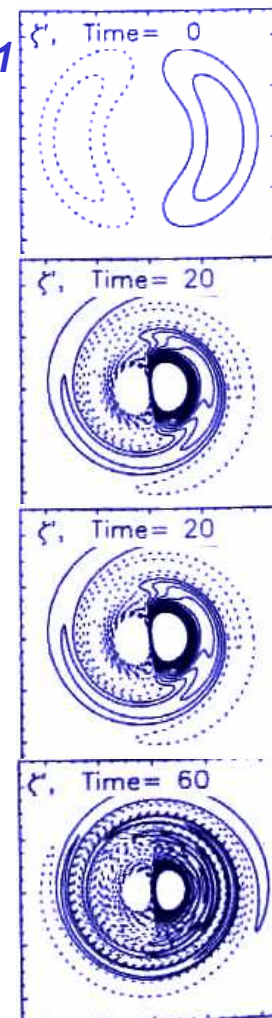
## BANDES EXTERNES (6)

Montgomery & Kallenbach, 1997 [ QJRMS, 123, 435-465 ]

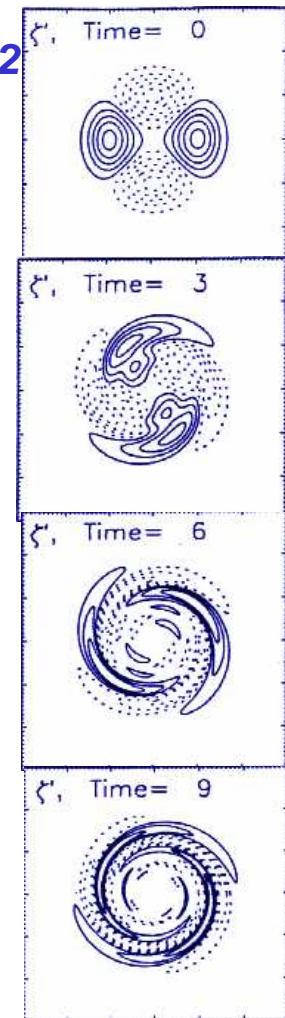
two-dimensional non-divergent inviscid flow in a « f-plane » :  
wavenumber-N Rossby waves propagate from a basic state  
characterized by a stable vorticity « monopole ».



Wavenumber-1

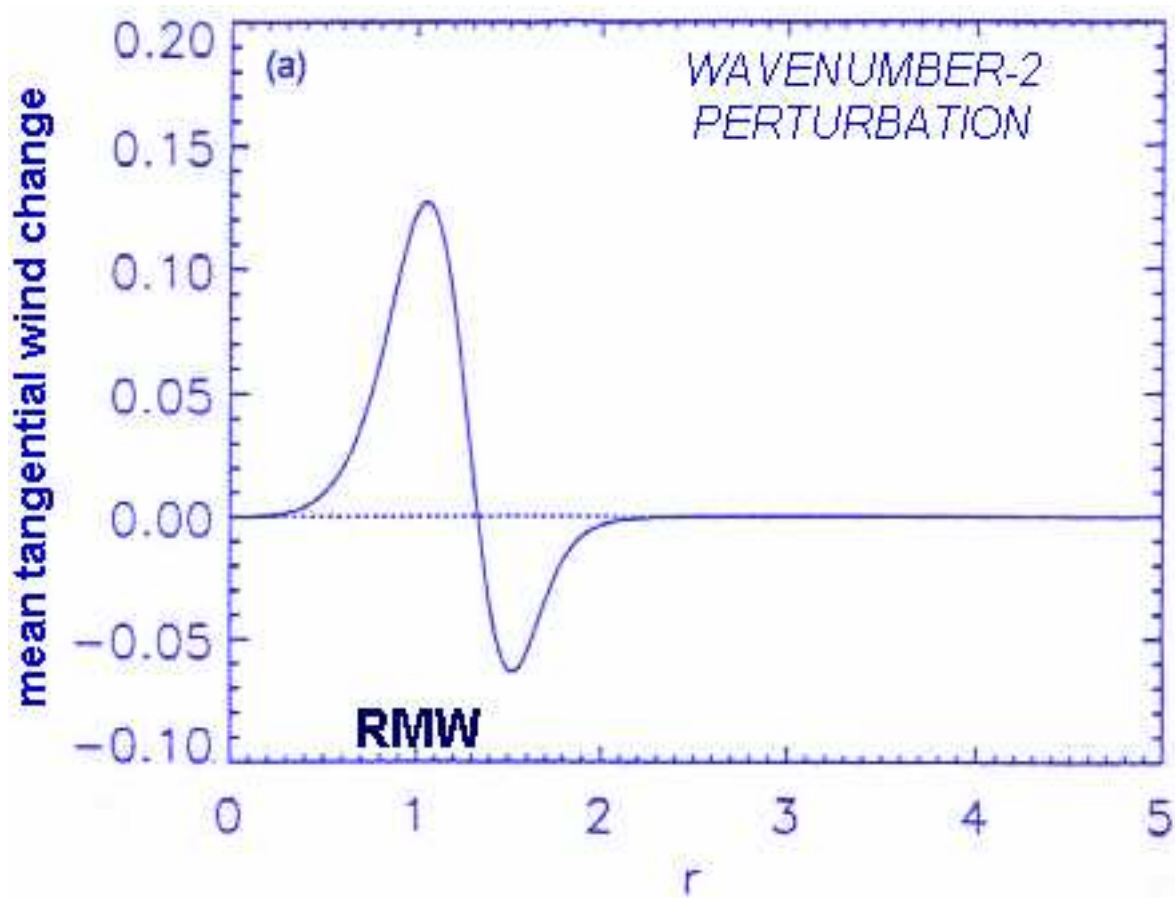


Wavenumber-2



## BANDES EXTERNES (7)

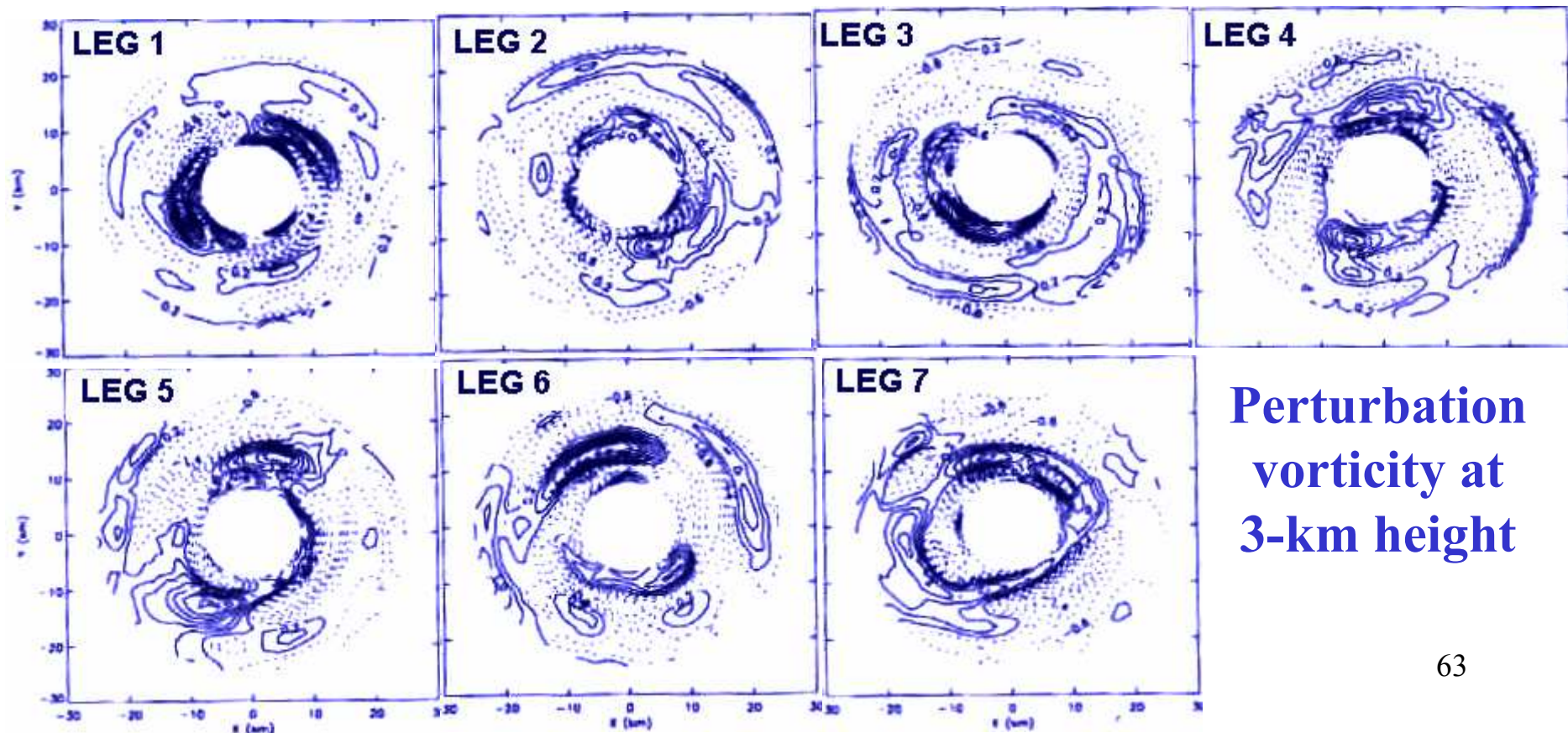
Interaction between the waves and the mean flow leads to an acceleration of the tangential wind inside the radius of maximum wind which increases the relative vorticity ( $2 V_T / r$ ) at low radii  
( $\rightarrow$  « monopole » distribution )



## BANDES EXTERNES (8)

Reasor *et al.*, 2000 [ *Mon. Wea. Rev.*, 128, 1653-1680 ]

An azimuthal wavenumber-2 feature dominates the asymmetry in relative vorticity below 3 km height in hurricane Olivia (1994) (from reflectivity and wind composites from airborne Doppler radar data)

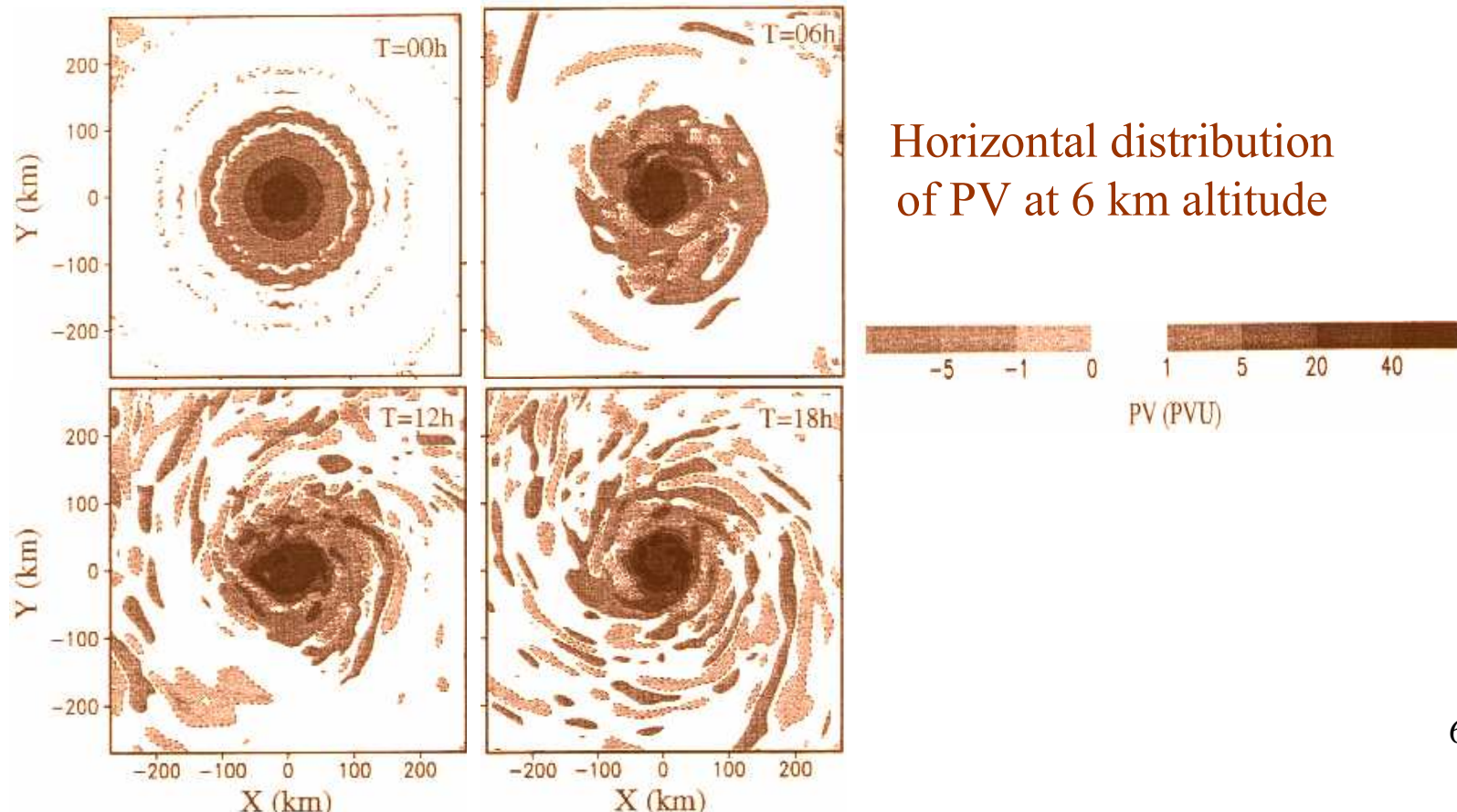


# BANDES EXTERNES (9)

Chen & Yau, 2001 [ *J. Atmos. Sci.*, 58, 2128-2145 ]

An initially axisymmetric hurricane was explicitly simulated using MM5  
(Liu *et al.* 1997 → constant SST=28°C)

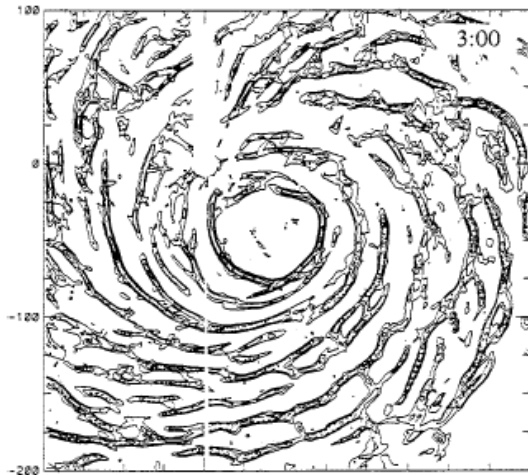
→ continuous generation of PV through latent heat release in the eyewall (+ spiral bands)



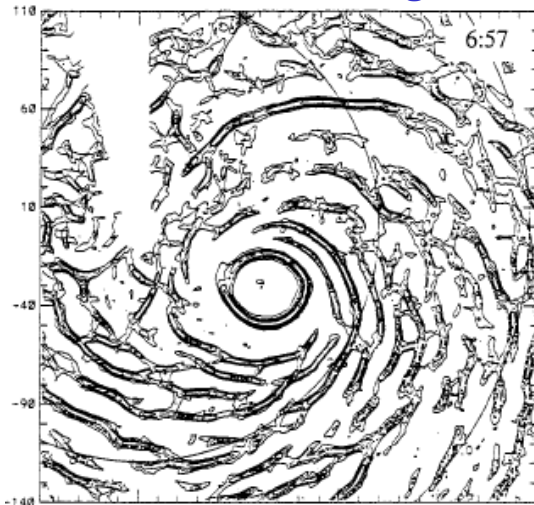
# STRUCTURES FINES (1)

Gall et al., 1998 [ *Mon. Wea. Rev.*, 126, 1749-1766 ]

Hugo - 22 Sep 89



Andrew - 24 Aug 92



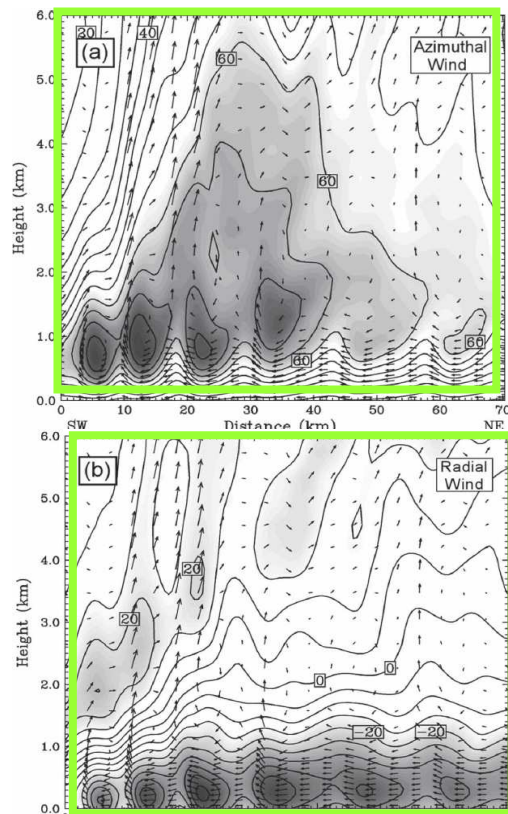
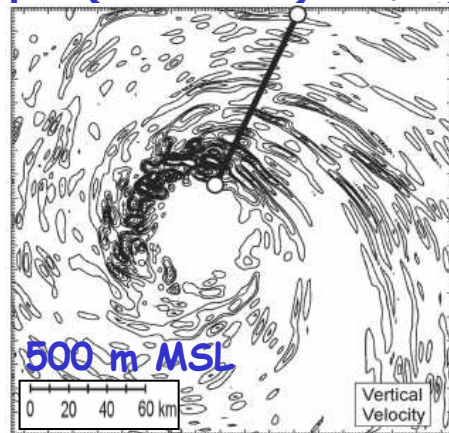
Radar reflectivity at 0.5° elevation : perturbation field = actual field - (7 gates x 7 rays) average + correlation between successive scans

properties of the small-scale spiral structures.

- 1) They spiral out from the storm center in a clockwise fashion.
- 2) The scale across the structures is of the order of 10 km.
- 3) They appear to extend around the storm for distances, along the spiral, of up to 100 km.
- 4) From the animation, they appear to move with the tangential wind.
- 5) Individual bands can be followed for periods of at least 1 h.
- 6) The bands form an angle of perhaps 10° with circles about the center of the hurricane.
- 7) Along a fixed radius from the hurricane center they would appear to move outward.
- 8) The variation in reflectivity across the bands is about 10 dBZ.

# STRUCTURES FINES (2)

Opal (5 Oct 95) 1km-grid

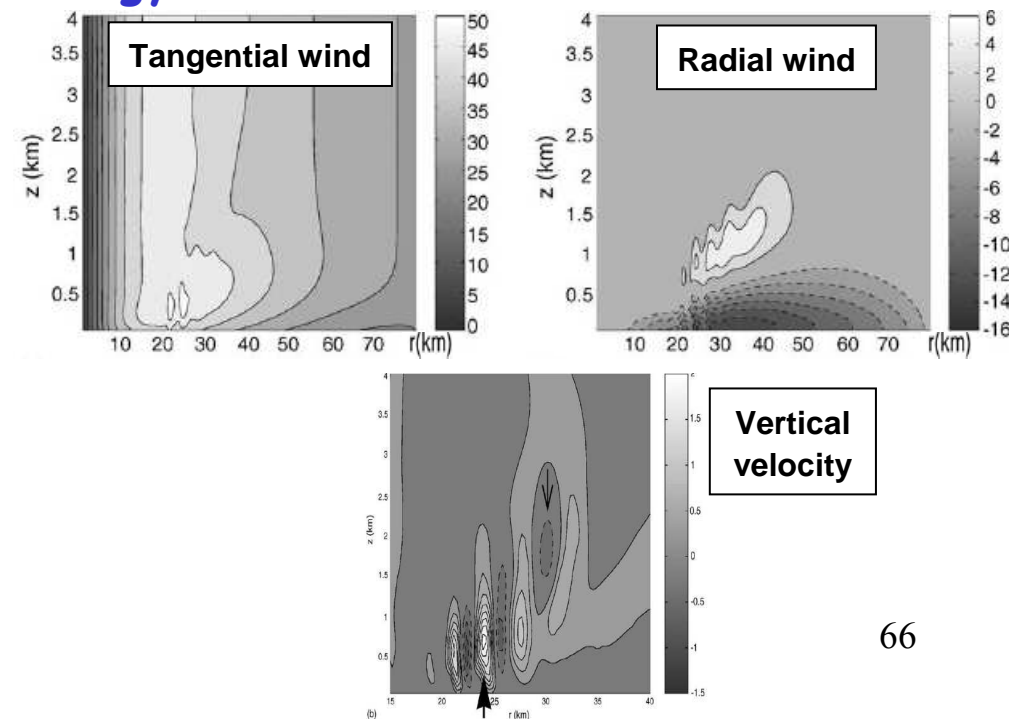


Romine & Wilhelmson, 2006 [ *Mon. Wea. Rev.*, 134, 1121-1139 ]

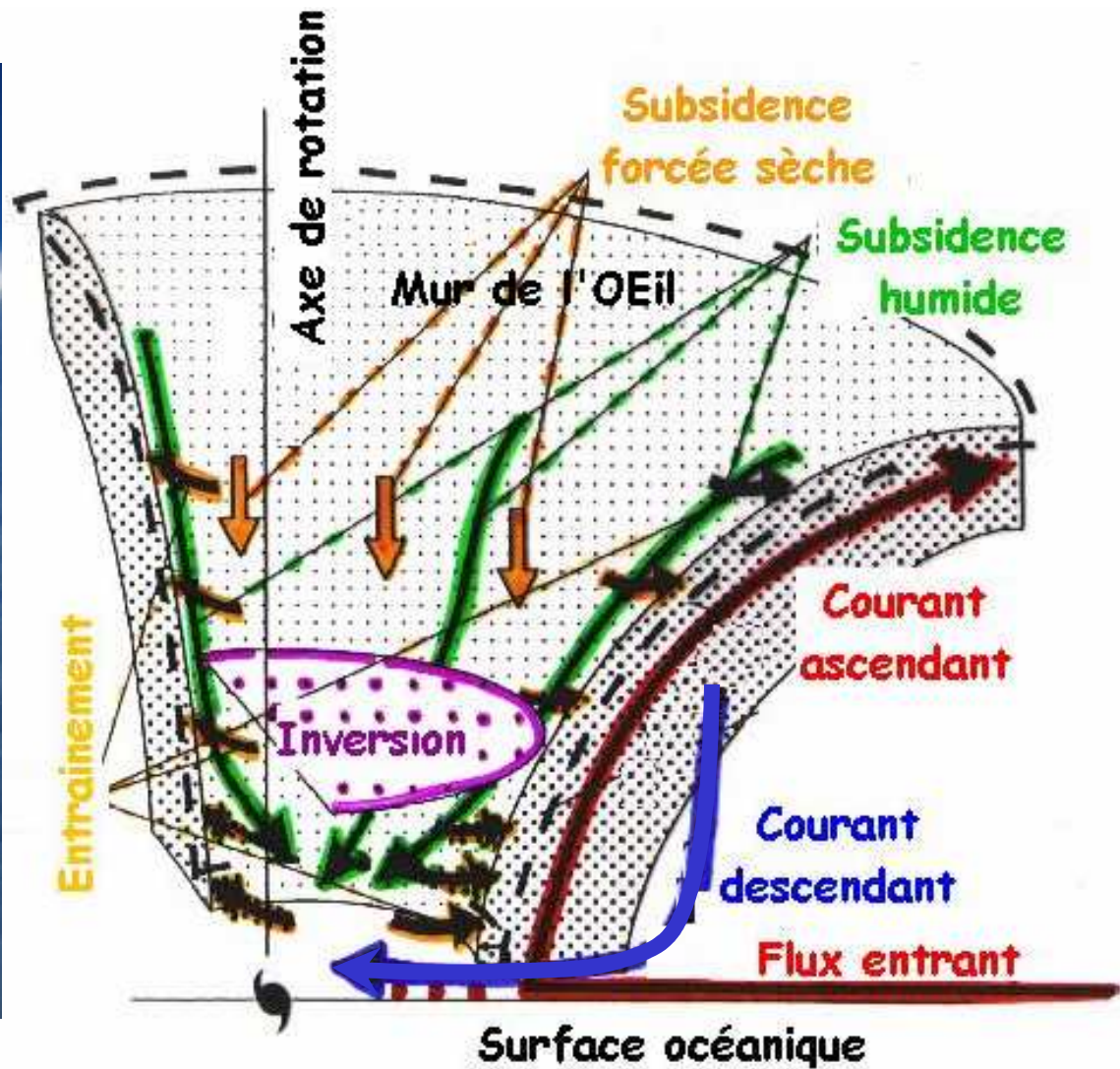
Most plausible mechanism : Kelvin-Helmholtz instability combined with boundary-layer radial and tangential wind shear.

Nolan 2005 [ *Dyn. Atmos. Oceans.*, 40, 209-236 ]

Quasi-streamlines rolls, with radial wavelength of 4-10 km, acquire their energy from the vertical shear

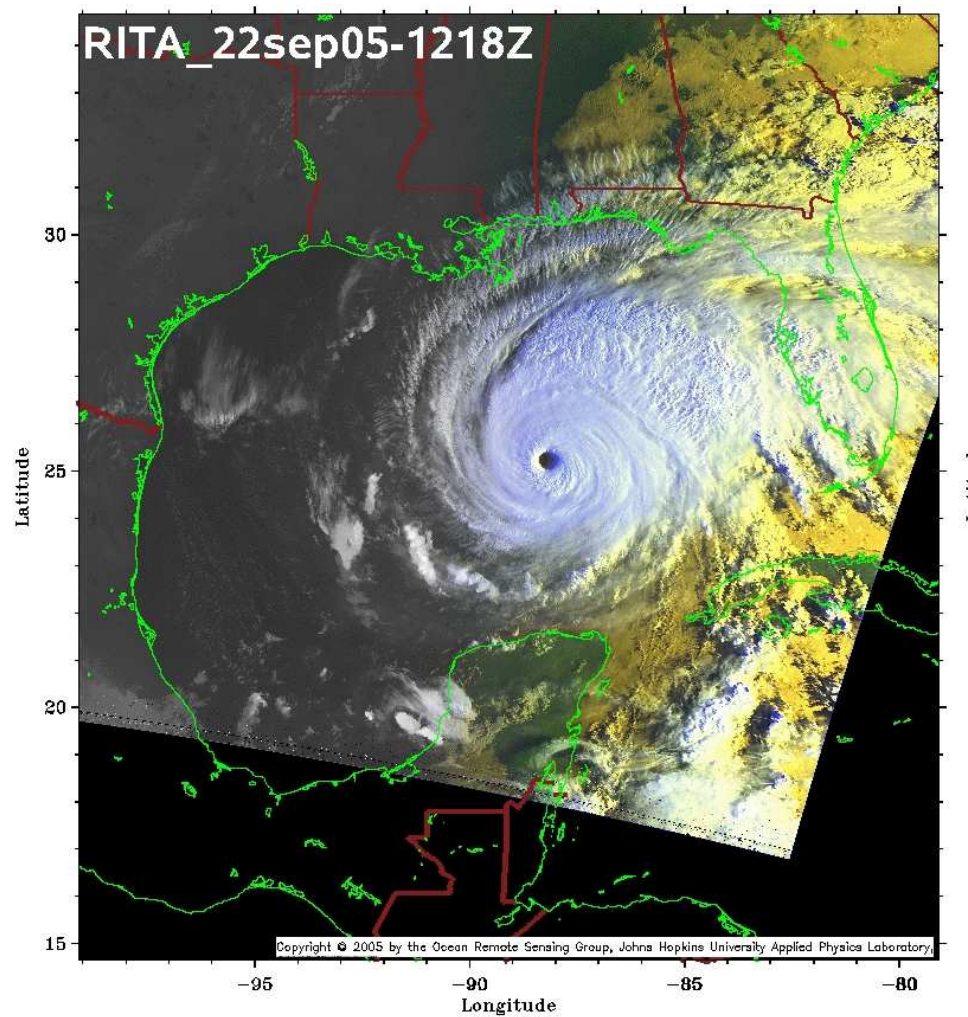


# LA CIRCULATION DANS L 'ŒIL (1)

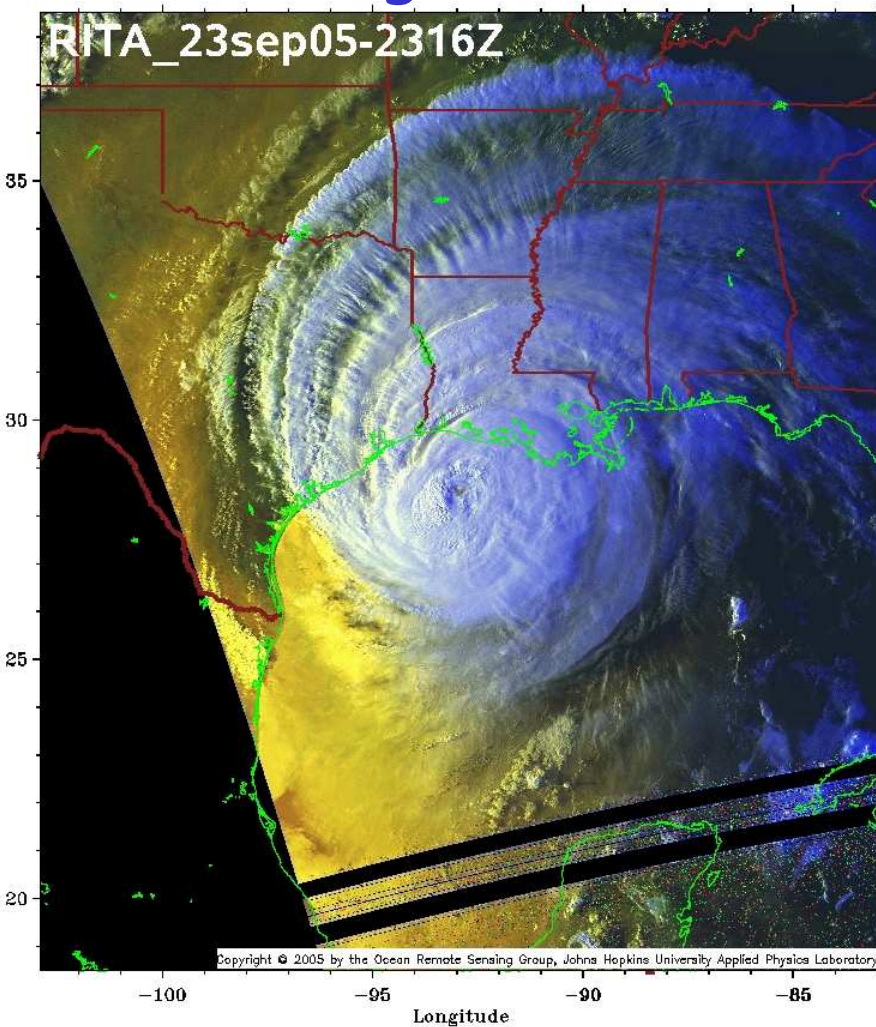


# LA CIRCULATION DANS L 'ŒIL (2)

Catégorie 5



Catégorie 3

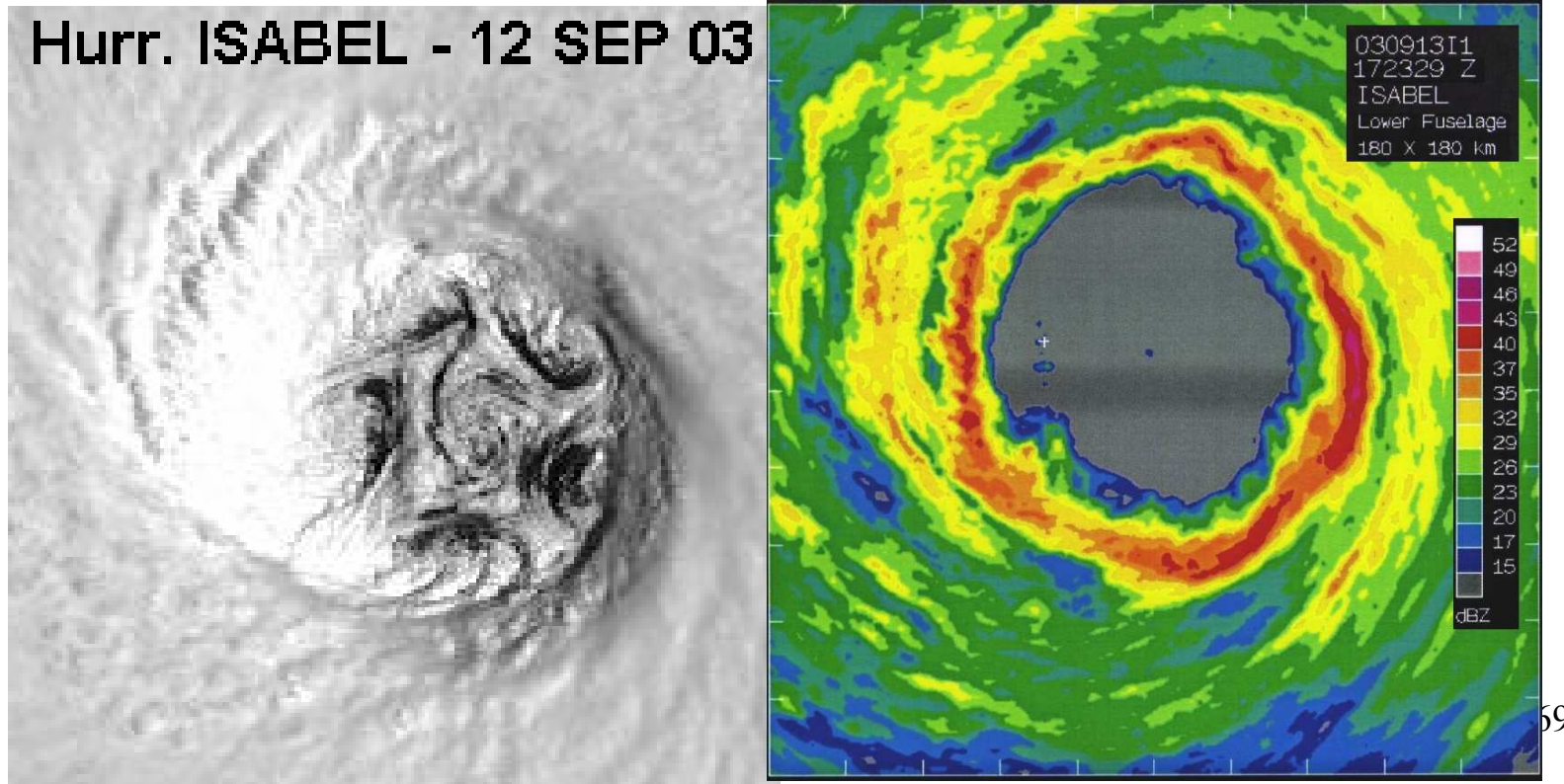


# L 'ŒIL POLYGONAL (1)

Schubert *et al.*, 1999 [ *J. Atmos. Sci.*, 56, 1197-1223 ]

Tropical cyclone eyewall occassionnally show polygonal (triangular to hexagonal) shapes. Other observations reveal the existence of intense « mesovortices » within or near the eye region.

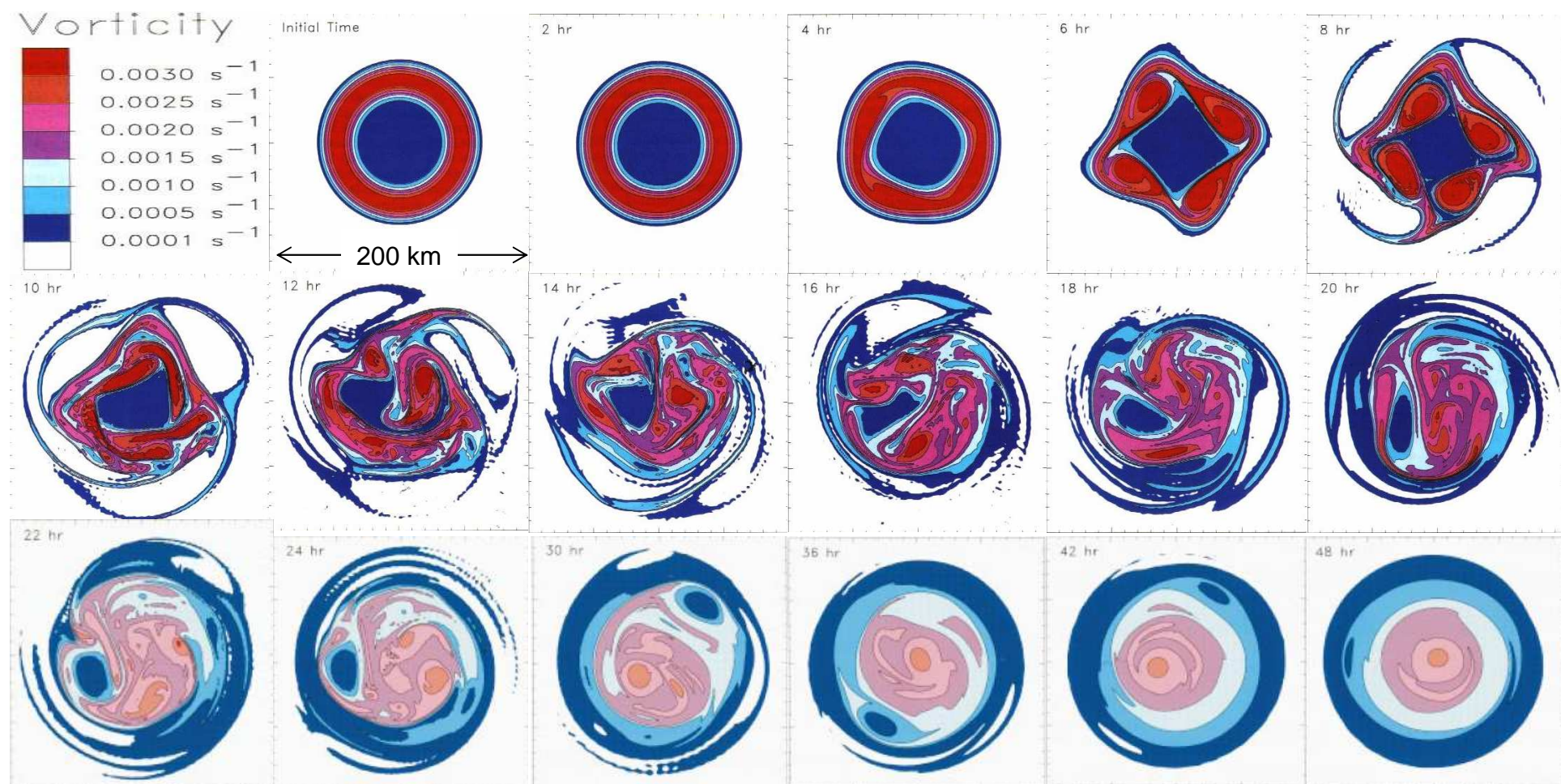
Hurr. ISABEL - 12 SEP 03



## L 'ŒIL POLYGONAL (2)

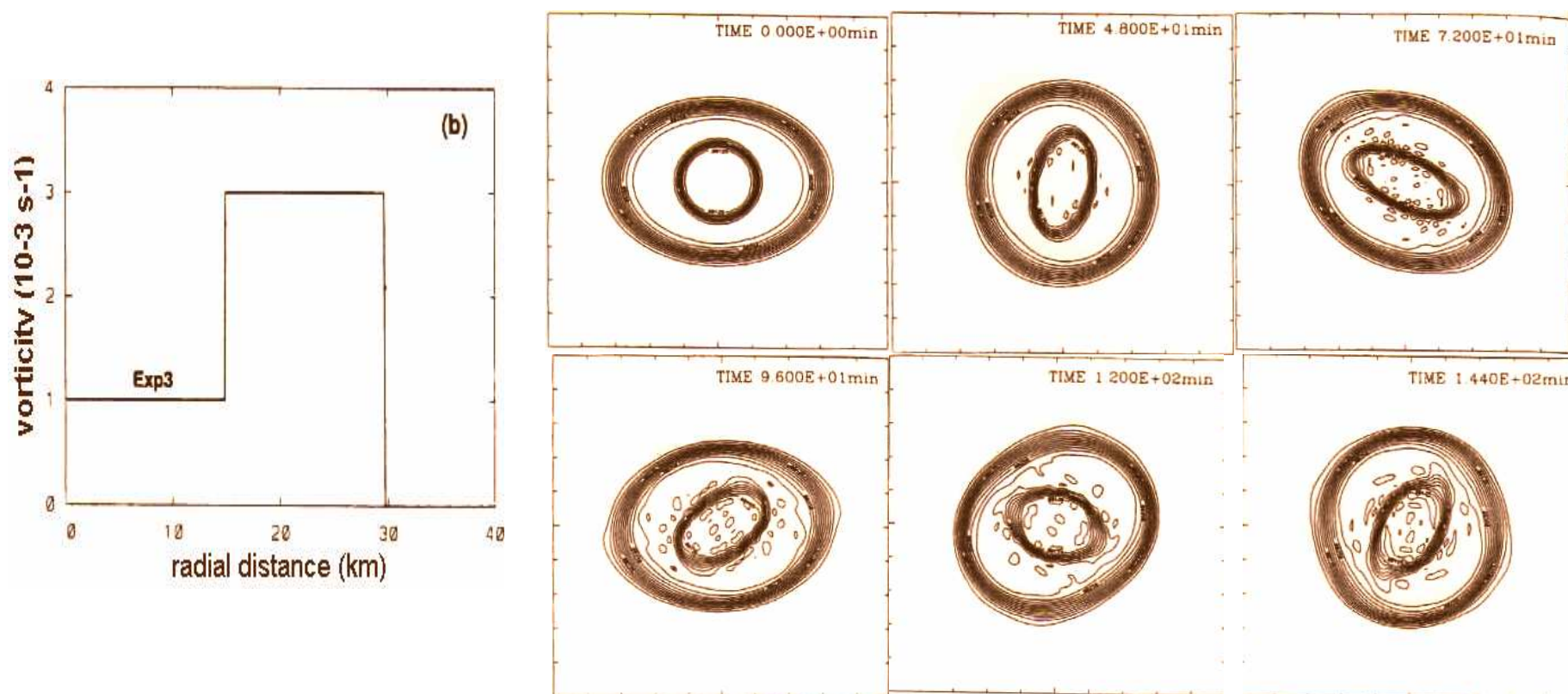
Barotropic non-divergent model of 200 km x 200 km initialized with a ring of high PV in the eyewall, at some distance from the storm center.

When the instability grows to finite amplitude, the vorticity of the eyewall region pools into discrete areas, creating the appearance of polygonal eyewalls with embedded mesovortices.



## L 'ŒIL POLYGONAL (3)

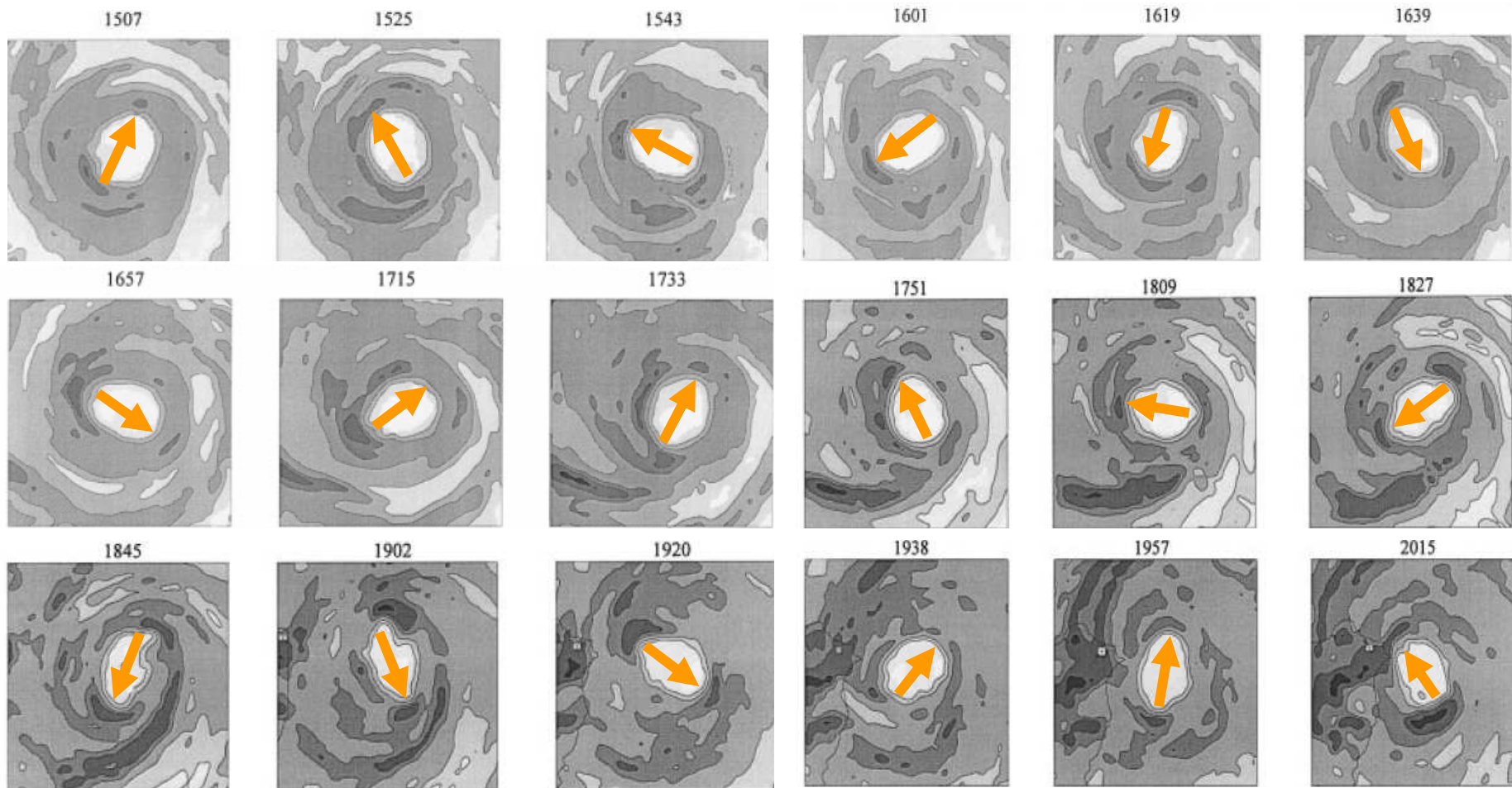
- barotropic dynamics in the presence of both a cyclonic mean flow and a high (potential) vorticity gradient near the edge of the eye leads to :
  - the propagation of vortex Rossby waves in the cyclonic mean flow make the eye rotate cyclonically
  - the rotation period is longer than the period of advected parcels because the vortex Rossby waves propagate upwind



# L 'ŒIL POLYGONAL (4)

Kuo *et al.* 1999 [ *J. Atmos. Sci.*, 56, 1659-1673 ]

The elliptical eye of typhoon Herb (1996) with a semi-major axis of 30 km and a semi-minor axis of 20 km rotated cyclonically with a period of approximately 145 min

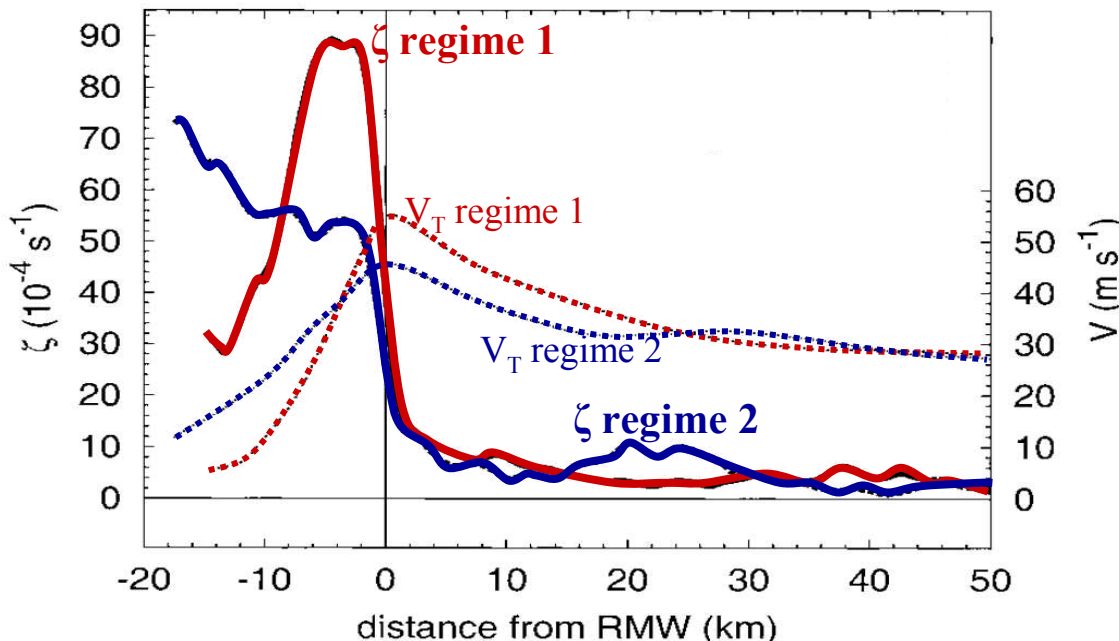


## L 'ŒIL POLYGONAL (5)

Kossin & Eastin, 2001 [ *J. Atmos. Sci.*, 58, 1079-1090 ]

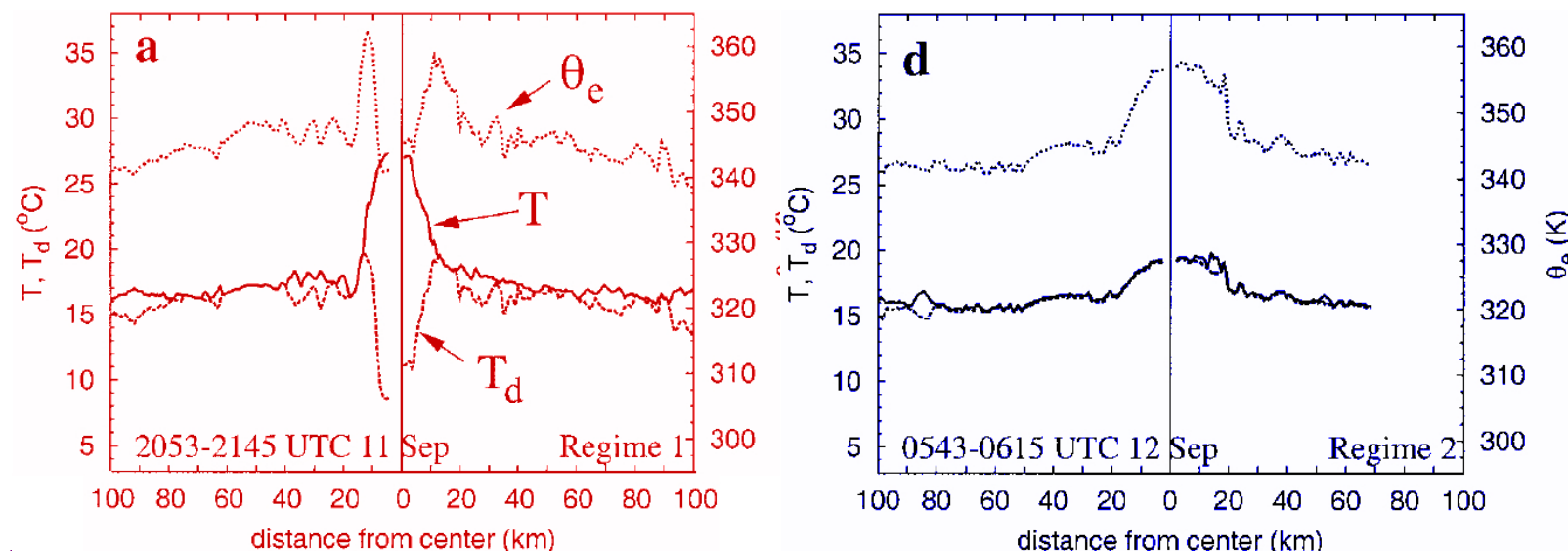
Aircraft flight level data show two distinct regimes of the kinematic and thermodynamic distribution within the eye and the eyewall :

- 1st regime : angular velocity is greatest within the eyewall and relatively depressed within the eye
- 2nd regime : radial profile of vorticity is nearly monotonic with maximum found at the eye center
- transition from 1st to 2nd regime can occur in less than 1 h, accompanied with dramatic changes in the thermodynamic structure

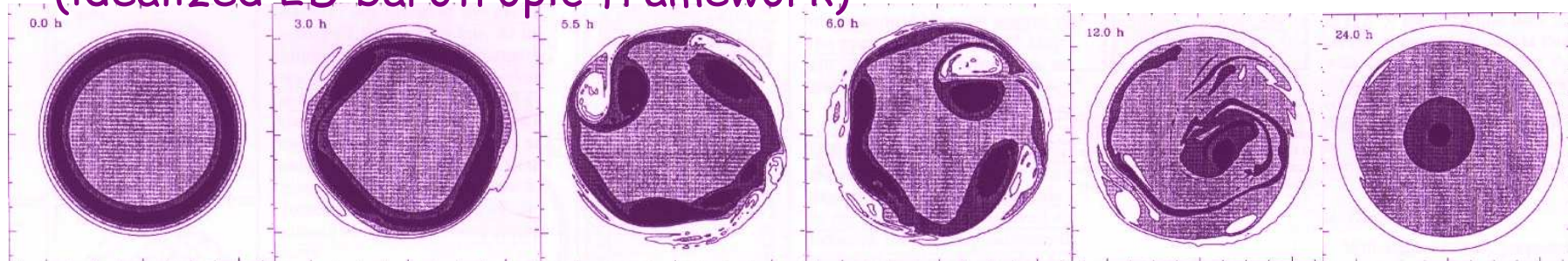


# L 'ŒIL POLYGONAL (6)

- Regime 1 : the eye is warm and dry,  $\theta_e$  is high in the eyewall and depressed in the eye
- Regime 2 : eye temperature may be lower, higher or unchanged; relative humidity is higher,  $\theta_e$  decreases monotonically from the storm center



This evolution can be explained through horizontal vorticity mixing  
(idealized 2D barotropic framework)



## L 'ŒIL POLYGONAL (7)

Nuissier et al., 2005 [ Quart. J. Roy. Meteor. Soc., 131, 155-194 ]  
Perturbations of the horizontal and vertical wind induced by the  
(wavenumber-2) Rossby-waves trigger spiral rainbands in the inner core.

